DTIC FILE COPY

ITATION PAGE

AD-A231 163

(1)

T DATE 1990	3 REPORT TYPE AND DATES COVERED THESIS/DISSERTATION

4 TITLE AND SUBTITLE

A Two-Dimensional Photochemical Model of the Troposphere

5 FUNDING NUMBERS

6. AUTHOR(S)

Meade W. Carlson

7. PERFORMING ORGANIZATION NAME(S) AND ADDRESS(ES)

AFIT Student Attending: Florida State University

8. PERFORMING ORGANIZATION REPORT NUMBER

AFIT/CI/CIA-90-147

9. SPONSORING MONITORING AGENCY NAME(S) AND ADDRESS(ES)

AFIT/CI
Wright-Patterson AFB OH 45433-6583

10. SPONSORING, MONITORING AGENCY REPORT NUMBER

11. SUPPLEMENTARY NOTES

12a. DISTRIBUTION/AVAILABILITY STATEMENT

Approved for Public Release IAW 190-1
Distributed Unlimited
ERNEST A. HAYGOOD, 1st Lt, USAF
Executive Officer

12b. DISTRIBUTION CODE

13. ABSTRACT (*Maximum 200 words*)

14. SUBJECT TERMS			15 NUMBER OF PAGES 99
			16. PRICE CODE
17. SECURITY CLASSIFICATION OF REPORT	18. SECURITY CLASSIFICATION OF THIS PAGE	19. SECURITY CLASSIFICATION OF ABSTRACT	20 LIMITATION OF ABSTRACT

THE FLORIDA STATE UNIVERSITY

COLLEGE OF ARTS AND SCIENCES

A TWO-DIMENSIONAL PHOTOCHEMICAL MODEL OF THE TROPOSPHERE

By

MEADE W. CARLSON

A Thesis submitted to the
Department of Meteorology
in partial fulfillment of the
requirements for the degree of
Master of Science

Degree Awarded:

Fall Semester, 1990

The members of the Committee approve the Thesis of Meade W. Carlson defended on August 28, 1990.

Paul H. Ruscher
Professor Co-directing Thesis

Jack Fishman
Professor Co-directing Thesis

T. N. Krishnamurti
Committee Member

David W. Stuart
Committee Member

The members of the Committee approve the Thesis of Meade W. Carlson defended on August 28, 1990.

Paul H. Ruscher
Professor Co-directing Thesis

Jack Fishman
Professor Co-directing Thesis

T. N. Krishnamurti
Committee Member

David W. Stuart
Committee Member

A Two-dimensional Photochemical Model of the Troposphere

by Meade W. Carlson, Capt, USAF

1990
99 pages
Degree Awarded: M.S. by The Florida State University

Abstract

An experiment using a time-dependent, two-dimensional photochemical model of the troposphere to model the vertical and zonal distribution of ozone and its precursors is presented. The experiment examines two cases. Case I simulates vertical transport due to diffusion and zonal transport due to advection, with surface emissions of ozone precursors in the center of the model domain representing an urban environment with light wind conditions favorable for the formation of ozone in concentrations greater than 80 parts per billion by volume (ppbv). In Case II, an elevated source of ozone and its precursors is introduced at the upstream boundary in order to investigate the role of advection of these chemical species on ozone concentrations.

The first simulation produces surface ozone concentrations greater than 120 ppbv in the air above the urban area, and the second simulation produces an increase of 3 - 10 percent in this region. A comparison of Case I and Case II results shows that enhanced photochemical production of ozone due to the addition of ozone's precursors plays an important role in this increase.

Acknowledgements

I am deeply indebted to my advisors, Dr. Paul Ruscher and Dr. Jack Fishman for their support and guidance, without which this work would not have been accomplished. I am also deeply indebted to Dr. Tom Carney who led my initial research efforts despite the failing health which led to his passing in October 1989.

Thanks also go to Jennifer Richardson at NASA/Langley for her help and suggestions, to Dr. Jon Ahlquist for his work in creating the LaTeX macro used for this thesis and for his help and guidance in as I learned LaTeX, and to my committee members Prof. T. N. Krishnamurti and Prof. David Stuart for their support.

Contents

List of Tables

List of Figures

Abstract

An experiment using a time-dependent, two-dimensional photochemical model of the troposphere to model the vertical and zonal distribution of ozone and its precursors is presented. The experiment examines two cases. Case I simulates vertical transport due to diffusion and zonal transport due to advection, with surface emissions of ozone precursors in the center of the model domain representing an urban environment with light wind conditions favorable for the formation of ozone in concentrations greater than 80 parts per billion by volume (ppbv). In Case II, an elevated source of ozone and its precursors is introduced at the upstream boundary in order to investigate the role of advection of these chemical species on ozone concentrations.

The first simulation produces surface ozone concentrations greater than 120 ppbv in the air above the urban area, and the second simulation produces an increase of 3 – 10 percent in this region. A comparison of Case I and Case II results shows that enhanced photochemical production of ozone due to the addition of ozone's precursors plays an important role in this increase.

Chapter 1

Introduction

The presence of ozone (O_3) in the troposphere is a very significant environmental hazard. Ozone is estimated to cause greater than $1 billion of crop damage each year in the U.S. (Heck *et al.*, 1982). Human health is adversely impacted by ozone concentrations that commonly occur in parts of the United States during summer. A recent study shows exposure to ozone concentrations of 0.12 ppm (the current Environmental Protection Agency (EPA) standard) for one to six hour periods reduces the volume of air that a person is able to breath (Follinsbee *et al.*, 1988). Ozone also accelerates the aging of the lungs and causes other adverse bio-chemical changes to the lungs (Sun, 1988).

Ozone is an important infrared (IR) absorber in the troposphere because the 9.6 μm band of ozone is in the center of the IR window (Ramanathan, 1988). This makes ozone an important greenhouse gas. Changes to the amount of ozone present in the troposphere will change the radiative balance between the earth and the atmosphere, possibly resulting in changes to climate. Doubling the amount of ozone in the troposphere could result in

an average global temperature increase of 0.9 K (Fishman *et al.*, 1979). In comparison, a doubling of CO_2 could lead to an increase of 3.5 to 4.5 K (Ramanathan, 1988). This contribution is not as large as the contribution the major greenhouse gas, CO_2, would make with a similar increase, but the contribution due to ozone is still significant. Because tropospheric ozone may be increasing 3 - 5 times faster than CO_2 over the past 20-30 years (Logan, 1985), the impact on climate of these these two gases may be comparable (Vukovich and Fishman, 1986).

Episodes of widespread elevated ozone levels (greater than 80 ppbv) occur over the United States each summer. These episodes are frequently associated with air stagnation events characterized by weak, slow moving, persistent high-pressure systems (Logan, 1989). Some occurences of high ozone concentrations were explained by the occurrence of tropopause folding events in which a large amount of ozone rich stratospheric air is injected into the middle and lower troposphere (Danielsen, 1968), while normal concentrations of ozone at the surface were thought to originate in the stratosphere and be transported to the surface by other large scale motions (e.g., Fabian and Pruchniewicz 1973). In both cases, ozone was treated as chemically inert in the troposphere. The Logan (1989) analysis of meteorology for high ozone episodes indicates that transport of ozone from the stratosphere to the surface due to tropopause folding is not the primary mechanism for these high ozone occurrences.

Starting with Crutzen (1973), and Chameides and Walker (1973), studies of the tropospheric ozone budget were done with one dimensional models incorporating ozone photochemistry. These early photochemical studies were done under the hypothesis that photochemical processes were the dominant important source of ozone in the troposphere. These first models did not consider the role of atmospheric transport mechanisms in the ozone budget.

Current one dimensional models treat both photochemistry and vertical atmospheric transport mechanisms as contributors. The model used for this study is an expansion of Fishman and Carney (1984). It includes vertical transport by diffusion with simple models of the boundary layer, and also models transport due to fair weather cumulus clouds. The photochemical model includes reactions important in the tropospheric budget of ozone and its precursors. Of primary importance in this study are the reactions due to the oxides of nitrogen (NO_x), non-methane hydrocarbons (NMHC), and carbon monoxide (CO). These chemical species are precursors to the the formation of tropospheric ozone and as such, are very important factors in controlling ozone photochemistry in the troposphere (Fishman *et al.*, 1985). Studies have linked increased emissions of these chemical families due to fossil fuel burning and biomass burning to increases in tropospheric ozone (Logan 1985; Fishman and Crutzen 1978; Fishman *et al.*, 1985; Fishman *et al.*, 1990).

The primary goal of this research is to investigate the role of horizontal advection in the photochemical production of ozone during elevated ozone events. To accomplish this, a model of the photochemical generation and transport of ozone and its precursors over

a typical southeast U.S. air stagnation event is developed by expanding an existing one-dimensional time dependent photochemical model of the troposphere to two dimensions by including large scale advection in the vertical and in one horizontal direction. A wind field representative of the synoptic scale features of one such event is incorporated into the model.

Chapter 2

Methodology

The one-dimensional photochemical model described by Fishman and Carney (1984) serves as the starting point for the two dimensional Eulerian photochemical model used in this study. The one-dimensional model has been expanded to include a horizontal advection term and a vertical advection term.

2.1 The Continuity Equation

The general form of the two-dimensional (2D) continuity equation for a chemical species X_i is:

$$\begin{aligned}\frac{\partial[X_i]}{\partial t} &= E_i + P_i - [X_i]D_i + -w[M]\frac{\partial \mu_i}{\partial z} + \frac{\partial}{\partial z}\left(K_z[M]\frac{\partial \mu_i}{\partial z}\right) \\ &\quad - u[M]\frac{\partial \mu_i}{\partial x} + \frac{\partial}{\partial x}\left(K_x[M]\frac{\partial \mu_i}{\partial x}\right) \qquad (1)\end{aligned}$$

where

$[X_i]$ is the concentration of the chemical species X_i (molecules cm^{-3}),

E_i is the emission rate of X_i (molecules cm^{-3} sec^{-1}),

P_i is the photochemical production rate of X_i (molecules cm^{-3} sec^{-1}),

$[X_i]D_i$ is the photochemical destruction rate of X_i (molecules cm^{-3} sec^{-1}),

$[M]$ is the concentration of air molecules,

μ_i is the volume mixing ratio of X_i,

K_z is the vertical eddy diffusion coefficient,

K_x is the horizontal eddy diffusion coefficient,

w is the vertical velocity component, and

u is the horizontal velocity component.

This equation defines the rate of change of the molecular concentration of a chemical species in time as the net amount of production, destruction, vertical advection, vertical diffusion, horizontal advection, and horizontal diffusion. In this study, the horizontal diffusion term is ignored because emissions are given in terms of area sources, so small-scale horizontal details of concentration are smoothed out, and because the grid scale precludes resolution of small scale effects in the horizontal.

The domain of the model is a grid covering 12 km in the vertical and 1000 km in the horizontal (see figure 1.) Grid spacing is 50 km in the horizontal and irregular in the vertical. Above 2 km, vertical grid spacing is 1 km. Below 2 km, grid spacing is 250 m with an additional layer at 2 m which serves as the lowest level where species concentration is calculated. The grid points at the surface serve only as computational points for finite differencing. The grid is placed over the southeast United States so that the horizontal wind field is representative of a summertime Bermuda high situation which is often observed over

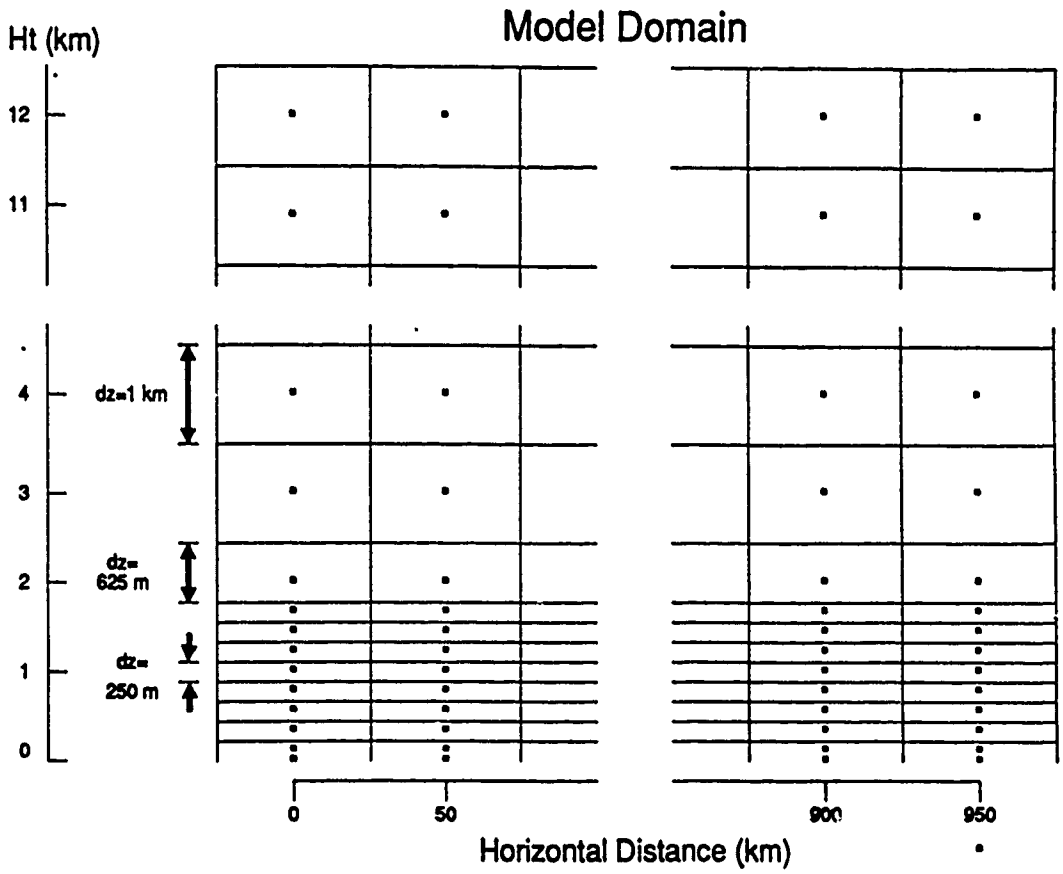

Figure 1: A schematic representation of the grid spacing used in this study.

the region during air stagnation events.

2.2 Photochemistry

The photochemical reactions used in this model are taken from the one-dimensional model described by Fishman and Carney (1984) with the addition of isoprene chemistry after Lurmann *et al.* (1986). The reaction rate coefficients used in this study are shown in Appendix A. The model allows for explicit numerical integration of the chemistry of long lived species such as the alkanes ethane, butane, and hexane, as well as the alkenes ethylene and propylene. It also generates concentrations for species such as acetaldehyde, peroxyacetylnitrate (PAN) and other partially oxidized compounds. These species have highly variable lifetimes and their concentrations are computed using implicit integration. The short-lived radicals, such as OH, HO_2 and their analogs derived from non-methane hydrocarbons are calculated using steady state approximations. No advection or diffusion of the short-lived species is calculated. Integration of the photochemical terms of the continuity equation is done using Euler-backward time differencing. A time step of 3 min has been used in this study.

Emission rates of CO, NMHC and NO_x are the independent variables in this study. The background surface emission rates are shown in Table 1. The emission rates for CO, NMHC, and NO_x at three grid points near the center of the horizontal domain were increased by a factor of twenty to simulate emission rates consistent with an urban environment.

Table 1: Background emission rates

Species	Chemical Formula	Emission Rate (mol cm^{-2} sec^{-1})
Oxides of Nitrogen	NO_x	0.5E 11
Carbon Monoxide	CO	3.75E 11
Ethane	C_2H_6	0.1E 11
Butane	C_4H_{10}	0.2E 11
Hexane	C_6H_{14}	0.1E 11
Ethene	C_2H_4	0.1E 11
Propene	C_3H_6	0.1E 11
Isoprene *	C_5H_8	5.0E 11

* Average daytime emission rate. Isoprene is not emitted at night.

2.3 The Wind Field

The wind field used in the model represents an idealized flow during a summertime Bermuda high situation over the southeast United States. The wind field taken as a guide in constructing the winds used in this model is from the European Centre for Medium Range Weather Forecasts (ECMWF) analysis for 1200 UTC, 26 July 1987.

During the period starting on July 16 through July 31, a persistent high pressure system was in place over the southeast United States. The high pressure system prevented large scale precipitation and kept skies generally clear. Temperatures were high during the period with many stations in the southeast reaching 100° F. While synoptic scale precipitation events were not present, isolated moist convection produced measurable rainfall amounts at some stations in the southeast. During this period, elevated levels of ozone were recorded throughout the Southeast and there were numerous violations of the ozone standard of 120

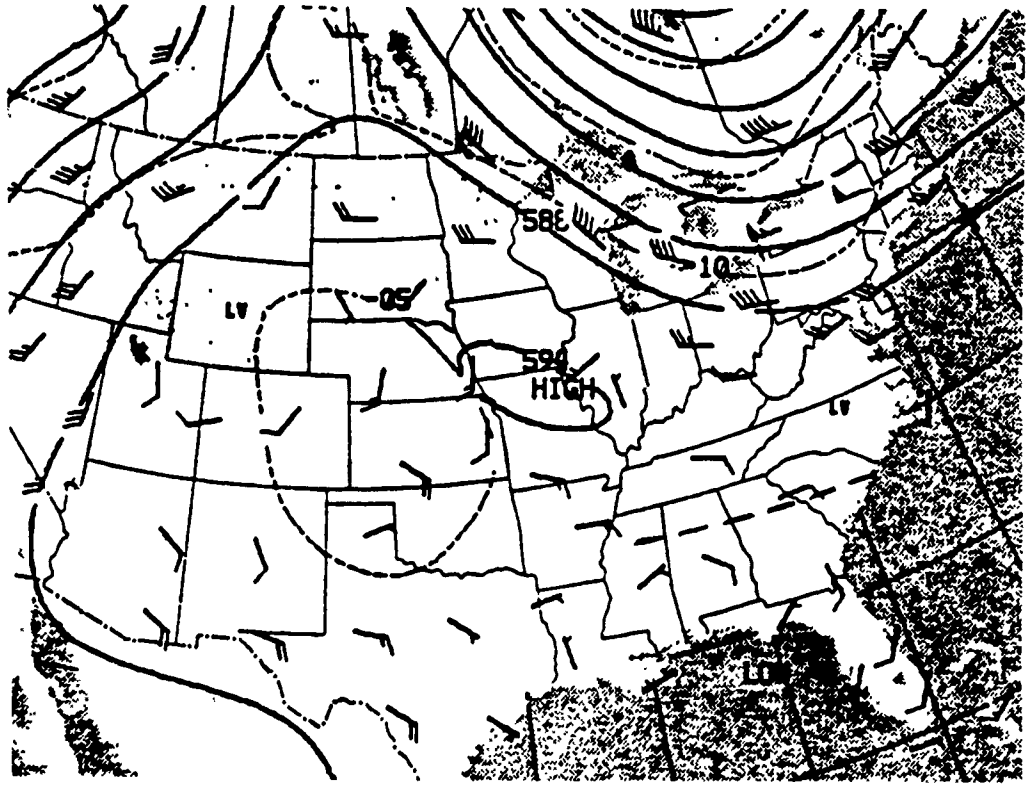

Figure 2: 500mb analysis for 1200 UTC, 26 July 1987. From Daily Weather Maps Weekly Series, July 26, 1987. Dashed line indicates the horizontal domain for model calculations.

ppbv for one hour (McNider, 1989). The 26 July, 1200 UTC surface analysis depicts a large high pressure area over the entire southeast with the high centered over southern Arkansas. Surface winds were generally light and variable throughout the entire region. Through 500 mb, winds over the region remained light. Synoptic conditions are depicted in figures 2 and 3.

The ECMWF winds for the standard pressure levels are depicted on figures 22 - 26 in appendix B. They show a weak westerly (positive) zonal wind component over the Southeast at 1000 mb, and a variable zonal wind component at 850 mb. At 700 mb and above, the zonal wind component is easterly (negative) over the region. The vertical motion for the 26 July

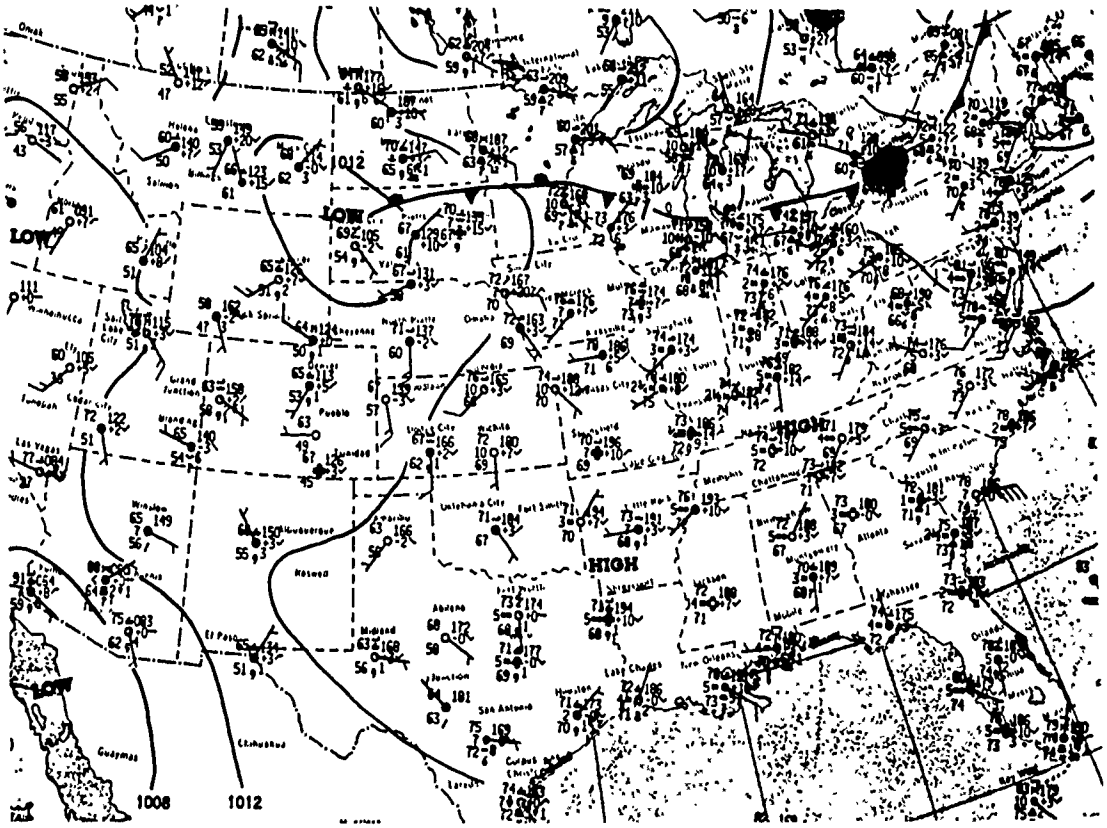

Figure 3: Surface analysis for 1200 UTC, 26 July 1987 (Daily Weather Maps Weekly Series, July 26, 1987).

1987, 1200 UTC wind field was calculated by the kinematic method. The resultant vertical motion field has a maximum value of 0.6 cm s^{-1}. This is four orders of magnitude smaller than zonal wind values. However, vertical gradients of the trace species that this study is concerned with are greater than their horizontal gradients. Thus, fluxes of trace species due to synoptic scale vertical motion may be as much as one to ten percent of horizontal fluxes and thus may play a significant role in the transport of these species in the free troposphere. In the planetary boundary layer (PBL), transport due to turbulent eddy motions is much more important than transport due to any synoptic scale vertical motions. This study is an initial attempt to examine the feasability of expanding the Fishman and Carney (1984) model to two dimensions and is primarily concerned with horizontal advective effects For these reasons, and to simplify interpretation of model output, the effects of vertical motion are ignored in these experiments.

The wind field used in the model is further simplified by requiring zonal homogeneity, thereby eliminating a horizontal gradient in the wind field. The resultant wind continues to emulate some specific characteristics of flow over the southeast United States during a Bermuda high, namely light westerlies are present in the lower PBL with light easterlies above. This feature was considered important for the present study because it may provide a mechanism for recirculating ozone and its precursors from the boundary layer that have been advected away from an emission source back over the region where it originated. This flow reversal is illustrated in figure 4.

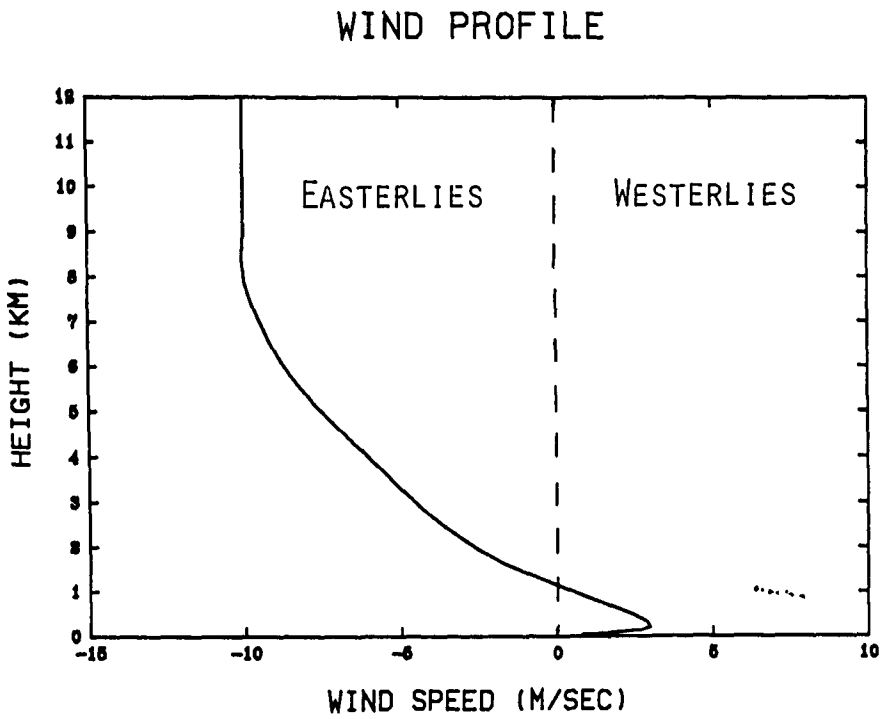

Figure 4: The wind profile used in this study.

2.4 Boundary Conditions

"Clean" air enters any upstream boundary; the horizontal gradients of all chemical concentrations are assumed to be zero outside the model domain so that concentrations at upstream boundaries are not changed by the advection terms. Vertical motion at both upstream and downstream boundaries is set to zero. Vertical motion throughout the model domain is set to zero with the exception of the chemical species listed in Table 2 where deposition velocities are prescribed for the surface grid points.

At 12 km, vertical gradients of most species are set to zero so that net changes in concentrations due to diffusion are zero. Downward fluxes of 6.6×10^{10} mol cm^{-2} sec^{-1} for ozone (Mahlman *et al.*, 1980) and 2×10^{8} mol cm^{-2} sec^{-1} for reactive nitrogen (Levy

Table 2: Deposition velocities (After Fishman and Carney 1984).

Species	Chemical Formula	W_d (cm sec^{-1})
Ozone	O_3	0.5 (night) 1.5 (day)
Oxides of Nitrogen	NO_x	0.5
Nitric acid	HNO_3	0.5
Dinitrogen pentoxide	N_2O_5	0.5
Hydrogen peroxide	H_2O_2	0.2 *
Formaldehyde	H_2CO	0.2
Acetaldehyde	CH_3CHO	0.2
All nonmethane hydrocarbons	C_xH_y	0.1
PAN	$CH_3CO_3NO_2$	0.05
Isoprene	C_5H_8	0.0

* deposition velocity for all peroxides

et al., 1980) are the two exceptions.

2.5 Boundary Layer Parameterization

Turbulent transport of chemical species in the boundary layer is modeled by allowing the profile of the vertical eddy diffusion coefficient K_z to vary with the time of day. Carney (1984) and Fishman and Carney (1984) have enlisted a model of the convective PBL and a model of the nocturnal PBL to predict the height of the well mixed layer at hourly intervals.

2.5.1 The Convective PBL

The model used to predict the height of the convective PBL is taken from Zeman and Tennekes (1977). The convective mixed layer grows through turbulent entrainment at its upper

boundary. This model applies a parameterized turbulent kinetic energy (TKE) equation to the base of a temperature inversion at the top of the PBL. The TKE equation is solved to provide a ratio of the heat flux near the surface and the negative heat flux at the inversion base:

$$\frac{F_i}{F_s} = \frac{C_f - C_d w_b \frac{h}{w^*}}{1 + C_t (w^*)^2 \frac{T_s}{gh\Delta\theta}} \tag{2}$$

where

F_i is the heat flux at the inversion base,

F_s is the heat flux at the earth's surface,

C_f, C_d, and C_t are empirical coefficients,

w_b is the Brunt-Väisälä frequency in the stable air above the boundary layer,

h is the height of the mixed layer,

w^* is the convective velocity scale,

T_s is the temperature at the surface,

g is the acceleration due to gravity, and

$\Delta\theta$ is the inversion strength (temperature jump).

With the ratio between the heat flux at the surface and at the inversion determined, equations 3 and 4 may be solved numerically for the height of the mixed layer and the inversion strength:

$$-F_i = (\Delta\theta)\frac{\partial h}{\partial t} \tag{3}$$

The prognostic equation for the potential temperature difference ($\Delta\theta$) is:

$$\frac{\partial(\Delta\theta)}{\partial t} = \gamma\frac{\partial h}{\partial t} - \frac{F_s - F_i}{h} \tag{4}$$

where γ is the vertical gradient of potential temperature in the air above the inversion. The resultant daytime PBL height ranges from about 200 m at sunrise to 1800 m at 1630 local time.

2.5.2 The Nocturnal Bounday Layer

Fishman and Carney (1984) use the model from Smeda (1979) to determine the height of the nocturnal boundary layer. Based on similarity theory, it assumes growth of the PBL is due to mechanical turbulence from interaction of wind with the surface. The prognostic equation for the growth of the PBL is:

$$\frac{\partial h}{\partial t} = C_1\frac{(u^*)^2}{hf}\left[1 - \left(\frac{C_2 hf}{u^*}\right)\alpha\right] \tag{5}$$

where C_1, C_2 and α are empirical constants,

u^* is the friction velocity, and

f is the Coriolis parameter.

Values of C_1, C_2 and α are taken to be 0.60, 3.3, and 3. respectively after Smeda (1979).

As the nocturnal PBL is formed, the remnants of the convective PBL are decoupled from the effects of the surface. The time required for the turbulence above the nocturnal

PBL to dissipate was estimated to be four hours by Benkley and Schulman (1979). This time interval is incorportated into the model by Fishman and Carney (1984). The resultant nocturnal PBL height profile decreases rapidly from 1800 m at 1630 local (L) to 200 m at midnight where it remains though the remainder of the nighttime hours.

2.5.3 Vertical Diffusion

The O'Brien (1970) K formula is used to to determine the K_z profile as a function of the heights provided by the PBL models. This gives a cubic profile for K_z in the PBL. Additionally, residual turbulence is allowed to dissipate after sunset as a function of the PBL height. The formulation is allowed to produce a maximum value for K_z of approximately 10^2 m^2 sec^{-1} while preserving an average tropospheric value of 10 m^2 sec^{-1}.

2.6 Numerical Techniques

Two techniques are employed to intergrate the continuity equation. For long lived species, the advection terms are integrated by the conservation of second order moments method after Prather (1986) and the remaining terms are integrated using the Euler-backward method. For short lived species, concentrations are assumed to be in steady state so that no integration is necessary.

2.6.1 Integration of Diffusion and Photochemical Terms

The Euler-backward method was used by Fishman (1977) to explicitly integrate the diffusion and photochemical terms of long lived species forward in time, and is the method used in

this study. This method has been shown by Matsuno (1966) to damp out high frequency oscillations that can develop during integration. This feature is important in this study because sharp gradients at the surface and the top of the boundary layer could otherwise create excessive computational dispersion. The cost of using this scheme is greater numerical diffusion in comparison to schemes such as the leapfrog method. Fishman (1977) shows that the Euler-backward method has accuracy comparable to forward time differencing when intergrating photochemical terms and thus these terms are not adversely impacted by its use. Spatial gradients are determined using second order centered finite differencing.

The Euler-backward scheme is a predictor-corrector scheme. The scheme is illustrated below by integrating the diffusion term. Ignoring all terms but vertical diffusion, the continuity equation is:

$$\frac{\partial[X_i]}{\partial t} = \frac{\partial}{\partial z}\left(K_z[M]\frac{\partial \mu_i}{\partial z}\right) \tag{6}$$

The predictor step creates a "first guess" of the concentration $[X_i]^*$ at the forward time step $n+1$.

$$[X_i]^{*(n+1)} = [X_i]^n + \frac{\partial}{\partial z}\left(K_z[M]\frac{\partial \mu_i}{\partial z}\right)\Delta t \tag{7}$$

From the first guess of the concentration $[X_i]^*$, a first guess of the species mixing ratio μ_i^* is found and is used in the next step. The next (corrector) step creates the final value for the concentration at the forward time step.

$$[X_i]^{n+1} = C_n + \frac{\partial}{\partial z}\left(K_z[M]\frac{\partial \mu_i^*}{\partial z}\right)\Delta t \tag{8}$$

2.6.2 Integration of the Advection Terms

Numerical integration of the advection equation presents a number of problems to the modeler. Conventional integration techniques create undesired computational dispersion, negative values, and numerical diffusion. The treatment of photochemical production and destruction in the model used in this study requires short time steps, amplifying the need for a scheme with minimal numerical diffusion. Large spatial gradients of chemical species near the surface and at the top of the PBL necessitate a scheme with little computational diffusion. Additionally, the scheme must conserve the species and be positive-definite because negative chemical concentrations cannot be dealt with and are physically unrealistic.

Two advection schemes were considered for use in this model. The first scheme examined was that of Smolarkiewicz (1983). This approach to the advection problem starts with the zero order "upstream" scheme and applies a correction to the upstream result. The correction step employs an "antidiffusion velocity" u_d which is the negative of velocity describing flux due to implicit diffusion and is described for the x direction by the following equation:

$$u_d = -\frac{K_{impl}}{[X_i]} \frac{\partial [X_i]}{\partial x} \tag{9}$$

where K_{impl} is the coefficient describing implicit diffusivity.

The second scheme, and the one that was ultimately chosen, is the conservation of second order moments scheme developed in Prather (1986). In this scheme the mixing ratio of a chemical species in each grid box is expressed as a second order polynomial.

$$\mu(x,z) = m_0K_0 + m_xK_x + m_{xx}K_{xx} + m_zK_z + m_{zz}K_{zz} + m_{xz}K_{xz} \qquad (10)$$

where $K_0 = 1$,

K_x and K_z are first order functions of x and z respectively,

K_{xx} and K_{zz} are second order functions of x and z respectively,

K_{xz} is a first order function of x and z,

m_0 is the zero order moment coefficient,

m_x and m_z are the first order x and z coefficients respectively,

m_{xx} and m_{zz} are the second order x and z coefficients respectively, and

m_{xz} is the cross term coefficient.

The functions K_j (for $j = x, xx, z, zz, xz$) are chosen to be orthogonal with each other. The moments S_j are then defined as the product of the mixing ratio and the orthogonal functions integrated over the volume of the grid box. Each moment S_j is further decomposed into two moments representing the portion remaining in the grid box and the portion leaving the grid box. The updated moments are recomposed from the moments representing the portion leaving the upstream grid box and the moments representing what remains in the grid box. The sum of these updated moments represents the updated mixing ratio of the center of the box.

The second order moments method is stable up to where the product of the wind speed and the time step equals the dimension of the grid box. It has been to shown produce errors of more than an order of magnitude smaller than the Smolarkiewicz scheme (Prather 1986). For a complete explanation of the method see Prather (1986).

Chapter 3

Experimental Design

3.1 Background

During a regional high ozone outbreak, cities in the region may exceed the EPA standard for ozone. In certain instances, local governments are then required to implement costly local pollution abatement measures. This approach assumes that high ozone levels are primarily due to local pollution sources. Furthermore, the success of these efforts depends on whether local pollution emissions are a strong forcing mechanism in tropospheric ozone production.

To test the validity of this assumption, an experiment is set up, using the two-dimensional model, to determine the role of local emissions of NO_x, NMHC, and CO in the production of ozone. In this experiment two cases are examined. The first case simulates increased surface emissions over an area in the center of the model domain that is 150 km wide. The second case simulates urban emissions identical to the first case, and also simulates the advection of polluted air into the model domain in a layer between 1.325 km and 3.5 km.

The second case determines if advection of ozone and its precusors from outside the region could be a strong forcing mechanism in the development of high concentrations along with local production of pollutants.

Model integration is carried out to five days. This length of time is representative of the residence time of the stagnant high pressure systems that this study is investigating (Vukovich and Fishman, 1986). At day 5, the model is very near steady state, hence model results are shown from day 5 only. Any additional integration has little change on the result.

3.2 Model Parameters

In Case I, surface emissions of NO_x, NMHC, and CO are increased to twenty times the background emission levels listed in table 1 at the gridpoints 400, 450, and 500 km from the model's western boundary. This level of emissions is approximately half of the values for urban emissions used by Richardson (1988) in a study of ozone production over Atlanta, Georgia. These lower emissions are compensated for by the broad area (150 km) over which they are emitted in the two-dimensional model.

In Case II, surface emissions of NO_x, NMHC, and CO are the same as Case I. Additionally, the flux of ozone and precursor rich air into the model is simulated by setting initial ozone concentrations at the upstream boundary to 50 ppbv in the layer between 1.325 km and 3.5 km. Photochemical production and vertical diffusion is allowed to change the concentration of ozone in the air advected into the model.

Flux of pollutants in the layer is simulated by requiring the average flux of pollutants

into the model due to horizontal advection to be 20 percent of the surface emission of pollutants occuring in the urban area of the model. This yields concentrations for NO_x up to 1.1 ppbv. The range of values measured by Buhr *et al.*, (1990) for NO_x at a surface site in central Pennsylvania is 1.5 to 6 ppbv. The concentration of pollutants in the air advected in from upstream is then reasonable, assuming a boundary layer origin.

3.3 Model Sensitivity

The model output indicates a high sensitivity to ozone deposition velocity. Fishman (1985) lists ozone deposition rates found in the literature. They range from 0.24 cm s^{-1} to 2.0 cm s^{-1} for mid-latitude forest land. Sillman *et al.* (1990) uses an ozone depositon velocity of 2.5 cm s^{-1} in a regional model over various parts of the contiguous United States. Model sensitivity is illustrated in figure 5 and figure 6. These figures show ozone concentrations at 1500L for day five of two model runs where ozone deposition velocities are set to 0.5 cm s^{-1} and 3.0 cm s^{-1}, respectively. The maximum concentration of ozone at the surface is reduced by more than 60 ppbv by raising the deposition velocity from 0.5 cm s^{-1} to 3.0 cm s^{-1}. The actual ozone maximum in figure 6 is elevated well above the surface. This illustrates the effect of the more intense ozone sink that a high deposition velocity creates. The dramatic change illustrates the need for a good understanding of surface deposition processes. Since this study concentrates on the role of horizontal advection rather than the role of surface sinks of ozone, a detailed test of model sensitivity to ozone deposition velocity is not carried out here. The values for ozone deposition velocity used in this study

are 1.5 cm s^{-1} during daytime hours and 0.5 cm s^{-1} during nighttime hours. These values are a compromise between the values found in the literature and are felt to be realistic parameterizations of ozone deposition in the Southeast.

Ozone concentration and concentrations of pollutants are also very sensitive to wind strength. Concentrations of ozone precursors in the lower PBL over the area of elevated emissions are inversely proportional to wind speed and therefore the contribution of urban emissions to urban ozone levels diminishes as surface wind speed increases and the wind is allowed to carry pollutants away.

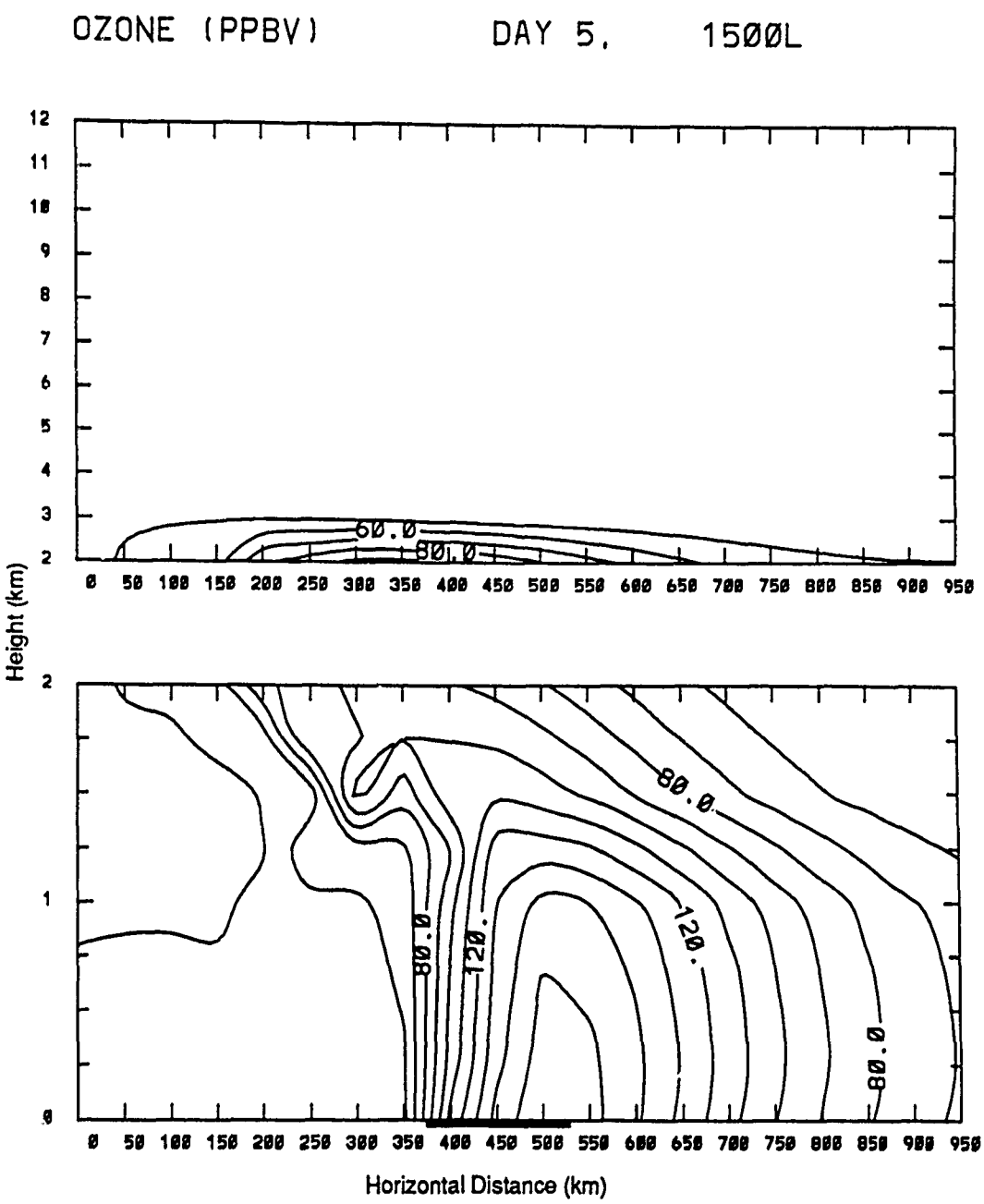

Figure 5: Ozone distribution of 1500L, day five of model run. Ozone deposition velocity is equal to 0.5 cm s^{-1}. The top of the figure shows the troposphere from 2-12 km, while the bottom figure expands the ordinate to show detail in the PBL. The abscissa indicates the horizontal extent of the computational domain. The bold line on the abscissa marks the urban emissons region.

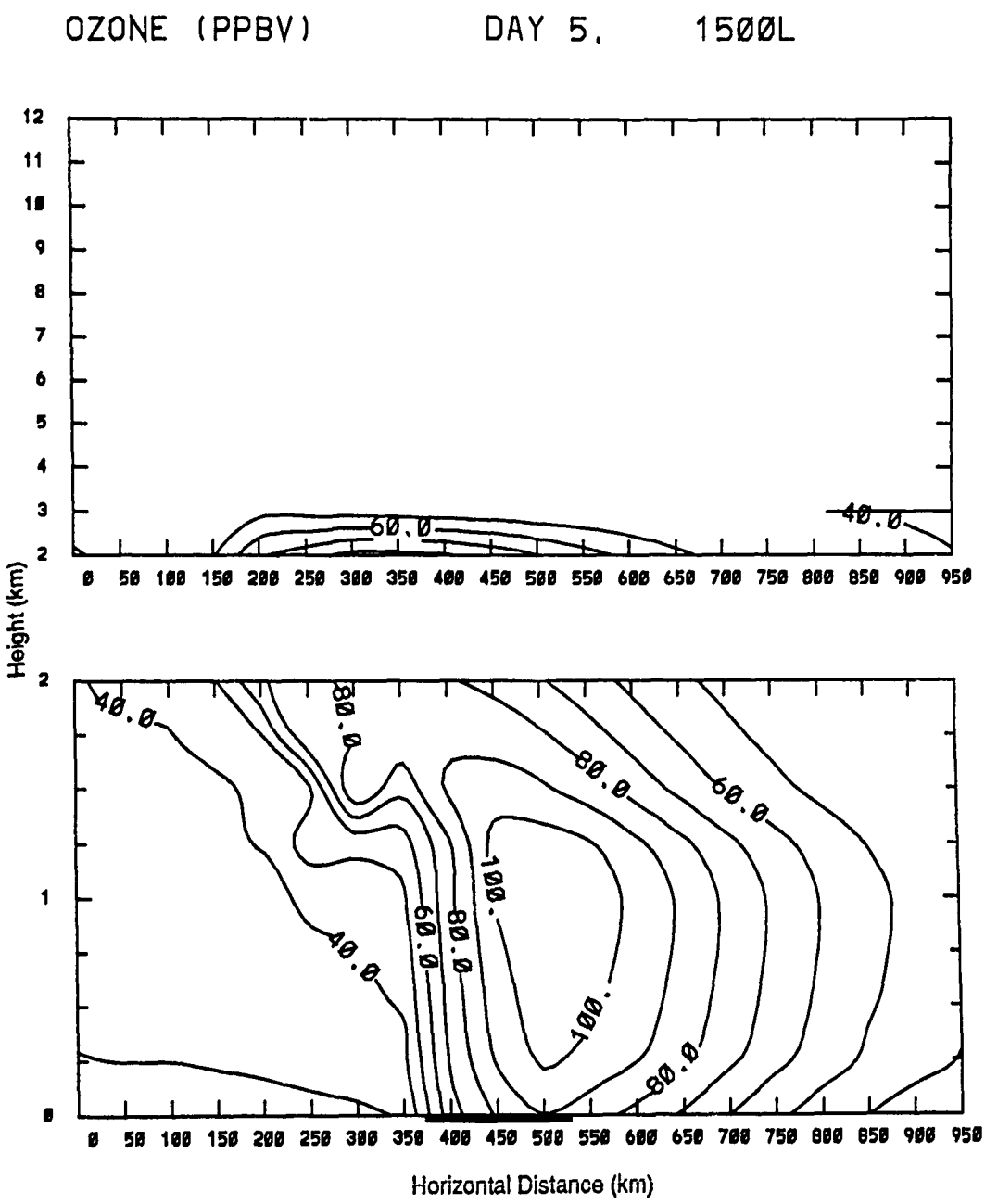

Figure 6: Same as figure 5 except ozone deposition velocity equal to 3.0 cm s^{-1}.

Chapter 4

Results

4.1 Results of Case I

Plots of ozone, NO_x, CO, and butane from 1500L, on day five of Case I are depicted on figure 7 through figure 10 respectively. Butane is included to show the distribution of a NMHC. By day five, ozone concentrations are approaching steady state with changes in ozone between day four and day five at 1500L less than five percent. However, ozone concentration shows the large diurnal change expected with the elimination of photochemical production at night. A more complete series of plots, showing concentrations at time invervals of six hours on day five, are located in Appendix C. Figures 27 through 30 show the reduction in ozone near the surface due to the absence of photochemical production at night. Figures 31 through 34 show a reservoir of NO_x accumulating at night due to the absence of photochemical oxidation processes. Likewise, CO and butane concentrations are greater near the surface during nighttime hours as illustrated by figures 35 through 38 and figures 39 through 42.

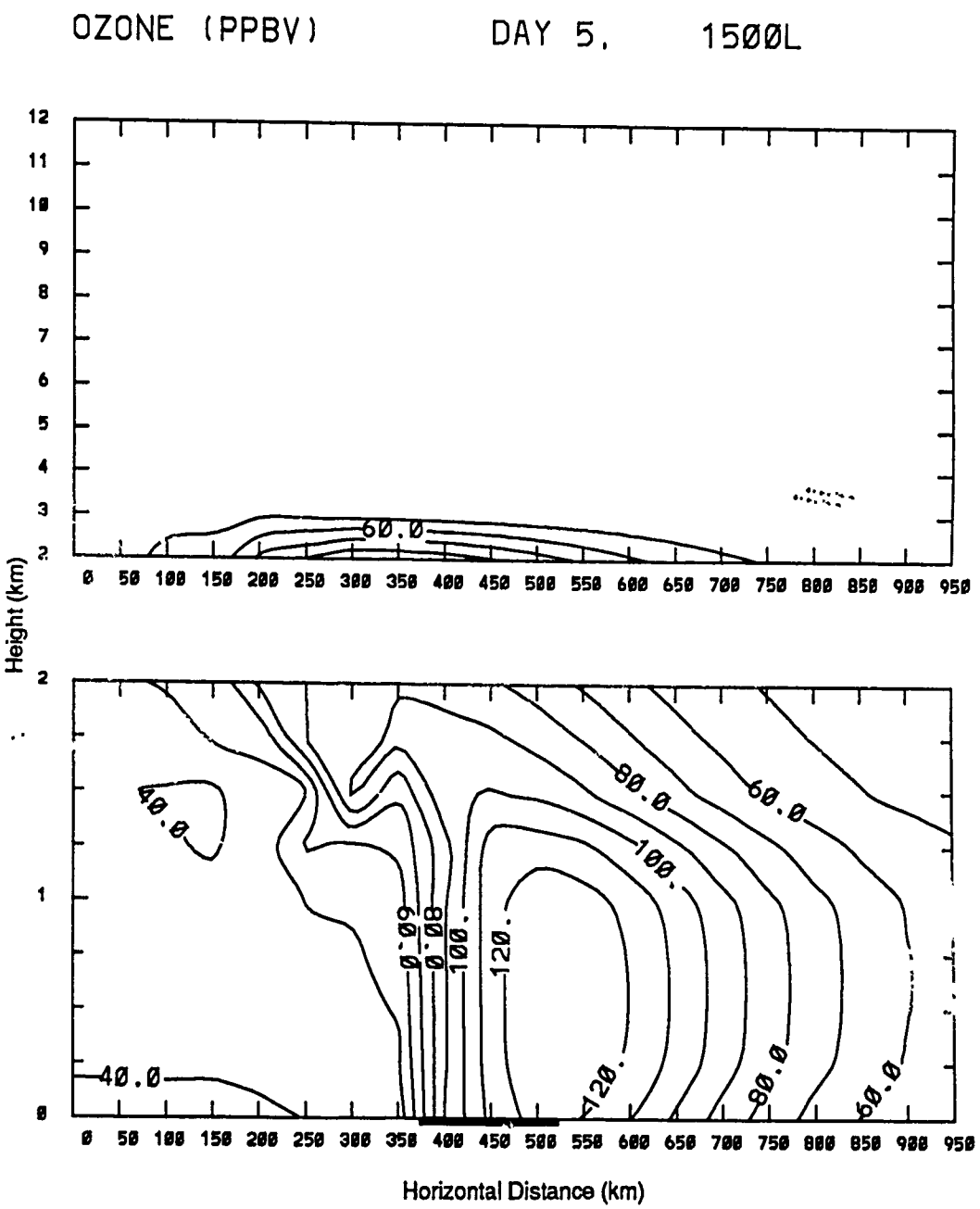

Figure 7: Forecast distribution for ozone at 1500L, day five of Case I. Contour increments are 10 ppbv. The top of the figure shows the troposphere from 2-12 km, while the bottom figure expands the ordinate to show detail in the PBL. The abscissa indicates the horizontal extent of the computational domain.

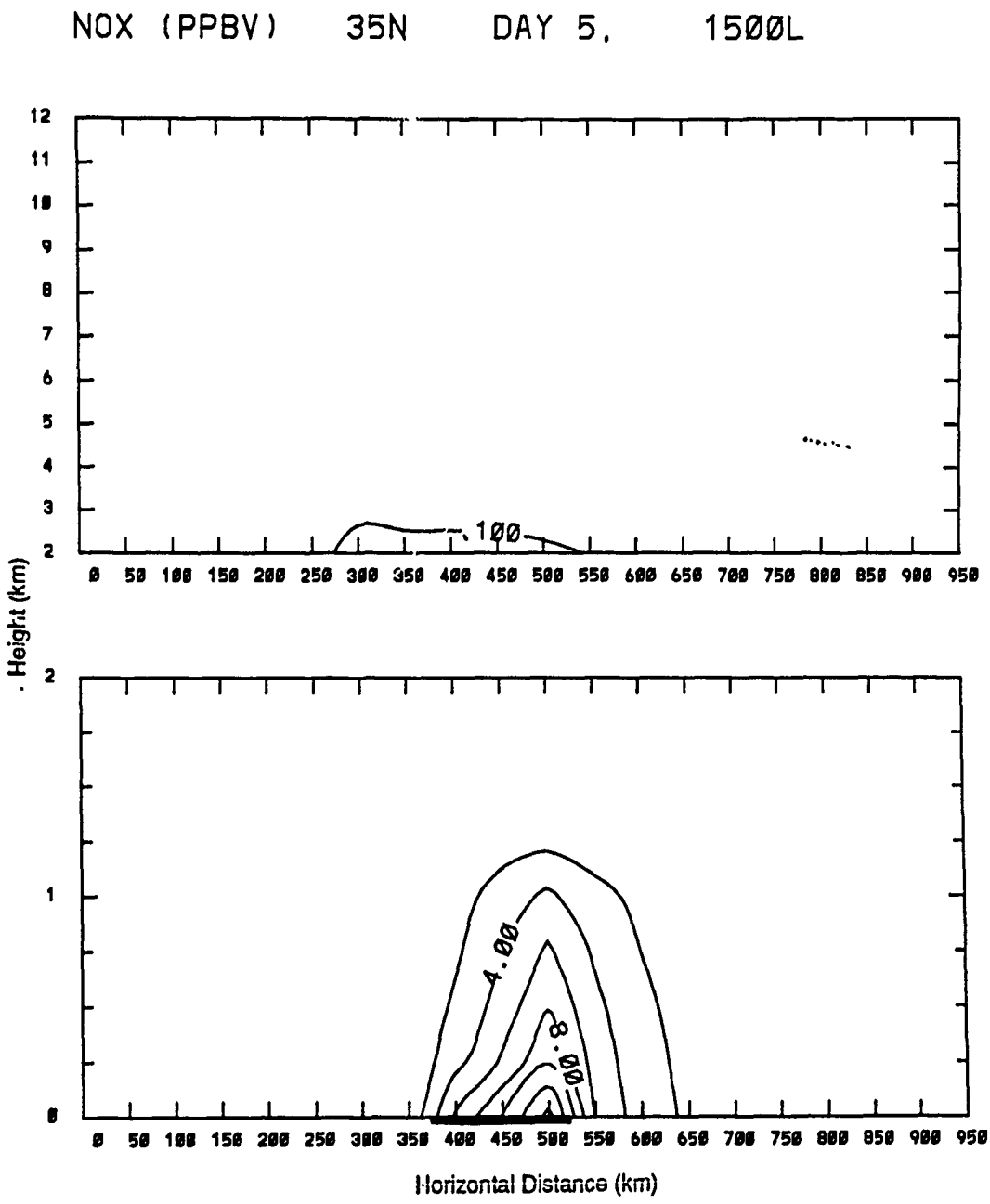

Figure 8: As in figure 7 for NO_x. Contour increments are 0.1 ppbv for the top figure and 2 ppbv for the bottom figure.

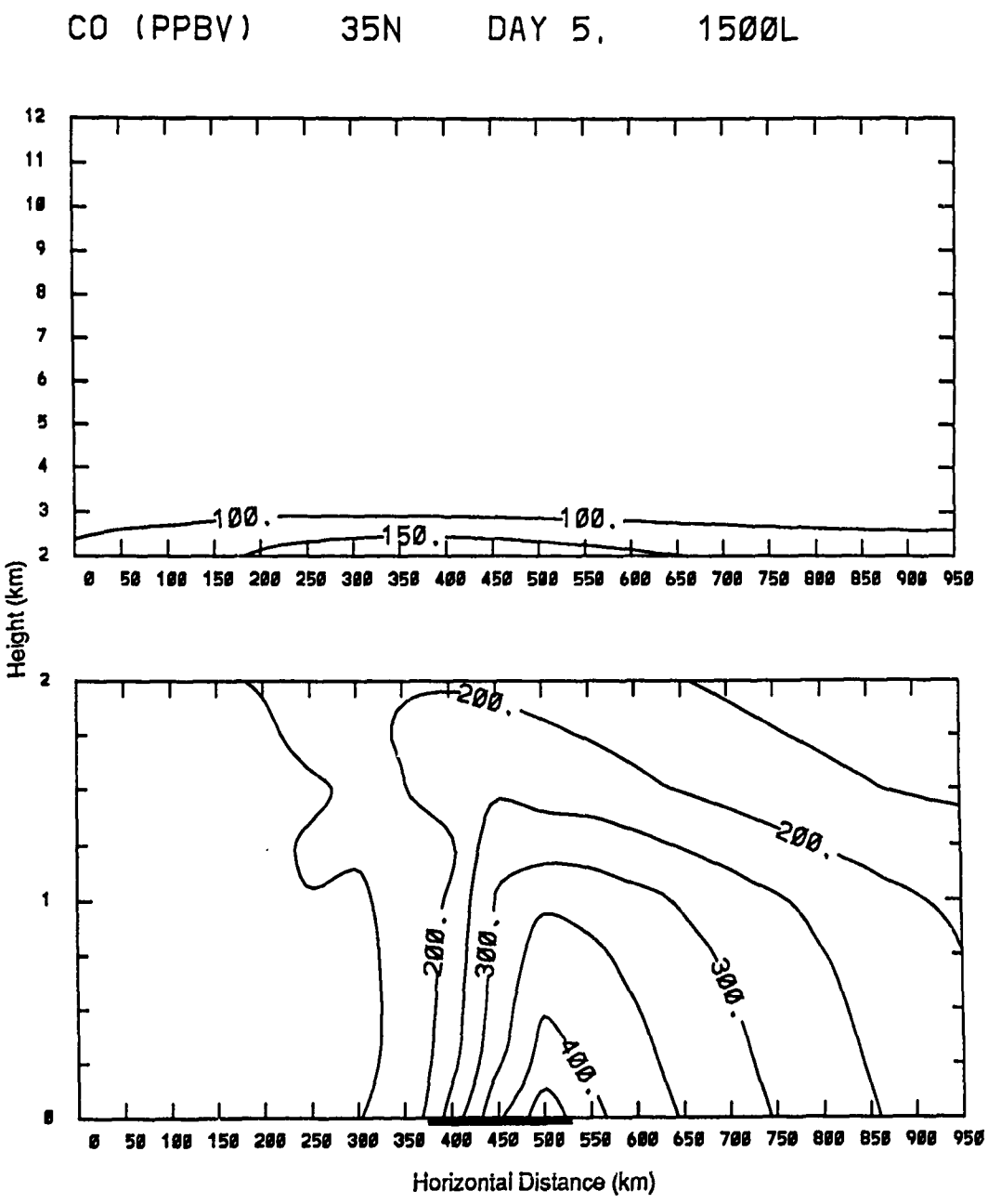

Figure 9: As in figure 7 for CO. Contour increments are 50 ppbv.

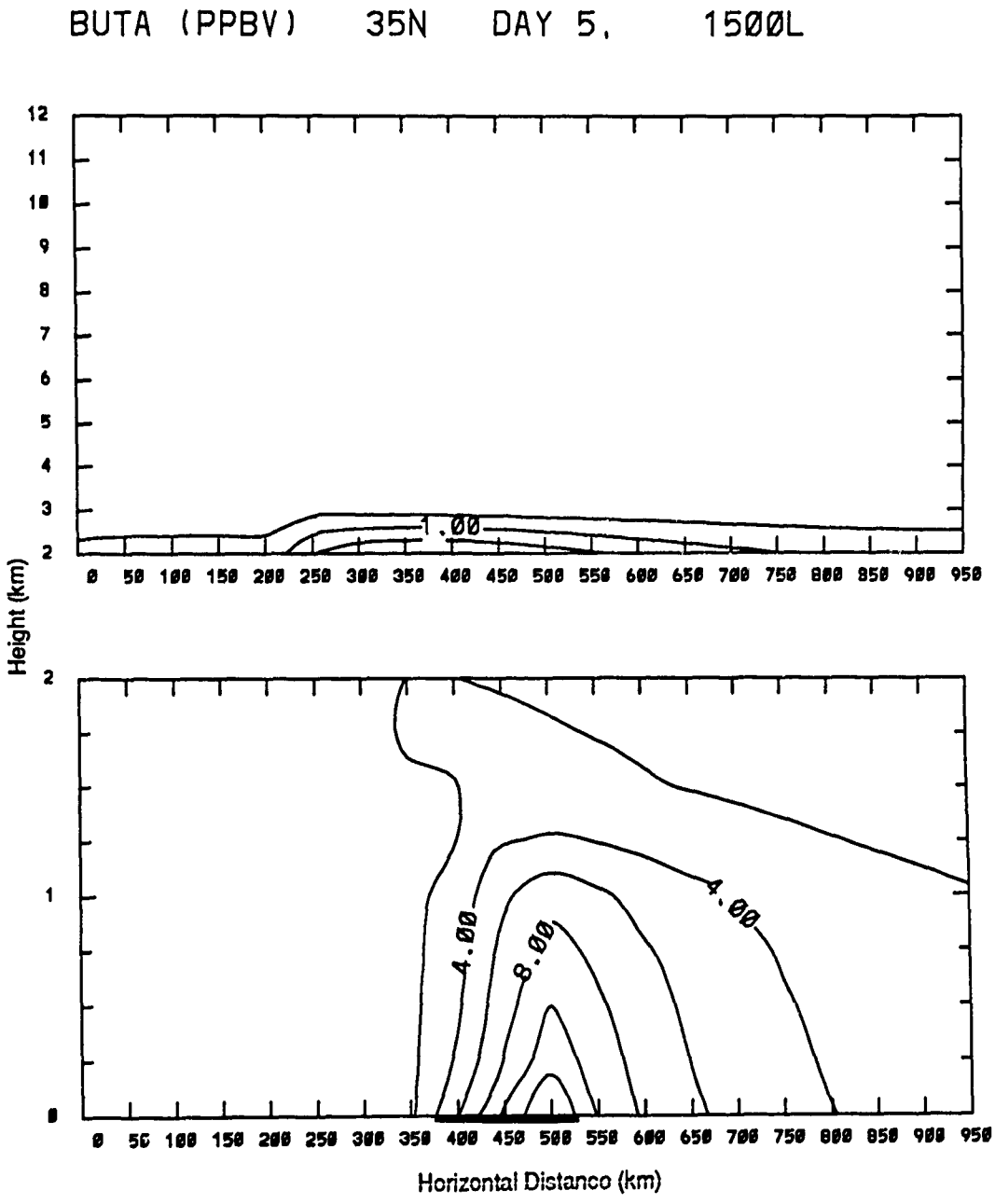

Figure 10: As in figure 7 for butane. Contour increments are 1 ppbv for the top figure and 2 ppbv for the bottom figure.

The effect of surface emissions on model output is negligible above 4 km due to less vertical diffusion in the free troposphere than in the PBL. CO has a longer chemical lifetime than the other species plotted (on the order of one week) and therefore would have the highest likelihood of being transported above 4 km by vertical diffusion. CO varies by less than 20 ppbv between 4 km and 12 km.

In contrast to the limited vertical extent of increased ozone levels, increased ozone levels are seen 500 km downwind of the area of high pollutants emissions. Ozone concentrations of 80 ppbv or more extend 250 km downwind. As a caveat to these results, one must remember that meridional homogeneity is assumed in the model. To more properly model an urban plume, it would be necessary to include horizontal diffusion effects. This would allow quicker dillution of the urban plume.

The remnants of an ozone maximum produced near the surface by the photochemical production of ozone during daylight hours of day four remain visible on figure 7 at a height of 1.5 km, 200 to 350 km from the origin. Two ozone maxima, created one and two days earlier by photochemical production, are visible on figure 28.

The forecast maximum agrees reasonably well with the surface ozone concentrations observed at Marietta and 40 km southwest at Atlanta, Georgia on 26 July. The concentration recorded at 1500L on that day is 149 ppbv at Marietta, and 85 ppbv at Atlanta (McNider, 1989), while the model produced a maximum surface concentration of 123 ppbv after five days of model integration. These values reflect the high concentrations associated with urban regions under air stagnation conditions. The model result is 17 percent lower than the observed value at Marietta and 45 percent higher than the observed value at Atlanta.

It is important to remember that the model was not intended to simulate this specific case, but these observations can serve to gauge the validity of the model parameters used for this study, such as the wind profile, and deposition velocities. The approximate agreement of the model results to surface observations suggests that the values used for these parameters are appropriate for this study.

4.2 Results of Case II

Figure 11 through figure 14 depicts the distribution of ozone, NO_x, CO, and butane at 1500L, on day five of Case II. The introduction of ozone and its precursors through the layer between 1.325 km and 3.5 km at the upstream boundary creates a layer of high ozone values that decreases from approximately 110 ppbv at the upstream boundary to approximately 85 ppbv at the downstream boundary. A modest increase in the concentration of ozone at the PBL maximum centered 525 km from the origin is achieved by the reduced upward flux of ozone and its precursors out of that region, brought on by the reduced gradient between the PBL and the free troposphere. The region at the surface with ozone concentrations exceeding the EPA standard of 120 ppbv expands from 70 km wide in Case I to 90 km wide in Case II. This is a 28 percent increase in the size of that region.

The rapid decrease of NO_x between 1.325 km and 3.5 km near the upstream boundary is visible on figure 12 and illustrates the short chemical lifetime of NO_x. An air parcel in the layer described above traverses the horizontal domain of the model with only small changes in concentrations of ozone, CO, and butane (see figures 11, 13 and 14) due to the longer

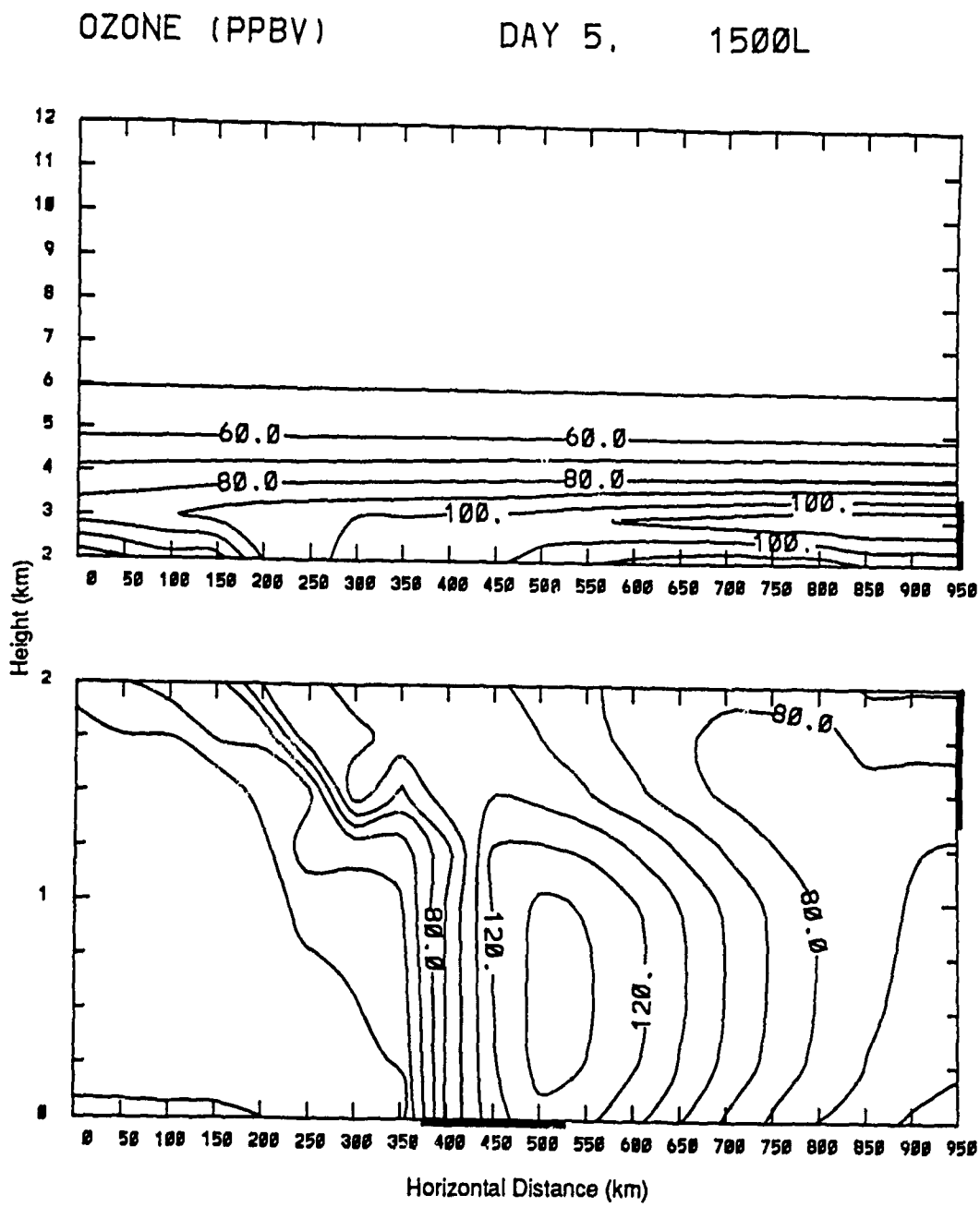

Figure 11: Forecast distribution of ozone at 1500L, day five of Case II. Contour increments are 10 ppbv. The top of the figure shows the troposphere from 2-12 km, while the bottom figure expands the ordinate to show detail in the PBL. The abscissa indicates the horizontal extent of the computational domain. The bold line at the upstream boundary marks the region of elevated emissions of ozone and precursors.

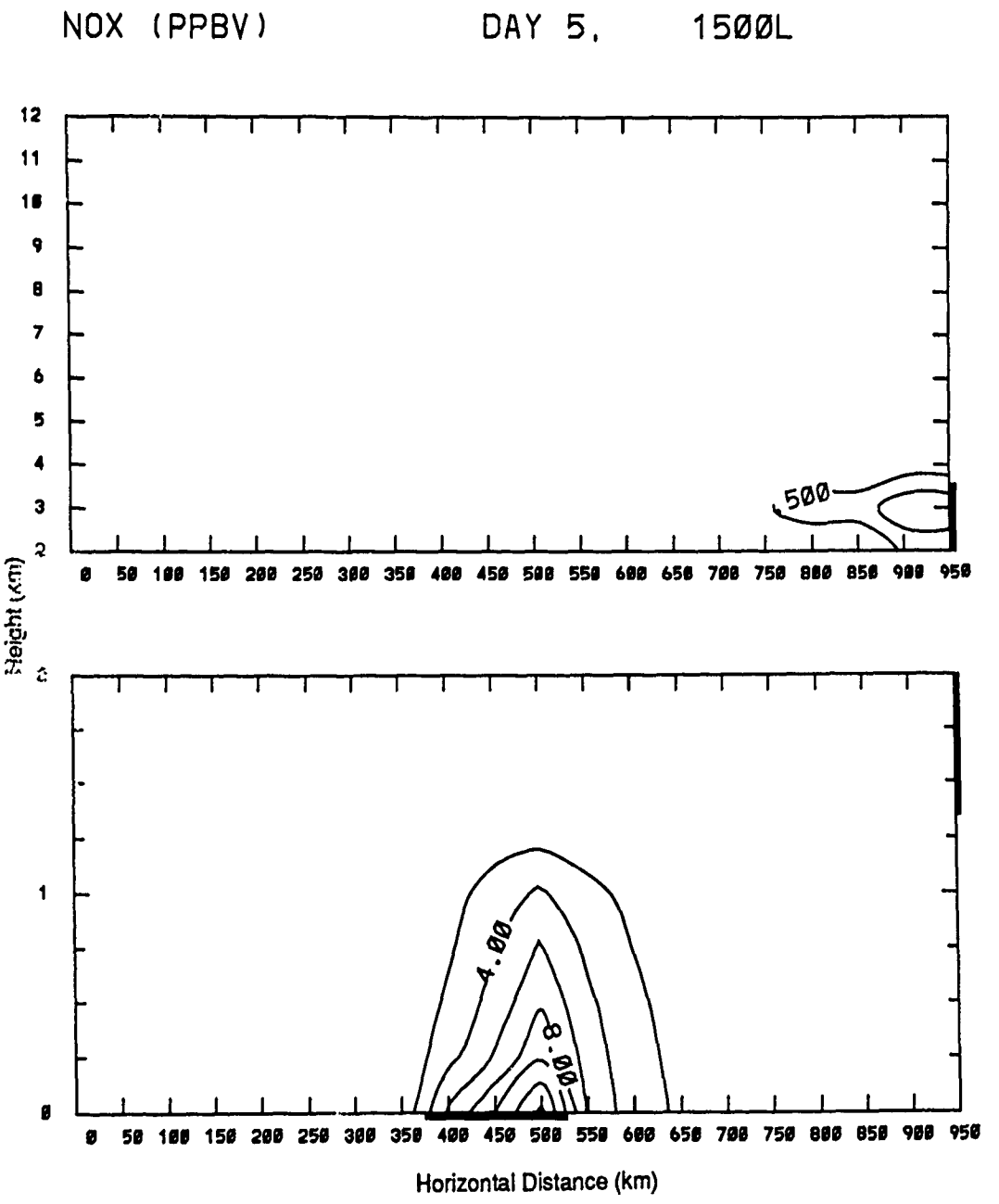

Figure 12: As in figure 11 for NO_x. Contour increments are 0.5 ppbv for the top figure and 2 ppbv for the bottom figure.

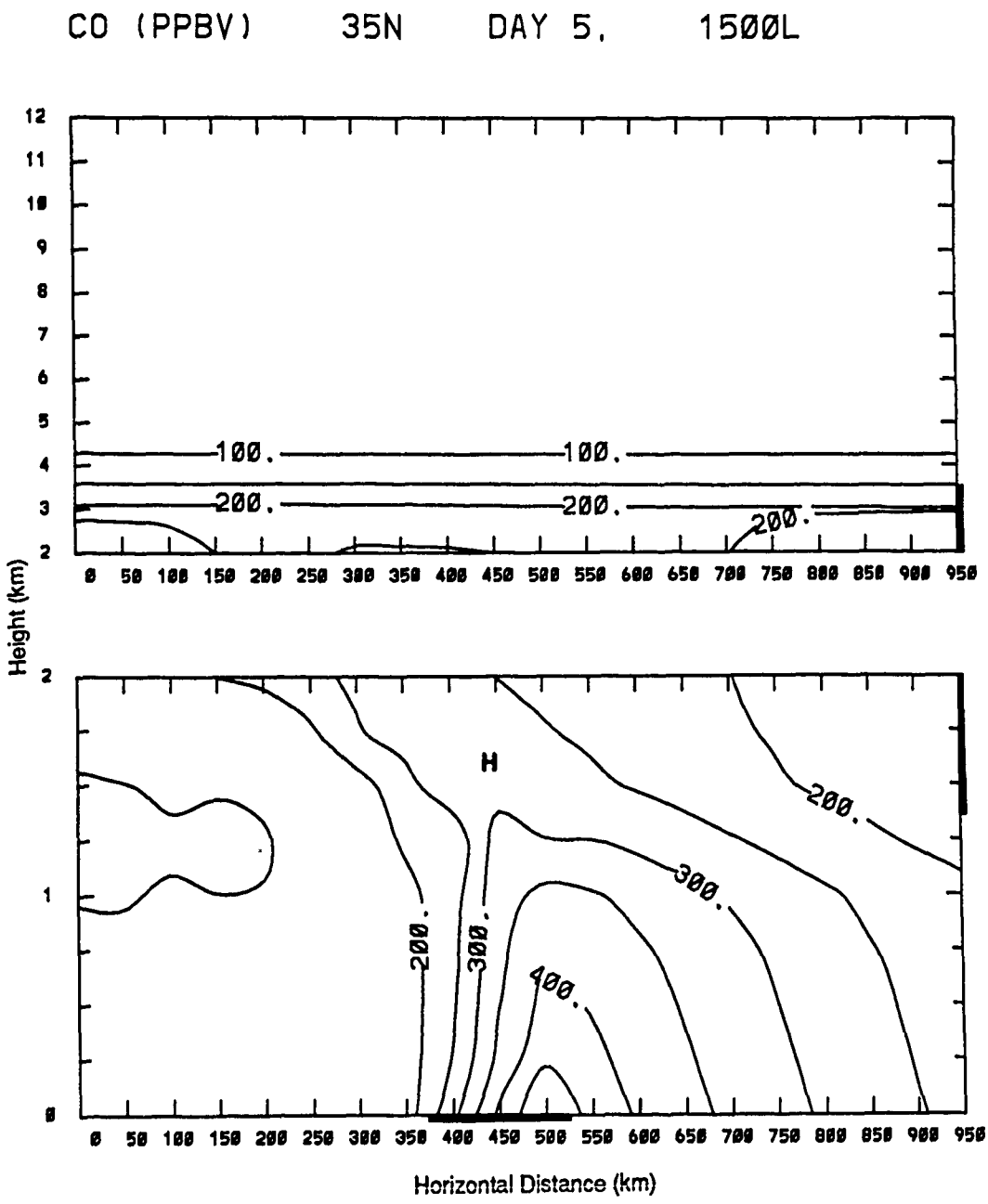

Figure 13: As in figure 11 for CO. Contour increments are 50 ppbv.

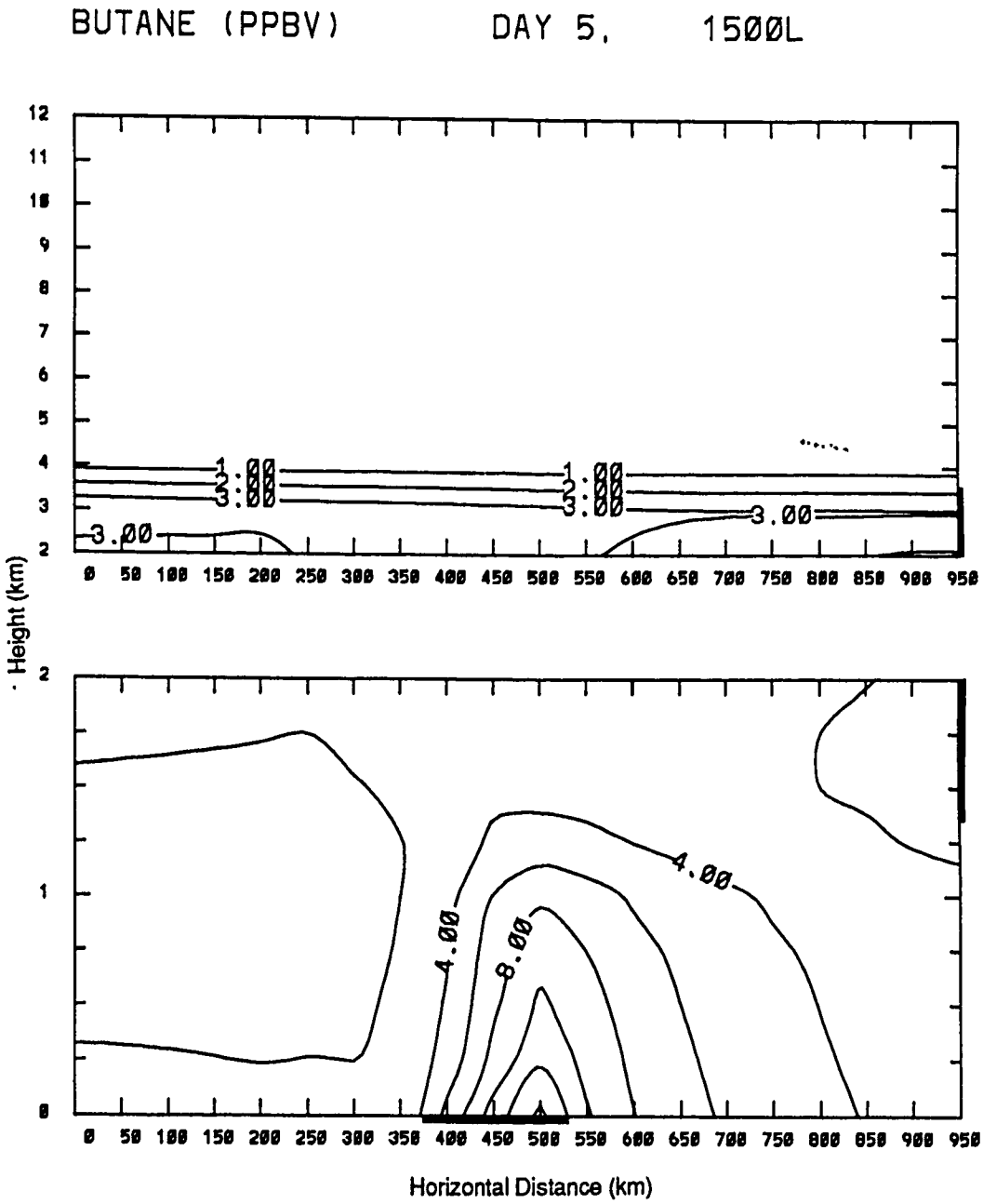

Figure 14: As in figure 11 for butane. Contour increments are 1 ppbv for the top figure and 2 ppbv for the bottom figure.

chemical lifetime of these species. Of the families of reactions involving the three ozone precursors NO_x, CO, and NMHC at concentrations found in the boundary layer, the NO_x family is more important in controling ozone photochemistry (Fishman *et al.*, 1985), but in this case, the rapid destruction of NO_x prevents a large addition to ozone production in the urban plume due to interaction with the elevated polluted layer.

Figure 15 depicts the difference in the ozone profiles of Case I and Case II at 1500L on day five of the model runs. It shows that the high concentration of ozone advected in from the upstream boundary was most effective in raising ozone concentrations where ozone levels were already high due to enhanced surface emissions of precursors in the center of the model domain. The relative maximum at 300 - 350 km downstream from the origin, at a height of 1.5 km shows that the high ozone and precursor concentrations advected into the model between 1.325 km and 3.5 km, were able to interact with the ozone maximum that was produced at the surface a day earlier. A similar but less robust maximum is seen at 500 km downstream, at a height of 0.75 km. This maximum is located at the same place as the ozone maximum seen on figure 7. These maxima on figure 15 are most likely due to a reduction in ozone and precursor gradients between the PBL and the free troposphere that occured when ozone and precursors were increased aloft. In turn, the reduction of the vertical gradient of ozone between the free troposphere and the top of the PBL reduced the net flux of ozone out of the PBL.

Figure 16 shows virtually no change in NO_x concentrations between Case I and Case II at 1500L on day five of the model runs due its shorter chemical lifetime. Figure 17 and figure 18 show features of CO distribution and butane distribution similar to ozone distribution

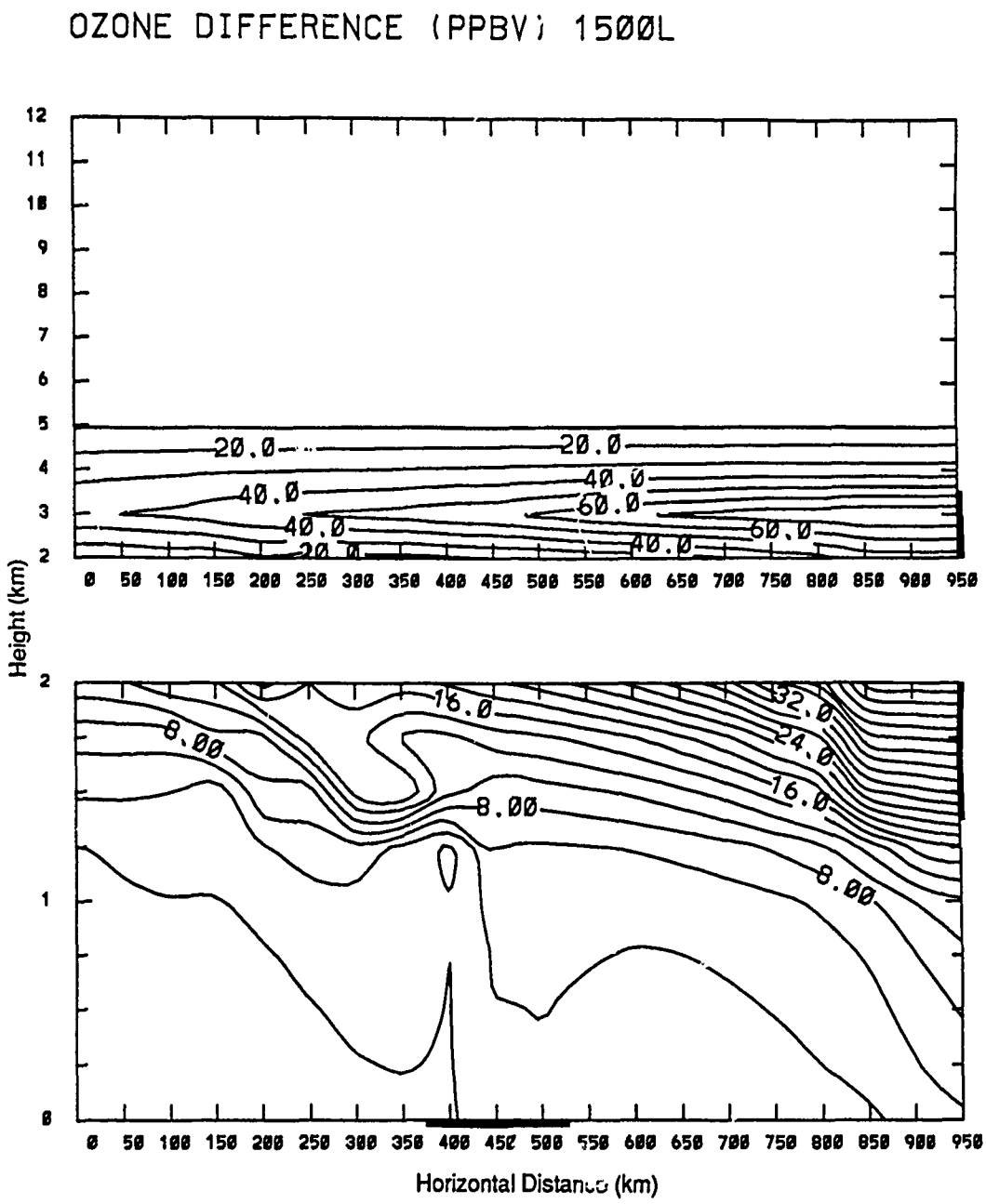

Figure 15: Forecast ozone distribution for Case II at 1500L, day 5, minus forecast distribution for Case I at the same time. Contour increments are 10 ppbv on the top figure and 2 ppbv on the bottom figure. The abscissa indicates the horizontal extent of the computational domain.

features on figure 15. Additionally, CO and butane increases are observed throughout the PBL and at the surface, downwind of the area of increased emissions. This increase is due to vertical eddy diffusion, which acts on ozone as well. In the case of CO and butane, the lack of a large sink at the surface allows the increase to remain near the surface. These long-lived species may then be advected over the area of increased surface emissions and help contribute to the increase in ozone over that region.

The area labeled M on figure 17 is an area where little difference exists for CO between Case I and Case II. This minimum may be partially caused by a small numerical error. Figure 13 shows a maximum in concentration of CO (labeled H) just upstream of area M. The gradient between these two points much greater in Case II than in Case I. The advective scheme used in this study may create a numerical error downstream of a large gradient (Prather, 1986). The dispersion error is smaller in Case I because the gradient between H and M is smaller. There is little evidence of this effect on figures showing distribution of other species because CO has a longer chemical lifetime. The numerical simulation of photochemical processes (and the simulation of vertical diffusion as well) in the model used for this study acts to diffuse sharp gradients and dampen high frequency waves such as those produced by the numerical advection scheme. This occurs because the photochemical term and vertical diffusion term act on the zero order moment (which equates to the average value of a grid box) and do not affect the higher order moments. Because the change in CO concentration due to photochemistry is small compared to other species, the damping effect is less. If the minimum at M is due to a numerical error, it does not present a serious problem in interpreting model results, but significantly reduces the value of the

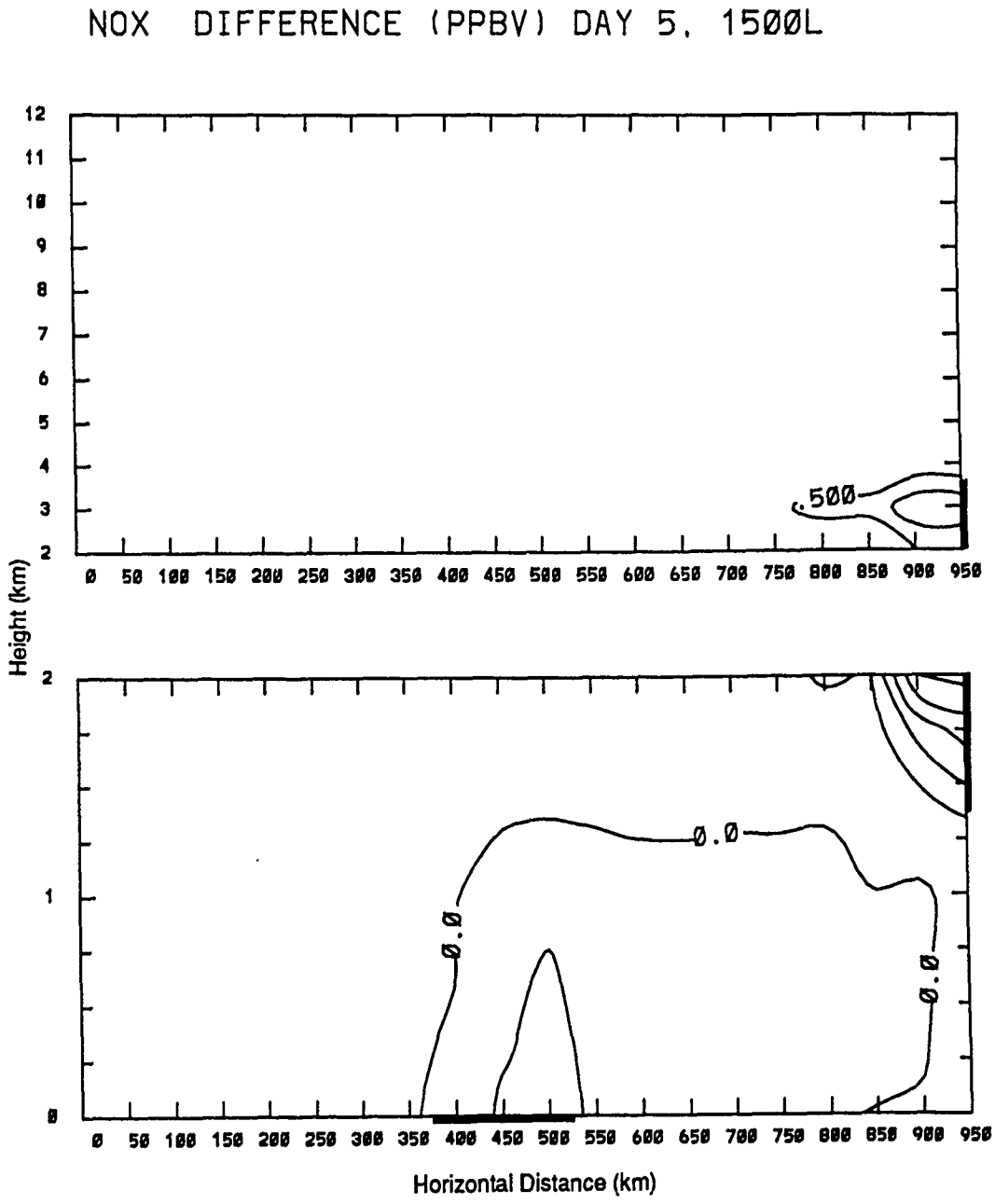

Figure 16: As in figure 15 for NO_x. Contour increments are 0.1 ppbv for the top figure and 2 ppbv for the bottom figure.

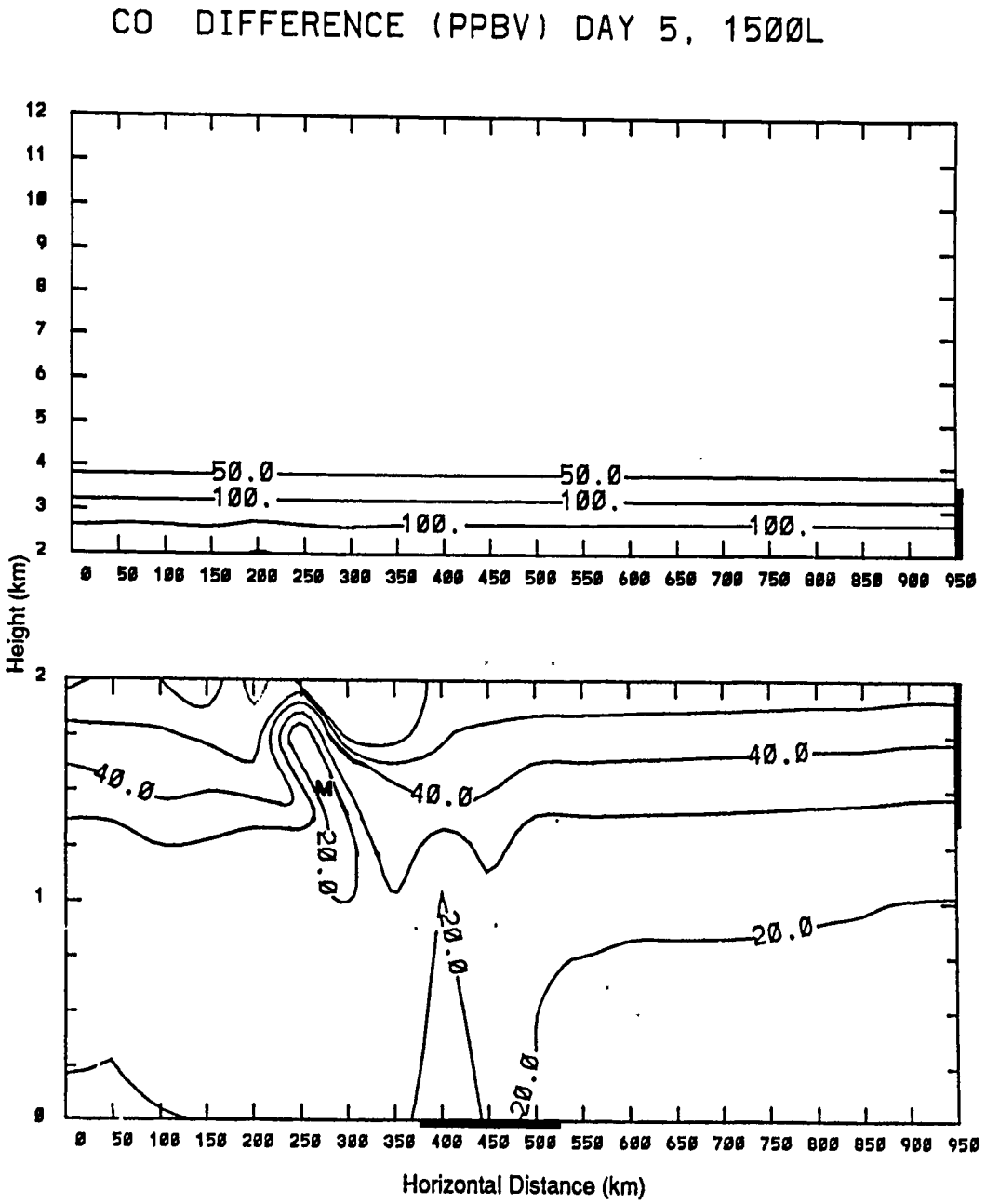

Figure 17: As in figure 15 for CO. Coutour increments are 50 ppbv for the top figure and 10 ppbv for the bottom figure.

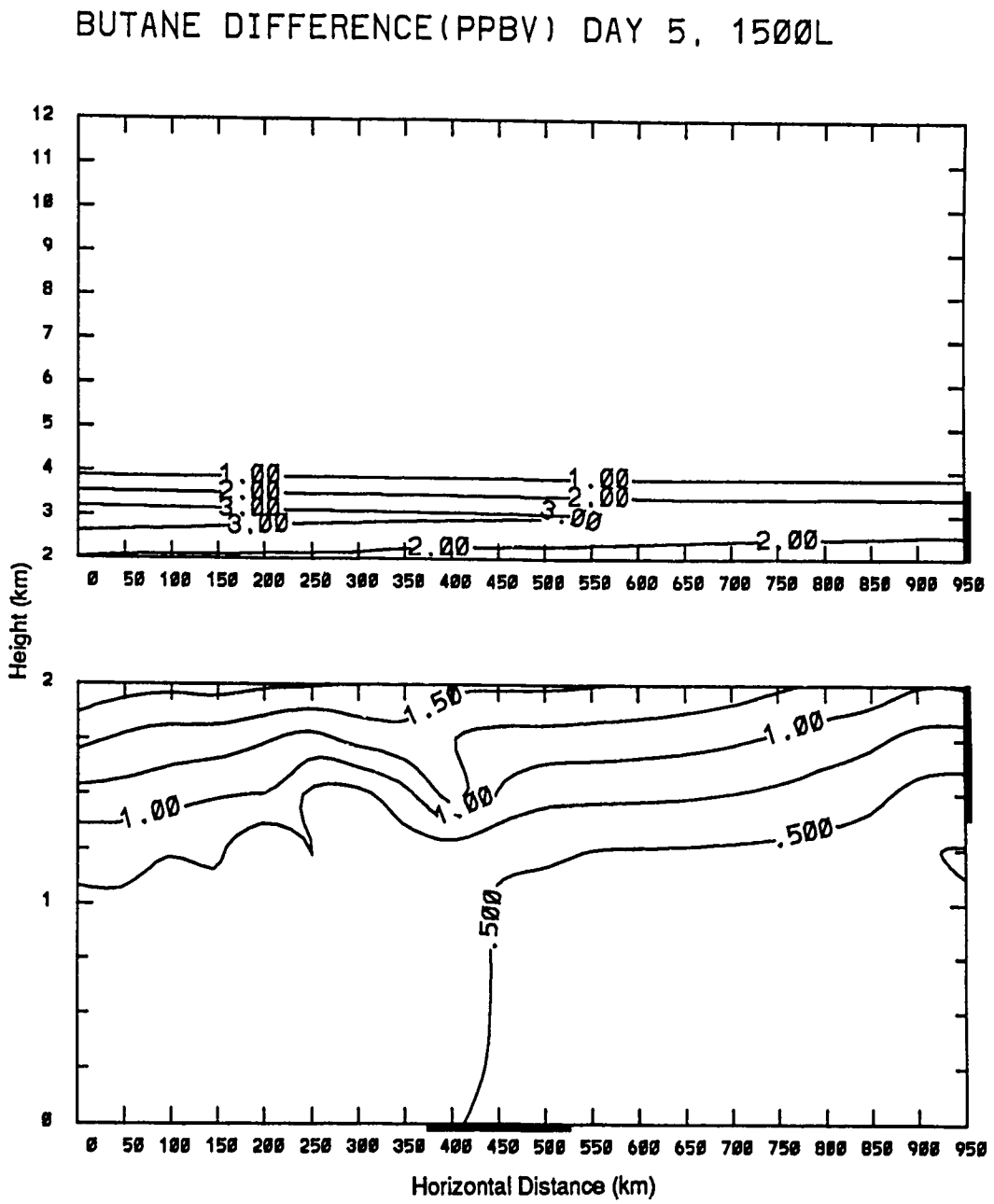

Figure 18: As in figure 15 for butane. Contour increments are 1 ppbv for the top figure and .5 ppbv for the bottom figure.

graphs showing the differences in tracer distributions between Case I and Case II. Some photochemical models incorporate more explicit numerical damping techniques to reduce the impact of these small-scale features. Had such a procedure been implemented for the model simulations, the area of concern would have produced a much smoother maximum difference.

It is interesting to note that the maximum of the ozone differences at 300 km on the horizontal axis and at a height of 1.5 km (shown in figure 15) is located downstream of the maxima of CO and butane (shown on figures 17 and 18 respectively). This suggests that enhanced photochemical production of ozone due to the increase of precursors is primarily responsible for the above mentioned net increase of ozone rather than diffusive vertical flux of ozone itself.

To investigate this possibility further, differences during a nighttime hour are examined. Figure 19 depicts the difference in the ozone profiles of Case I and Case II at 0000L on day five of the model runs. The small vertical gradient between 0.5 km and 1.8 km indicates that the residual turbulence from the daytime convective boundary layer has mixed the ozone introduced from above quite uniformly. The larger gradients above and below this layer show the effect of the sharply reduced diffusion.

The differences in CO and butane at 0000L on day five, shown in figures 20 and 21, show the same effect but to a lesser degree than ozone. Additionally, maxima are visible below 1.8 km, which are remnants of the maxima from the daytime hours (which are illustrated in figures 17 and 18 for day 5.) The fact that there is no such maximum for ozone in figure 19 illustrates the diurnal nature of the ozone maximum at point M on

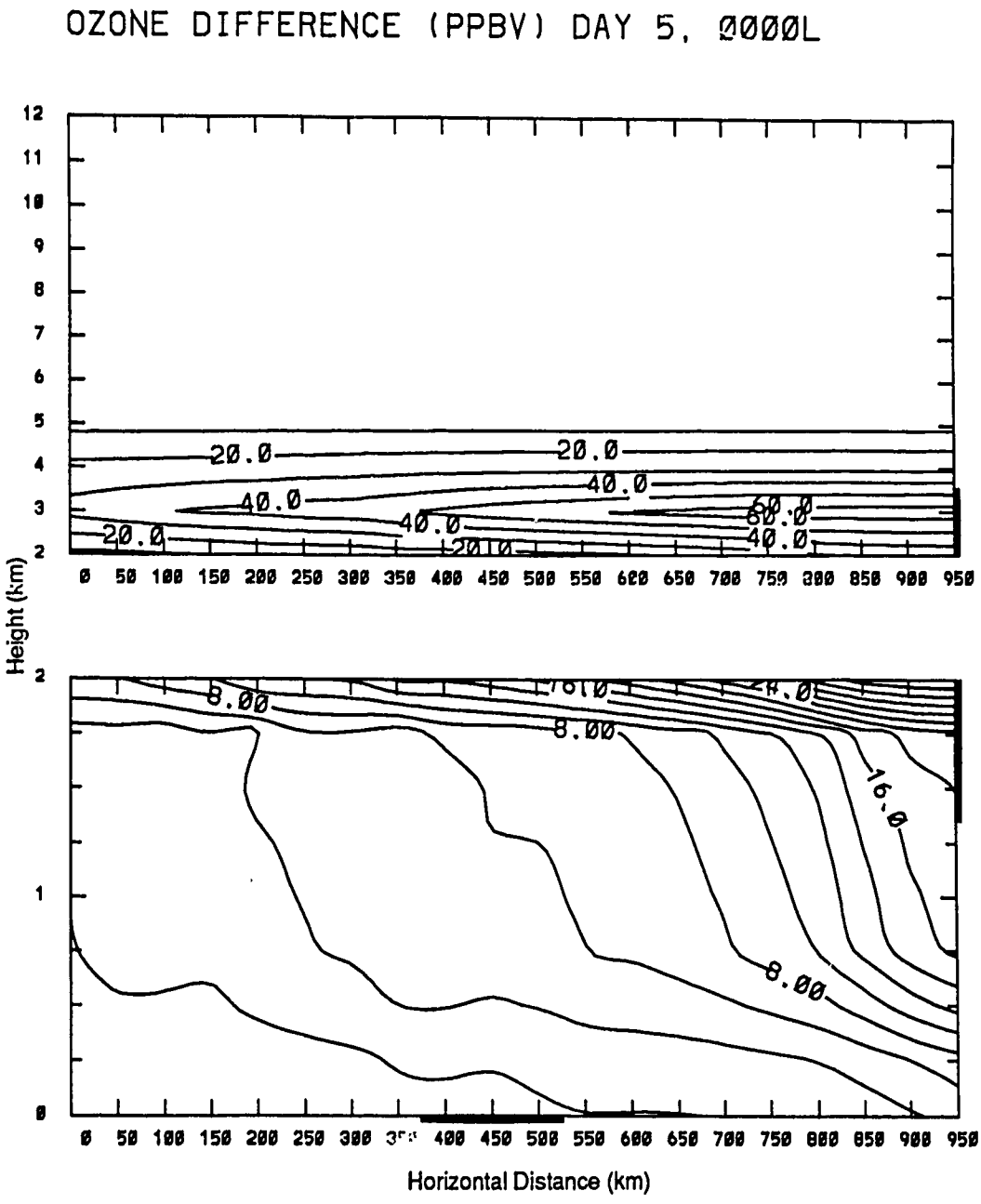

Figure 19: Forecast ozone distribution for Case II at 0000L, day 5, minus forecast distribution for Case I at the same time. Contour increments are 10 ppbv on the top figure and 2 ppbv on the bottom figure.

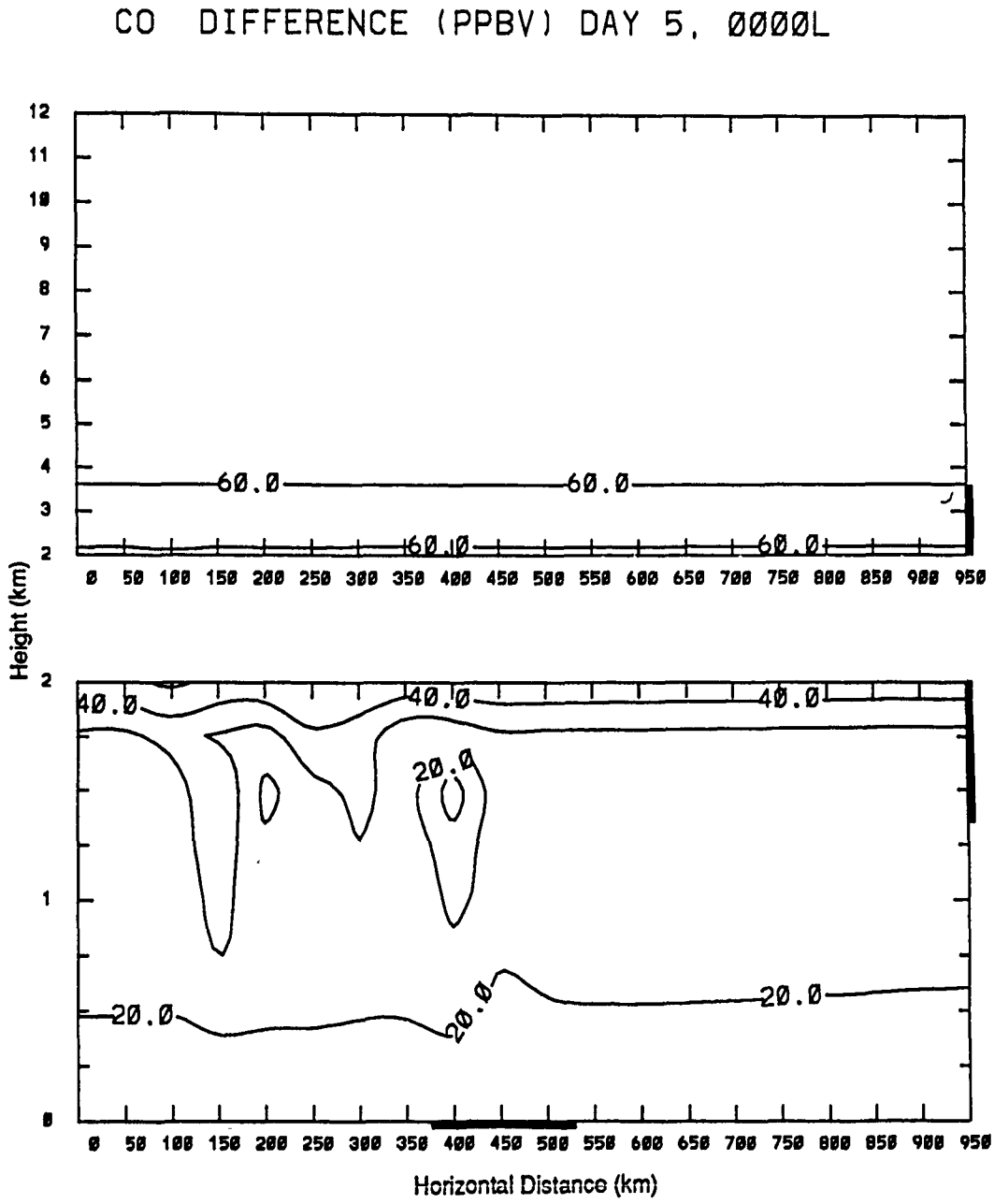

Figure 20: As in figure 19 for CO. Coutour increments are 50 ppbv for the top figure and 10 ppbv for the bottom figure.

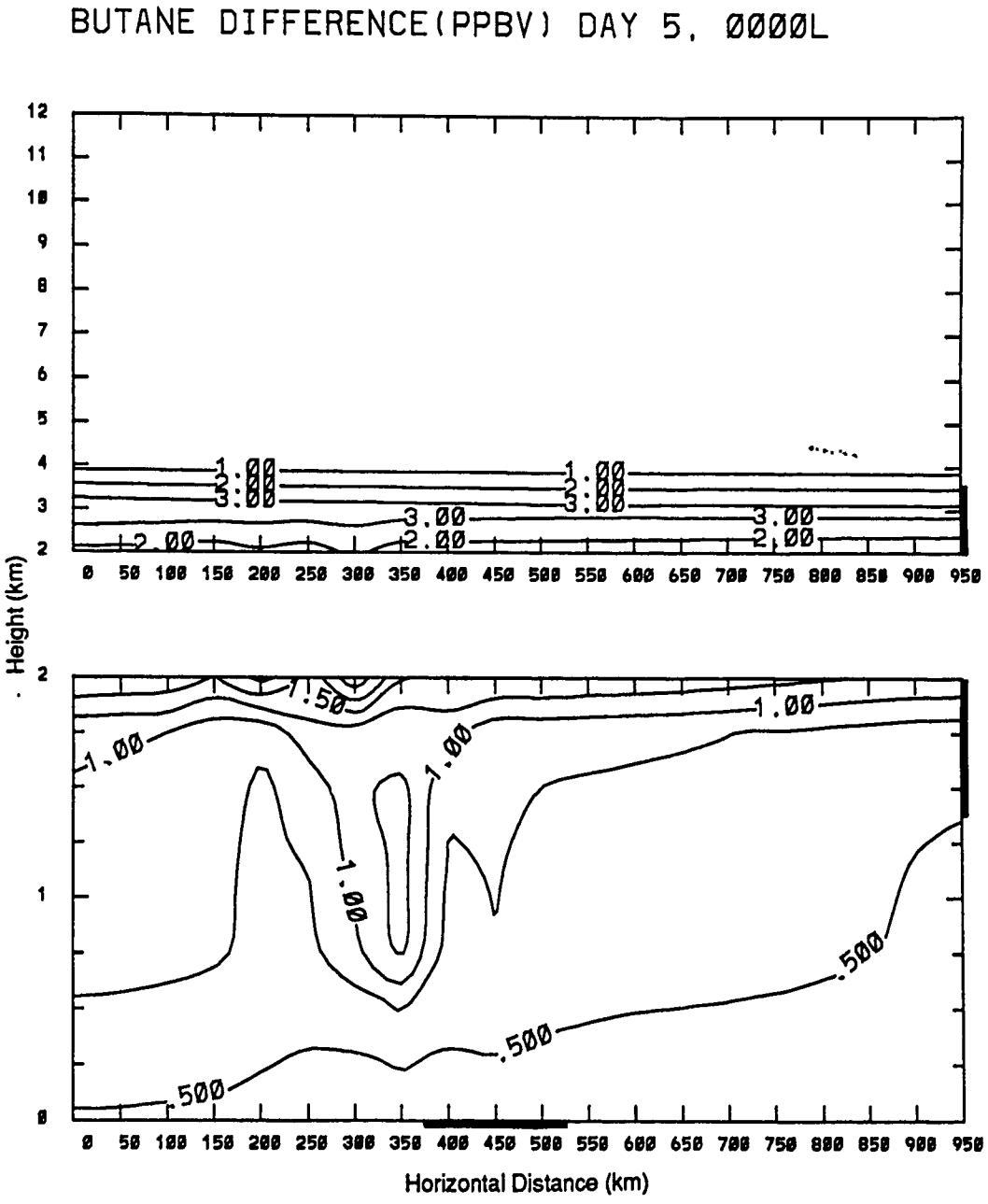

Figure 21: As in figure 19 for butane. Contour increments are 1 ppbv for the top figure and .25 ppbv for the bottom figure.

figure 15 and is further evidence that the enhanced increases in ozone at point M are due to the increased photochemical production brought on by the increased concentration of precursors upstream. This maximum represents 50 percent of the increase at point M, thus enhanced photochemical production apparently doubled the increase in ozone at M. If this maximum is indeed due entirely to photochemical production, advection of precursors in the manner simulated in this study can play as significant a role in the enhancement of ozone concentrations in the upper PBL over an urban area as does the advection of ozone in the manner simulated in this study.

The analysis presented here is primarily qualitative in nature and cannot lead to any definitive conclusion, but suggests that advection of precursors can play a significant role in enhancing ozone concentrations in the PBL, given the parameters used in the model for Case II. Further experimentation using the two- dimensional model presented here could help get a better estimate of the importance of the possible advection of precursors to ozone production. To take the problem a step further and achieve a quantative understanding, detailed measurements designed to yield horizontal and vertical structure of ozone and its precursors must be done to determine the relative importance of the roles that photochemistry and transport have on their two- and three- dimensional distributions.

Chapter 5

Summary

An experiment using a time-dependent, two-dimensional photochemical model of the troposphere to model the vertical and zonal distribution of ozone and its precursors has been presented. In Case I, the experiment simulates vertical transport due to diffusion and zonal transport due to advection, with surface emissions in the center of the model domain representing an urban environment and with light wind conditions favorable for the formation of ozone concentrations greater than 80 ppbv. To investigate the role of the advection of ozone and its precursors into a region under such conditions, an elevated source of these trace species is added at the upstream boundary (Case II) to simulate their advection into the model domain from a distant source.

The model incorporates parameterizations of the daytime convective boundary layer and the nocturnal boundary layer to simulate the flux of trace species between the PBL and the free troposphere due to vertical diffusion. Horizontal advection is simulated using a highly idealized wind profile derived from the meteorological conditions present during an

elevated ozone event over the southeastern United States in July 1987.

In Case I, the simulation of an urban emission source produces surface concentrations of ozone 120 ppbv up to 50 km downstream of the area of high surface emissions and surface concentrations 80 ppbv or greater as far as 225 km downstream. The vertical extent of the plume is less than 4 km.

The introduction of an elevated source of ozone and its precursors in Case II produces a modest increase of ozone (3 – 10 percent) in the region where high ozone values already exist due to high surface emissions. This increase partly due to enhanced photochemical production of ozone brought on by increased levels of the longer-lived precursors such as CO and NMHC, rather than NO_x, whose increase is very small due to its depletion prior to reaching the center of the model domain. The increase in ozone values is also due to reduced vertical flux of ozone out of the PBL brought on by a reduced ozone gradient between the PBL and the free troposphere. The surface region with ozone concentrations exceeding the EPA standard of 120 ppbv grows by 28 percent from 70 km wide in Case I to 90 km wide in Case II. An analysis of the change in concentrations of ozone, CO and butane between Case I and Case II shows that a maximum in the ozone increase at a point in the upper PBL in Case II is downstream of the maximum in increases of CO and butane. This suggests that enhanced photochemical production is responsible for this maximum in the PBL rather than downward flux due to vertical diffusion. The lack of this maximum at night supports this further by showing that the maximum has a diurnal cycle. The diurnal cycle is indicative of photochemical forcing. This maximum represents 50 percent of the increase of ozone in the region where it is located, and thus, enhanced photochemical production has apparently

doubled the increase in ozone in that region.

These results suggest that horizontal transport of ozone precursors may influence regional tropospheric ozone production, if transport of these precursors does indeed exist on the scale simulated in the model. Current observations are insufficient to determine if long range horizontal transport of ozone precursors does occur. The lack of observations of regional high ozone occurences other than relatively sparse surface observations and satellite derived columnar values restricts the ability to compare model simulations with observations. Future field studies may provide the needed data to answer these questions.

The model used in this study lacks the simulation of meteorological phenomena such as large and small scale vertical motions, terrain effects and a time dependent wind field. Each of these could be significant forcing mechanisms on ozone distribution, and future studies must address them. Future work will also require a three-dimensional model in order to fully understand the role of transport on the distribution of ozone and its precursors.

Despite its drawbacks and limitations, the two-dimensional model used in this study has utility in further investigations of the role of transport on ozone distribution. This study can be continued by devising new experiments to investigate the role of transport of ozone and its precursors in a quantitative manner. The State of Florida is interested in investigating the effect of sea-breeze circulations on ozone distribution (Florida Department of Environmental Regulation, 1990). This is an investigation for which the present model with an idealized time-dependent wind field appears well suited.

Appendices

A Reaction Rates

Table 3: Chemical reactions and rate constants following Richardson *et al.*, 1990

	Reaction	Reaction Rate (sec^{-1})	Reference
(1)	$O(^3P)+O_2(+M) \rightarrow O_3(+M)$	$6.2E-34*(T/300)^{-2}$	a
(2)	$O(^1D)(+M) \rightarrow O(^3P)(+M)$	$.79*1.8E-11\ \exp(107/T)$ $+.21*3.2E-11\ \exp(67/T)$	a
(3)	$O(^1D)+H_2O \rightarrow 2OH$	2.2E−10	a
(4)	$O(^1D)+H_2(+O_2) \rightarrow HO_2+OH$	9.9E−11	a
(5)	$O(^1D)+CH_4(+O_2) \rightarrow CH_3O_2+OH$	1.4E−10	a
(6)	$O(^1D)+CH_4(+O_2) \rightarrow H_2+CH_2O(+O_2)$	1.4E−11	a
(7)	$O_3+h\nu \rightarrow O(^1D)+O_2$	2.9E-5 *	f
(8)	$O_3+h\nu \rightarrow O(^3P)+O_2$	3.6E-4 *	f
(9)	$OH+O_3 \rightarrow HO_2+O_2$	$1.6E-12\ \exp(-940/T)$	a
(10)	$OH+H_2(+O_2) \rightarrow HO_2+H_2O$	$1.2E-11\ \exp(-2200/T)$	a
(11)	$OH+H_2O_2 \rightarrow HO_2+H_2O$	$3.1E-12\ \exp(-187/T)$	a
(12)	$OH+HO_2 \rightarrow H_2O+O_2$	$7+4[A][A_0]^{-1}(1.0E-11)$ †	a
(13)	$HO_2+HO_2 \rightarrow H_2O+O_2$	Temp. and Press. Dependent	a
(14)	$H_2O+h\nu \rightarrow 2OH$	4.0E−5 *	f
(15)	$HO_2+O_3 \rightarrow OH+2O_2$	$1.4E-14\ \exp(-580/T)$	a
(16)	$H_2O_2 \rightarrow$ Heterogeneous Loss	4.0E−05 ‡	f
(17)	$NO+HO_2 \rightarrow NO_2+OH$	$3.7E-12\ \exp(240/T)$	a
(18)	$NO+O_3 \rightarrow NO_2+O_2$	$2.2E-12\ \exp(-1430/T)$	a
(19)	$NO+NO_3 \rightarrow 2NO_2$	$8.0E-12\ \exp(250/T)$	a
(20)	$NO_2+OH(+M) \rightarrow HNO_3$	Temp. and Press. Dependent	a
(21)	$HNO_3+OH \rightarrow NO_3+H_2O$	$9.4E-15\ \exp(778/T)$	a
(22)	$HNO_3+h\nu \rightarrow OH+NO_2$	4.3E−7 *	f
(23)	$HNO_3 \rightarrow$ Heterogeneous Loss	4.0E−05 ‡	f
(24)	$NO_2+HO_2(+M) \rightarrow HNO_4(+M)$	Temp. and Press. Dependent	b
(25)	$HNO_4+OH \rightarrow NO_2+H_2O+O_2$	$1.3E-12\ \exp(380/T)$	a
(26)	$HNO_4 \rightarrow HO_2+NO_2$	Temp. and Press. Dependent	b
(27)	$HNO_4+h\nu \rightarrow HO_2+NO_2$	5.4E−6 *	f
(28)	$NO_2+NO_3(+M) \rightarrow N_2O_5(+M)$	Temp. and Press. Dependent	c
(29)	$N_2O_5+H_2O \rightarrow 2HNO_3$	1.3E−21	b
(30)	$N_2O_5 \rightarrow NO_2+NO_3$	$[\text{Rate}(28)](7.5E26*(300/T))^{.32}$ $*\ \exp(-11080/T)$	d
(31)	$N_2O_5+h\nu \rightarrow NO_2+NO_3$	2.2E−5 *	f
(32)	$NO_2+O_3 \rightarrow NO_3+O_2$	$1.2E-13\ \exp(-2450/T)$	a
(33)	$NO\text{-}2+h\nu \rightarrow O(^3P)+NO$	6.3E−3 *	f

Table 3 continued.

	Reaction	Reaction Rate (sec^{-1})	Reference
(34)	$NO_3+h\nu \rightarrow NO_2+O(^3P)$	2.3E−1 *	f
(35)	$NO_3+h\nu \rightarrow NO+O_2$	2.8E−2 *	f
(36)	$NO_2 \rightarrow$ Heterogeneous Loss	8.0E−7 ‡	f
(37)	$NO_3 \rightarrow$ Heterogeneous Loss	4.0E−7 ‡	f
(38)	$CH_4+OH(+O_2) \rightarrow CH_3O_2+H_2O$	2.4E−12 exp(−1710/T)	a
(39)	$CH_3O_2+NO \rightarrow CH_3O+NO_2$	4.2E−12 exp(180/T)	a
(40)	$CH_3O_2+HO_2 \rightarrow CH_3OOH+O_2$	7.7E−14 exp(1300/T)	a
(41)	$CH_3O_2+CH_3O_2 \rightarrow$ $1.4CH_2O+.8HO_2+.6CH_3OH+O_2$	1.5E−13 exp(220/T)	b
(42)	$CH_3O+O_2 \rightarrow CH_2O+HO_2$	9.2E−13 exp(−2200/T)	a
(43)	$CH_3OOH+OH \rightarrow CH_3O_2+H_2O$	2.6E−12 exp(−190/T)	a
(44)	$CH_3OOH+h\nu \rightarrow CH_3O+OH$	4.9E−6 *	f
(45)	$CH_3OOH \rightarrow$ heterogeneous loss	4.0E−5 †	f
(46)	$CH_3OH+OH \rightarrow HO_2+CH_2O+H_2O$	3.0E−12 exp(−327/T)	b
(47)	$CH_2O+OH(+O_2) \rightarrow CO+HO_2+H_2O$	1.0E−11	b
(48)	$CH_2O+h\nu \rightarrow CO+2HO_2$	2.6E−5 *	f
(49)	$CH_2O+h\nu \rightarrow CO+H_2$	4.8E−5 *	f
(50)	$CH_2O \rightarrow$ heterogeneous loss	4.0E−6 ‡	f
(51)	$CO+OH(+O_2) \rightarrow CO_2+HO_2$	Temp. and Press. Dependent	b
(52)	$C_2H_6+OH(+O_2) \rightarrow C_2H_5O_2+H_2O$	1.7E−11 exp(−1232/T)	b
(53)	$C_2H_5O_2+NO \rightarrow C_2H_5O+NO_2$	4.2E−12 exp(180/T)	b
(54)	$C_2H_5O_2+HO_2 \rightarrow C_2H_5OOH+O_2$	7.7E−14 exp(1300/T)	a
(55)	$C_2H_5O_2+C_2H_5O_2 \rightarrow 1.6CH_3CHO$ $+1.2HO_2+.4C_2H_5OH$	5.0E−14	b
(56)	$C_2H_5O(+O_2) \rightarrow CH_2O+CH_3O_2$	33.0	b
(57)	$C_2H_5O+O_2 \rightarrow ACHO+HO_2$	1.2E−13 exp(−1350/T)	a
(58)	$C_2H_5OOH+OH \rightarrow C_2H_5O_2+H_2O$	2.6E−12 exp(−190/T)	a
(59)	$C_2H_5OOH+h\nu \rightarrow CH_3O+OH$	4.9E−6 *	f
(60)	$C_2H_5OOH \rightarrow$ heterogeneous loss	4.0E−5 ‡	f
(61)	$C_2H_5OH+OH \rightarrow HO_2+CH_3CHO+H_2O$	1.0E−11 exp(−313/T)	b
(62)	$CH_3CHO+OH(+O_2) \rightarrow CH_3CO_3+H_2$	6.9E−12 exp(250/T)	b
(63)	$CH_3CHO+h\nu \rightarrow CH_3CO_3+HO_2$	5.6E−8 *	f
(64)	$CH_3CHO+h\nu \rightarrow CO+HO_2+CH_3O_2$	4.0E−6 *	f
(65)	$CH_3CHO \rightarrow$ heterogeneous loss	4.0E−6 ‡	f
(66)	$CH_3CO_3+NO \rightarrow CH_3O_2+NO_2+CO_2$	4.2E−12 exp(180/T)	b

Table 3 continued.

	Reaction	Reaction Rate (sec^{-1})	Reference
(67)	$CH_3CO_3+NO_2 \rightarrow PAN$	4.7E−12	b
(68)	$PAN \rightarrow CH_3CO_3+NO_2$	1.95E16 exp(−13543/T)	b
(69)	$CH_3CO_3+HO_2 \rightarrow MAP+O_2$	3.0E−1	b
(70)	$MAP+OH \rightarrow .5CH_3CO_3$ $+.5GLYC+.5OH+H_2O$	1.0E−11	b
(71)	$MAP+h\nu \rightarrow OH+HO_2+CH_2O$	5.E−4[Rate(NO $+h\nu$)]	b
(72)	MAP → heterogeneous loss	4.0E−5 ‡	f
(73)	$C_2H_4+OH \rightarrow ETHO2+H_2O$	1.66E−12 exp(474/T)	b
(74)	$ETHO2+NO \rightarrow NO_2+.2GLYC+$ $1.6CH_2O+HO_2$	4.2E−12 exp(180/T)	b
(75)	$ETHO2+HO_2 \rightarrow EP$	3.0E−12	b
(76)	$ETHO2+ETHO2 \rightarrow 1.2GLYC+1.2HO_2$ $+0.4C_2H_5OH+0.4CH_3CH$	5.0E−14	b
(77)	$GLYC+OH \rightarrow .5GCO3+.5GLYX$ $+H_2O+.5HO_2$	1.6E−11	e
(78)	$GLYC+h\nu \rightarrow CH_2O+2HO_2+CO$	2[Rate(CH_3CHO] $+h\nu$ to CH_3O_2)]	b
(79)	GLYC → heterogeneous loss	4.0E−5 ‡	f
(80)	$EP+OH \rightarrow .5ETHO2+.5GLYC$ $+.5OH+H_2O$	1.0E−11	b
(81)	$EP+h\nu \rightarrow OH+HO_2+GLYC$	5.E−4[Rate(NO $+h\nu$)]	b
(82)	EP → heterogeneous loss	4.0E−5 ‡	f
(83)	$GCO3+NO \rightarrow NO_2+HO_2+CH_2O+CO_2$	4.2E−12 exp(180/T)	b
(84)	$GCO3+NO_2 \rightarrow GPAN$	4.7E−12	b
(85)	$GPAN \rightarrow GCO3+NO_2$	1.95E16 exp(−13543/T	b
(86)	$GLYX+OH \rightarrow HO_2+2CO+H_2O$	1.15E−11	b
(87)	$C_2H_4+O_3 \rightarrow CH_2O+.4CH_2O+.12HO_2$ $+.42CO+.06CH_4+.21H_2O+.18CO_2+H_2$	1.2E−14 exp(−2633/T)	b
(88)	$CH_2O_2+NO \rightarrow CH_2O+NO_2$	7.0E−12	b
(89)	$CH_2O_2+NO_2 \rightarrow CH_2O+NO_3$	7.0E−13	b
(90)	$CH_2O_2+H_2O \rightarrow HCOOH$	4.0E−18	b
(91)	$HCOOH+OH \rightarrow HO_2+H_2O+CO_2$	3.2E−13	b

Table 3 continued.

	Reaction	Reaction Rate (sec^{-1})	Reference
	isoprene reactions		
(I1)	C_5H_8+OH → RIO_2	2.5E−11 exp(409/T)	g
(I2)	RIO_2+NO → .9(NO_2+HO_2+CH_2O) +.45(MVK+MACR)+.1(products)	4.2E−12 exp(180/T)	b
(I3)	RIO_2+HO_2 → RIOOH	3.0E−12	g
(I4)	RIOOH+OH → RIO_2	1.0E(−11)	g
(I5)	RIOOH+$h\nu$ → OH+CH_2O +HO_2+.5(MVK+MACR)	5.E−4[Rate(NO +$h\nu$)]	b
(I6)	RIOOH → Heterogeneous Loss	4.0E−05 ‡	f
(I7)	MVK+OH → VRO_2	3.0E−12 exp(500/T)	b
(I8)	VRO_2+NO → .9NO_2 +.6(HAC+CH_3CO_3) +.3(HO_2+CH_2O+MGLY)	4.2E−12 exp(180./T)	b
(I9)	VRO_2+HO_2 → VROOH	3.0E−12	g
(I10)	VROOH+OH → VRO_2	1.0E−11	g
(I11)	VROOH+$h\nu$ → OH+CH_2O +HO_2+MGLY	5.0E−4[Rate(NO_2+$h\nu$)]	b
(I12)	VROOH → Heterogeneous Loss	4.0E−05 ‡	f
(I13)	HAC+OH → HACO	1.5E−11	b
(I14)	HAC+$h\nu$ → CH_2O+2HO_2+CO	4.0E−6	f
(I15)	HAC → Heterogeneous Loss	4.0E−06 ‡	f
(I16)	HAC+NO_2 → HNO_3+HACO	5.2E−16	b
(I17)	HACO+NO_2 → IPAN	4.7E−12	b
(I18)	IPAN → HACO+NO_2	1.95E+16 exp(−13500/T)	b
(I19)	HACO+NO → NO_2+HO_2+CH_2O	4.2E−12 exp(180/T)	b
(I20)	HACO+HO_2 → products	3.0E−12	b
(I21)	MGLY+OH → CH_3CO_3+CO	1.7E−11	b
(I22)	MGLY+$h\nu$ → CH_3CO_3+HO_2+CO	4.0E−6	f
(I23)	MGLY → Heterogeneous Loss	4.0E−06 ‡	f
(I24)	MACR+OH → MAO_3	1.02E−11	b
(I25)	MAO_3+NO_2 → MPAN	4.7E−12	b
(I26)	MPAN → MAO_3+NO_2	1.95E+16 exp(−13500/T)	b
(I27)	MAO_3+NO → NO_2+MAO_2	4.2E−12 exp(180/T)	b
(I28)	MAO_2+HO_2 → products	3.0E−12	b

Table 3 continued.

	Reaction	Reaction Rate (sec^{-1})	Reference
(I29)	$MAO_2+NO \rightarrow NO_2+MAO$	4.2E−12 exp(180/T)	b
(I30)	$MAO+HO_2 \rightarrow$ products	3.0E−12	b
(I31)	$MAO+NO \rightarrow NO_2+HO_2+MGLY$	4.2E−12 exp(180/T)	b
(I32)	$MAO_3+HO_2 \rightarrow$ products	3.0E−12	b
(I33)	$MACR+OH \rightarrow MRO_2$	3.86E−12 exp(500/T)	b
(I34)	$MRO_2+NO \rightarrow .9(NO_2+HO_2$ $+CH_2O+MGLY)+.1$(products)	4.2E−12 exp(180/T)	b
(I35)	$MRO_2+HO_2 \rightarrow MROOH$	3.0E−12	a
(I36)	$MROOH+OH \rightarrow MRO_2$	1.0E−11	a
(I37)	$MROOH+h\nu \rightarrow CH_2O+HO_2+MGLY$	5.E−4[Rate(NO $+h\nu$)]	b
(I38)	MROOH → Heterogeneous Loss	4.0E−05 ‡	f
(I39)	$C_5H_8+O_3 \rightarrow$ $.5CH_2O+.3$(MACR+MAOO) $+.2(CH_2O-+MVK+MVKO+CO)$	7.0E−15 exp(1900/T)	b
(I40)	$CH_2O_2+NO \rightarrow NO_2+CH_2O$	7.0E−12	b
(I41)	$CH_2O_2+HO_2 \rightarrow$ products	3.0E−12	b
(I42)	$MVKO+NO \rightarrow MVK+NO$	4.2E−12 exp(180/T)	b
(I43)	$MVKO+HO_2 \rightarrow$ products	3.0E−12	b
(I44)	$MAOO+NO \rightarrow MACR+NO_2$	4.2E−12 exp(180/T)	b
(I45)	$MAOO+HO_2 \rightarrow$ products	3.0E−12	b
(I46)	$MVK+O_3 \rightarrow .5(CH_2O+MGLY)$ $+.2(CH_2O_2+HO_2+MCRG+CO)$ $+.15(ACHO+CH_3CO_3)$	4.0E−15 exp(−2000/T)	b
(I47)	$MCRG+NO \rightarrow MGLY+NO_2$	4.2E−12 exp(180/T)	b
(I48)	$MCRG+HO_2 \rightarrow$ products	3.0E−12	b
(I49)	$MACR+O_3 \rightarrow .5$(CH-2O+MGLY) $+.4CO+.2(CH_2O_2+HO_2+MCRG)$ $+.15CH_3O_2$	4.4E−15 exp(−2500/T)	b

[a]DeMore *et al.*, (1982)
[b]Lurmann *et al.*, (1986)
[c]Kircher *et al.*, (1984)
[d]Malko and Troe (1982)
[e]Niki *et al.*, (1984)
[f]Richardson *et al.*, (1990)
[g]Jacob and Wofsy (1988)

* for 500m at noon
† A=atmospheric number density: A_0= atmospheric number density at the surface
‡ Heterogeneous loss rates within the boundary layer

B ECMWF Wind Fields

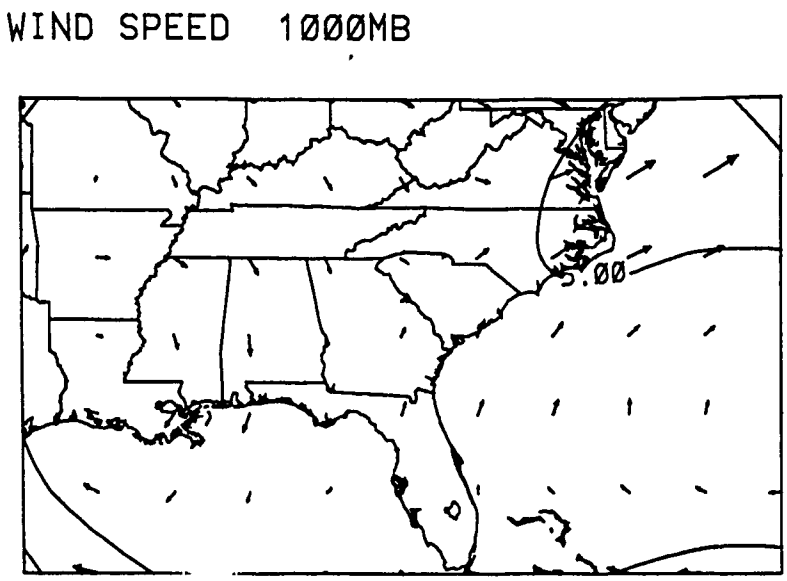

Figure 22: ECMWF wind field for 1000mb, 1200 UTC, 25 July 1987. All wind speeds are under ten m/sec.

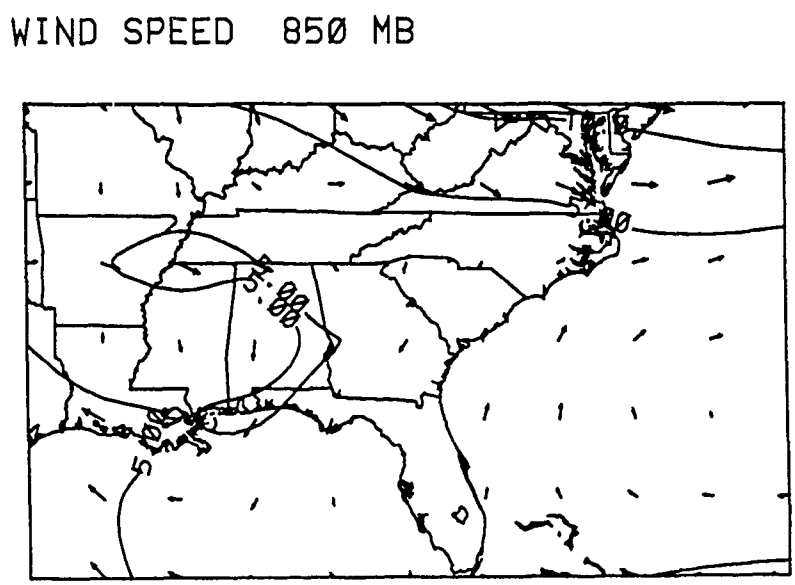

Figure 23: As in figure 22 for 850mb.

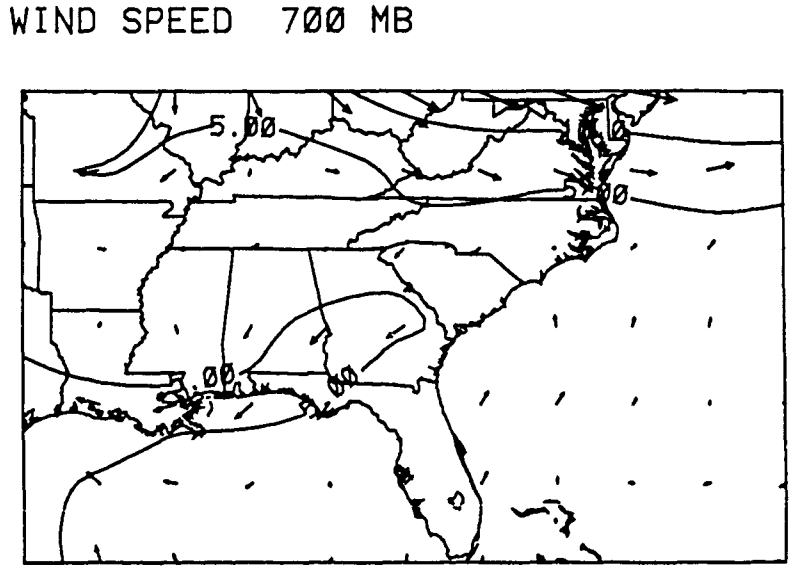

Figure 24: As in figure 22 for 700mb.

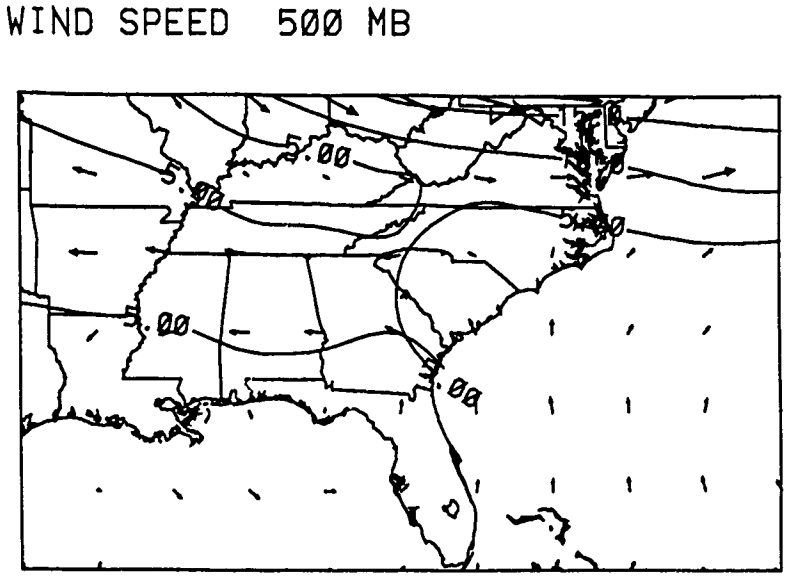

Figure 25: As in figure 22 for 500mb.

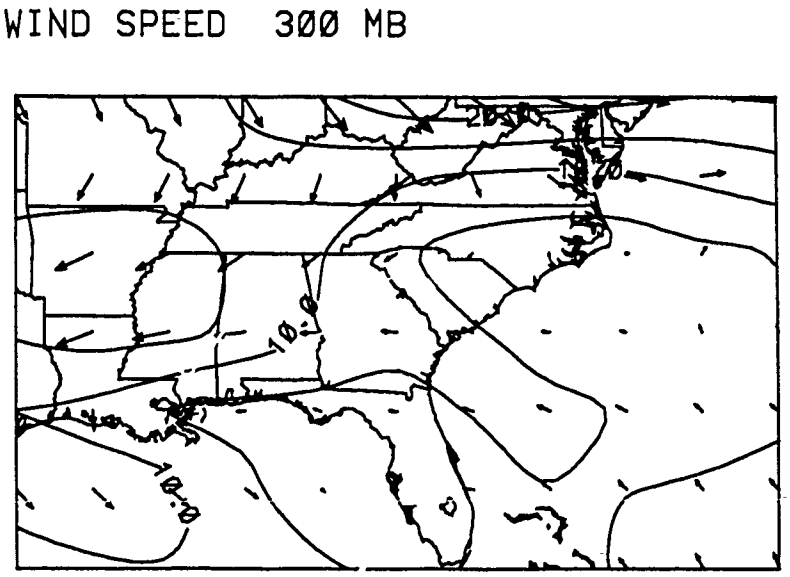

Figure 26: As in figure 22 for 300mb.

C Trace Gas Distibutions - Case I

Figures 27 through 30 depict ozone distribution for 0000L, 0600L, 1200L and 1800L on day 5 of the Case I model run. Figures 31 through 34 depict NO_x distribution for 0000L, 0600L, 1200L and 1800L on day 5 of the Case I model run. Figures 35 through 38 depict CO distribution for 0000L, 0600L. 1200L and 1800L on day 5 of the Case I model run. Figures 39 through 42 depict Butane distribution for 0000L, 0600L, 1200L and 1800L on day 5 of the Case I model run.

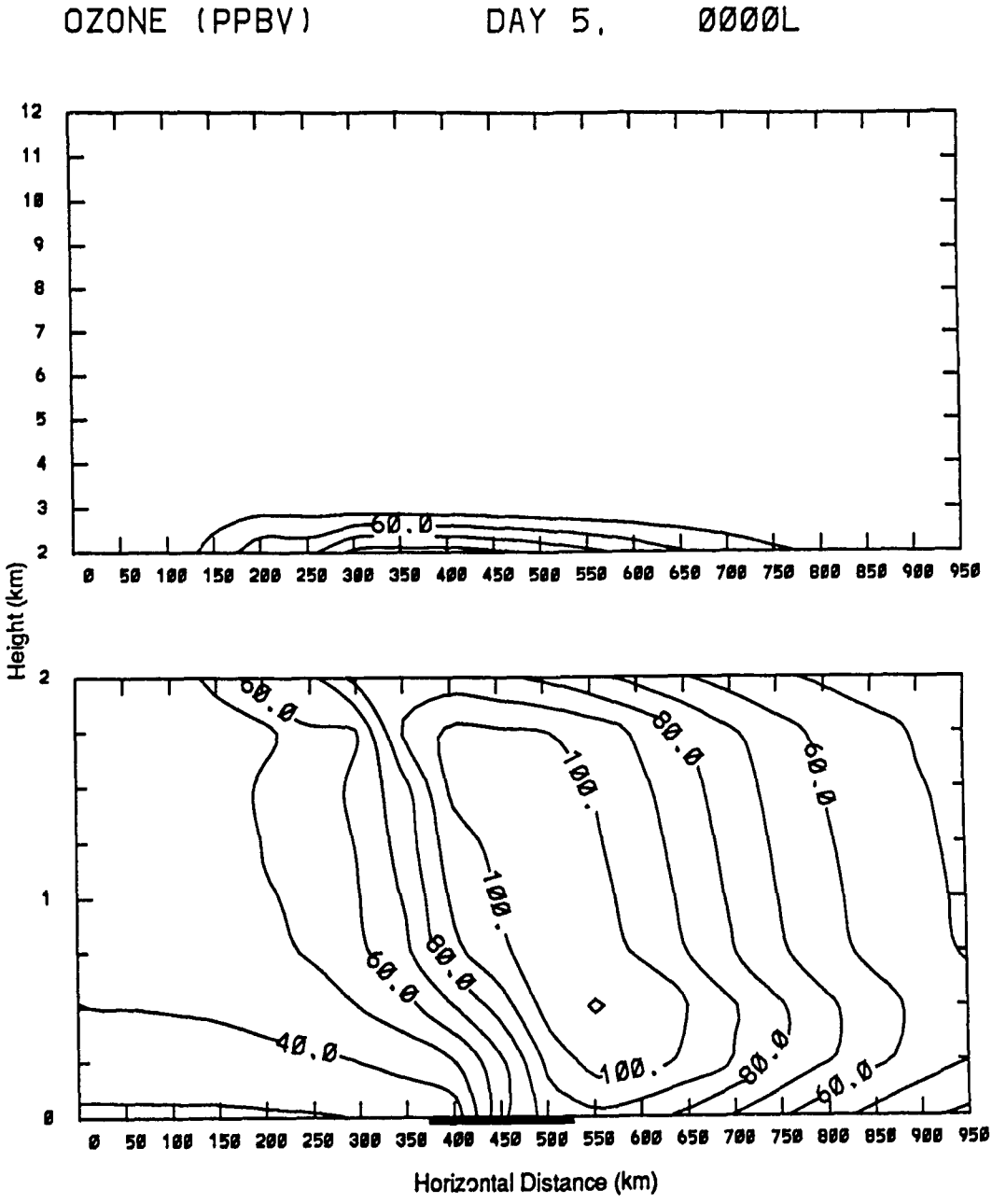

Figure 27: Forecast distribution of ozone for Case I at 0000L on day 5. Contour increment is 10 ppbv. The top figure shows the troposphere from 2-12 km, while the bottom figure expands the ordinate to show detail in the PBL. The abscissa indicates the horizontal extent of the computational domain.

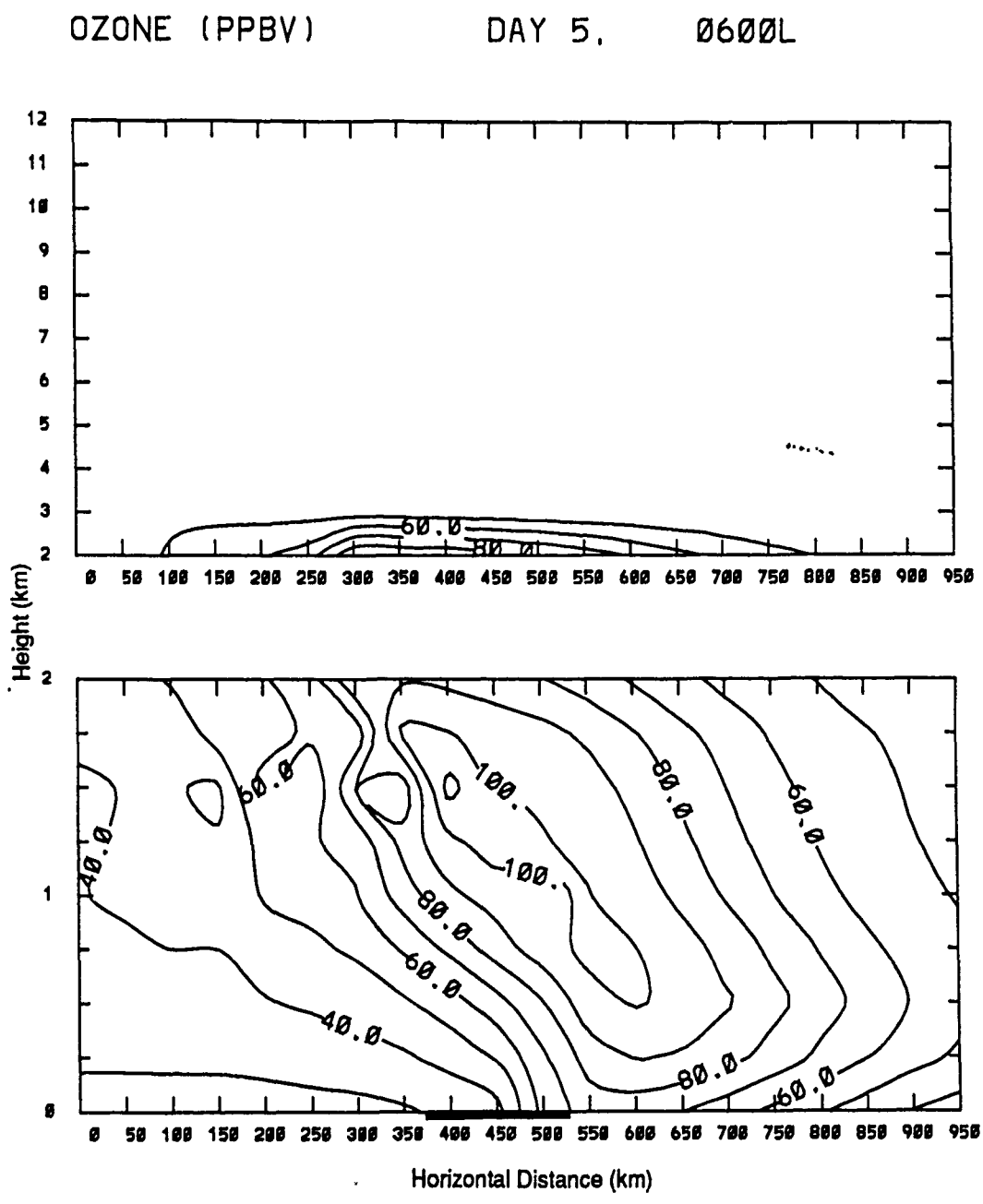

Figure 28: As in figure 27 for 0600L on day 5.

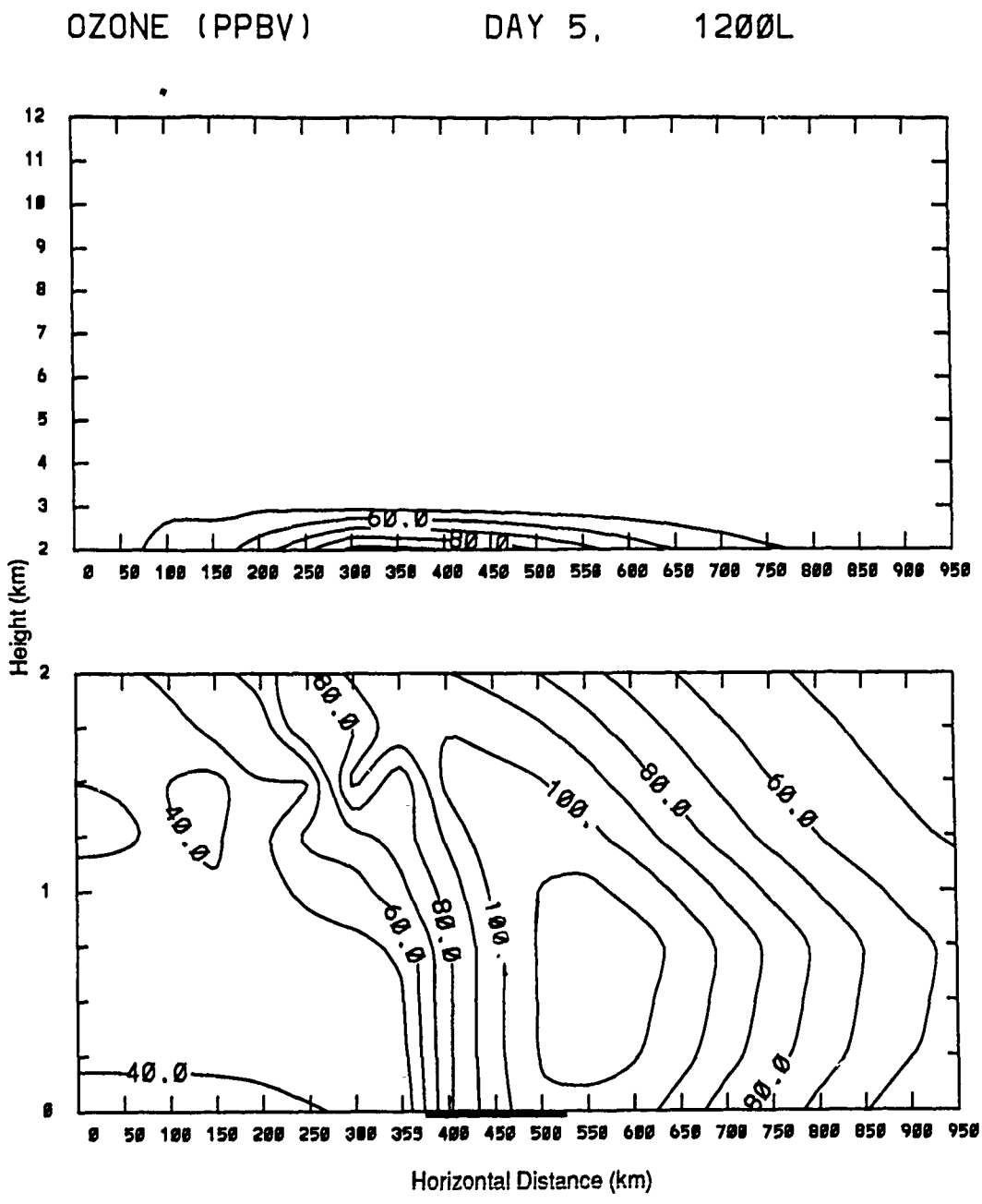

Figure 29: As in figure 27 for 1200L on day 5.

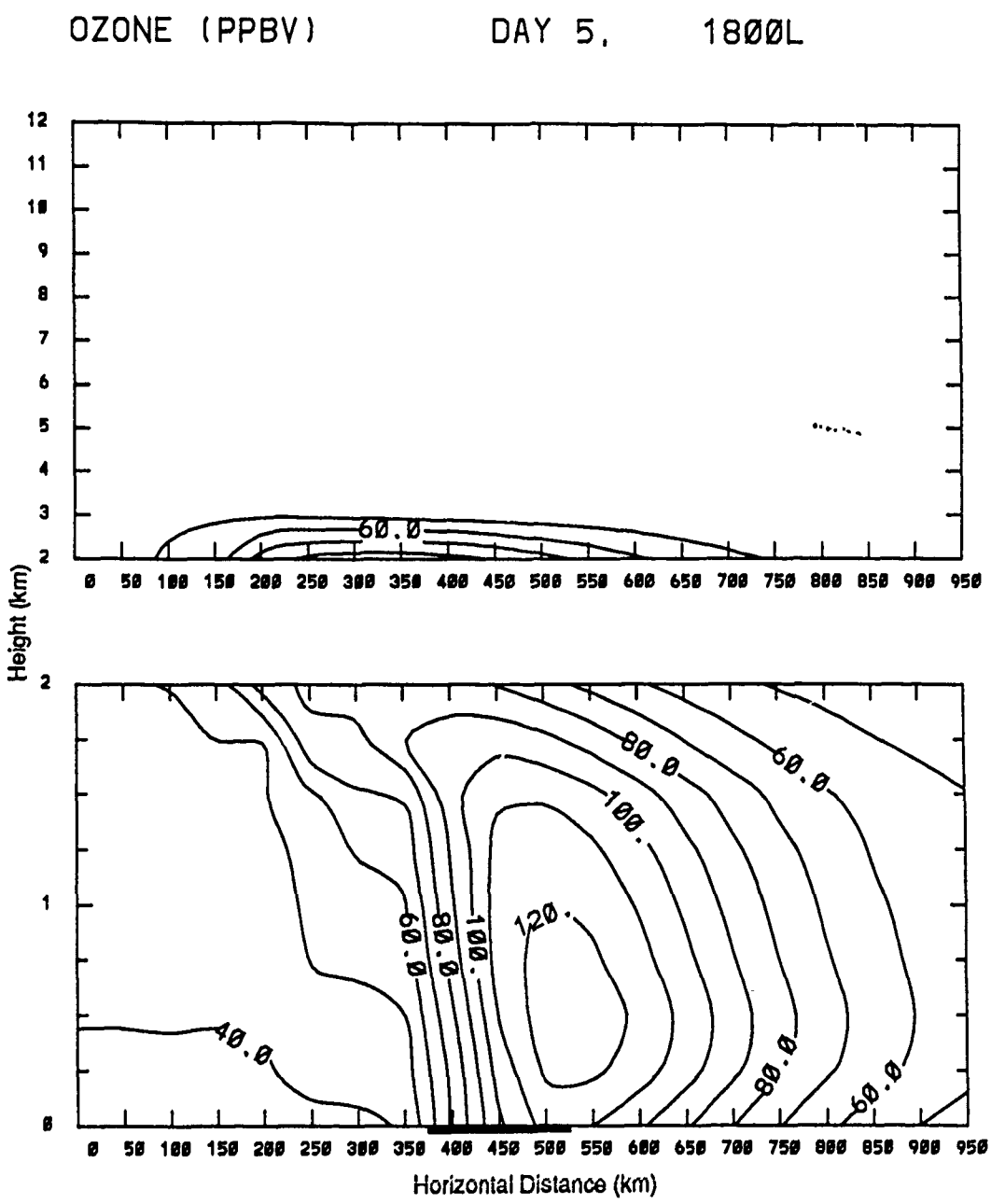

Figure 30: As in figure 27 for 1800L on day 5.

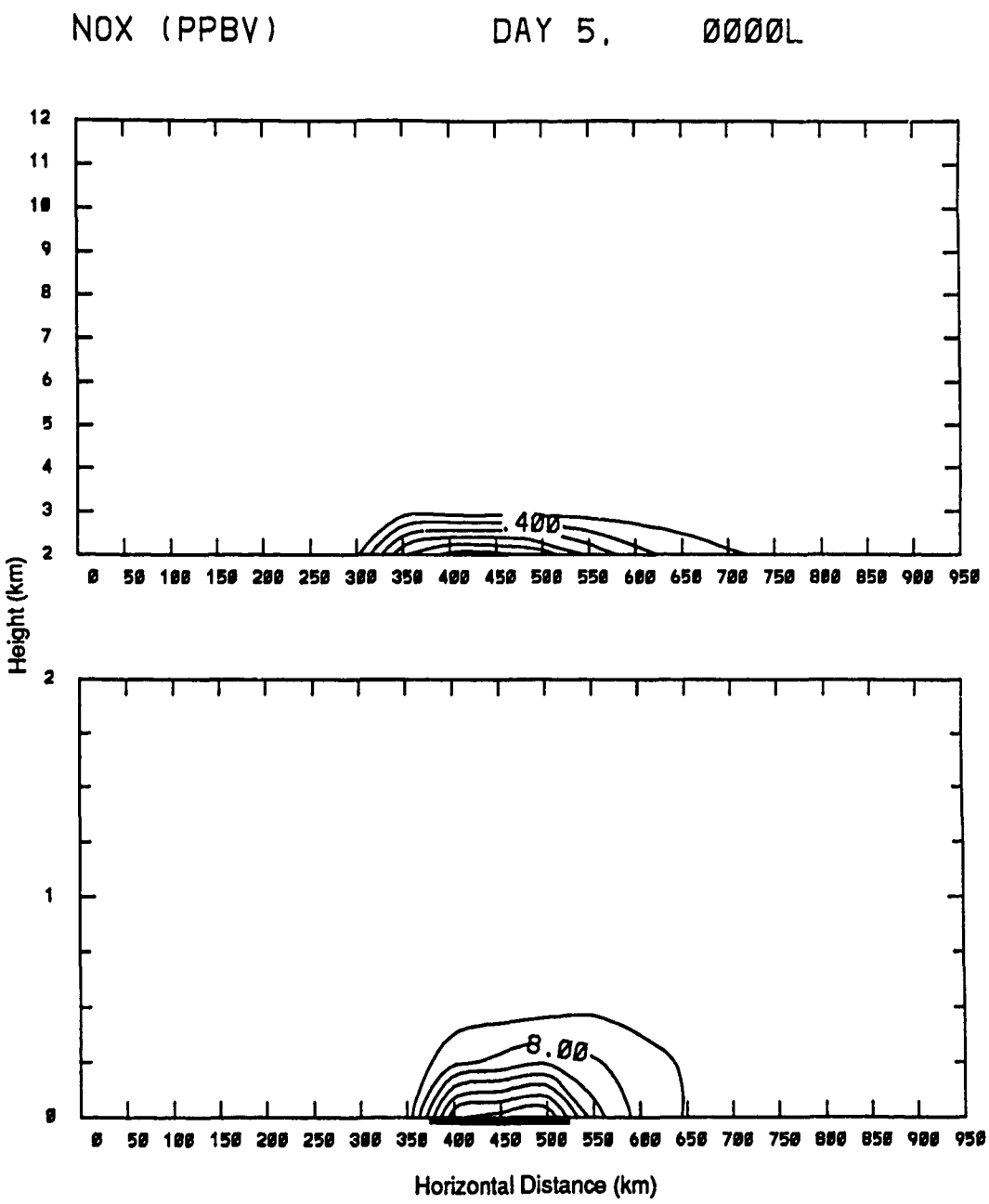

Figure 31: Forecast distribution of NO_x for Case I at 0000L on Day 5. Contour increment is 0.2 ppbv for the top figure, 4 ppbv for the bottom figure.

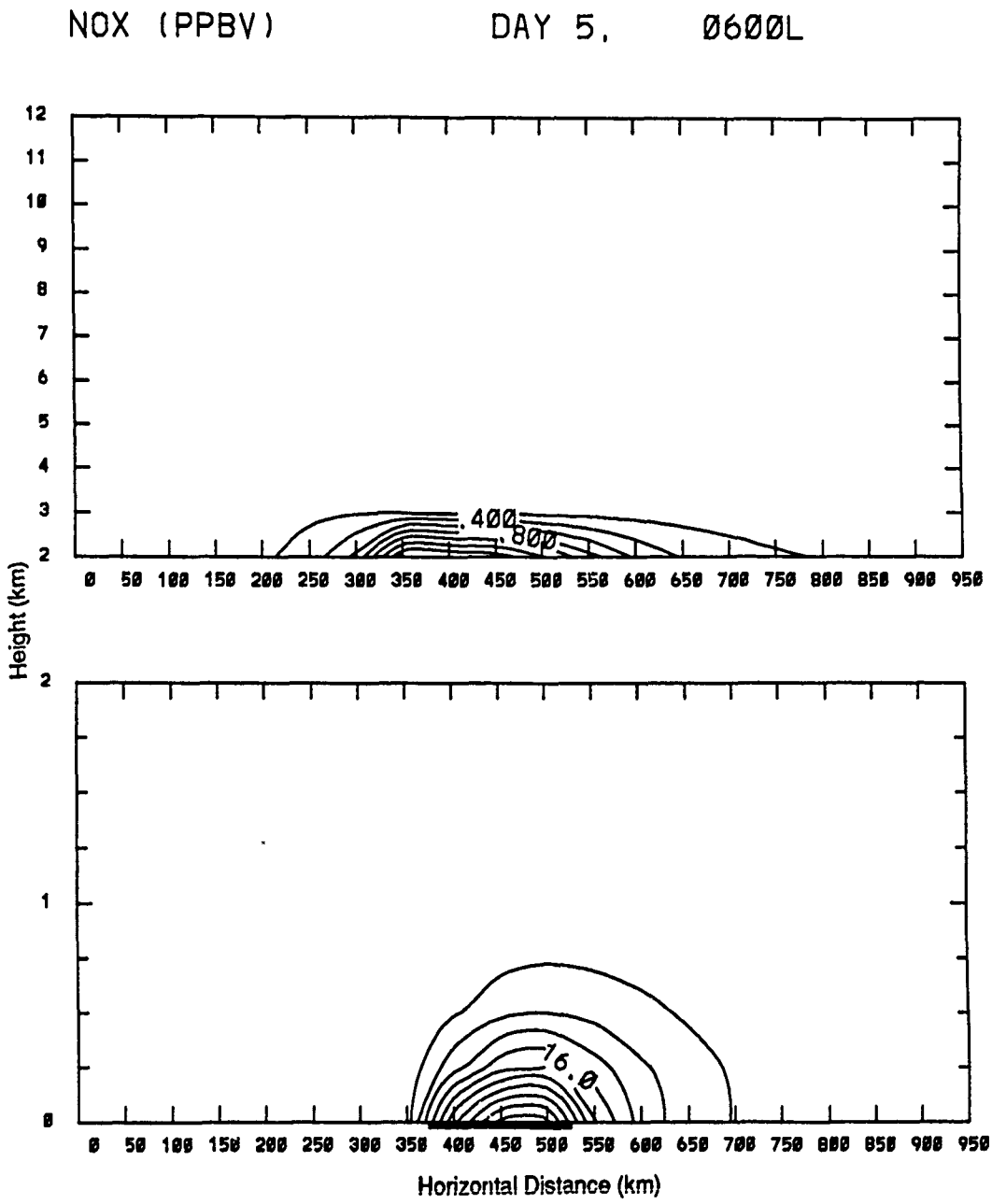

Figure 32: As in figure 31 for 0600L on day 5.

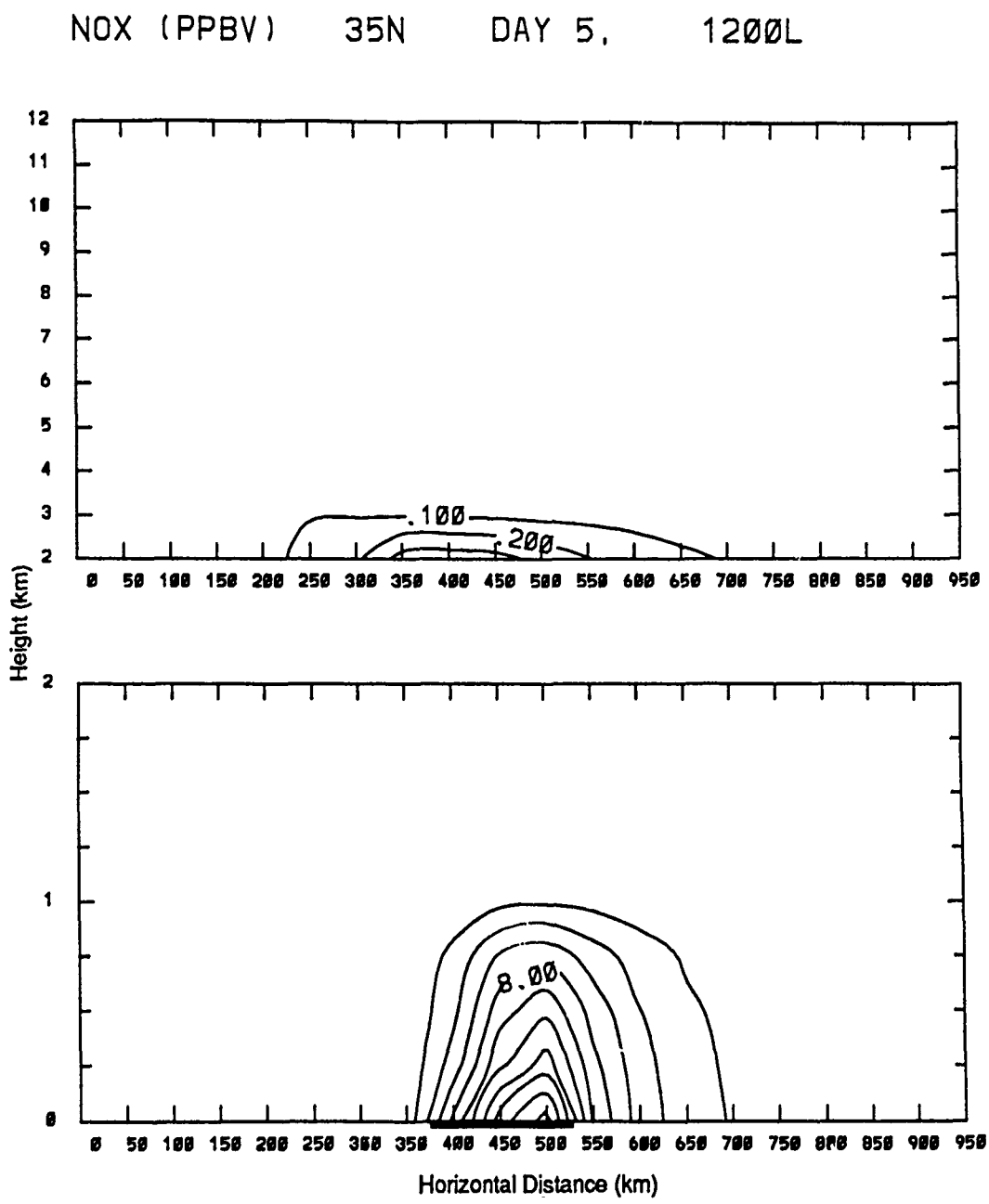

Figure 33: As in figure 31 for 1200L on day 5. on day 5. Contour increment is 0.1 ppbv for the top figure, 2 ppbv for the bottom figure.

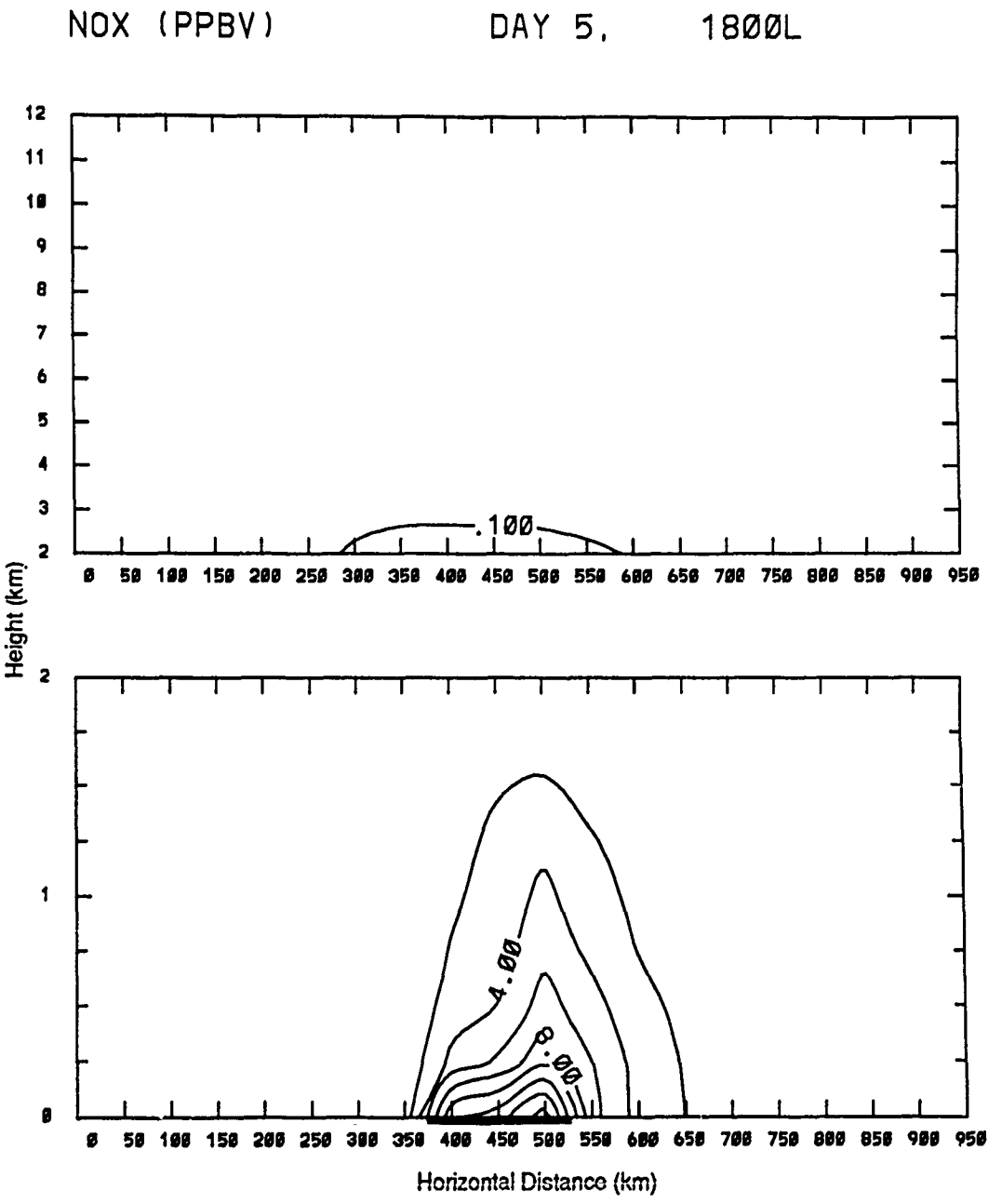

Figure 34: As in figure 31 for 1800L on day 5.

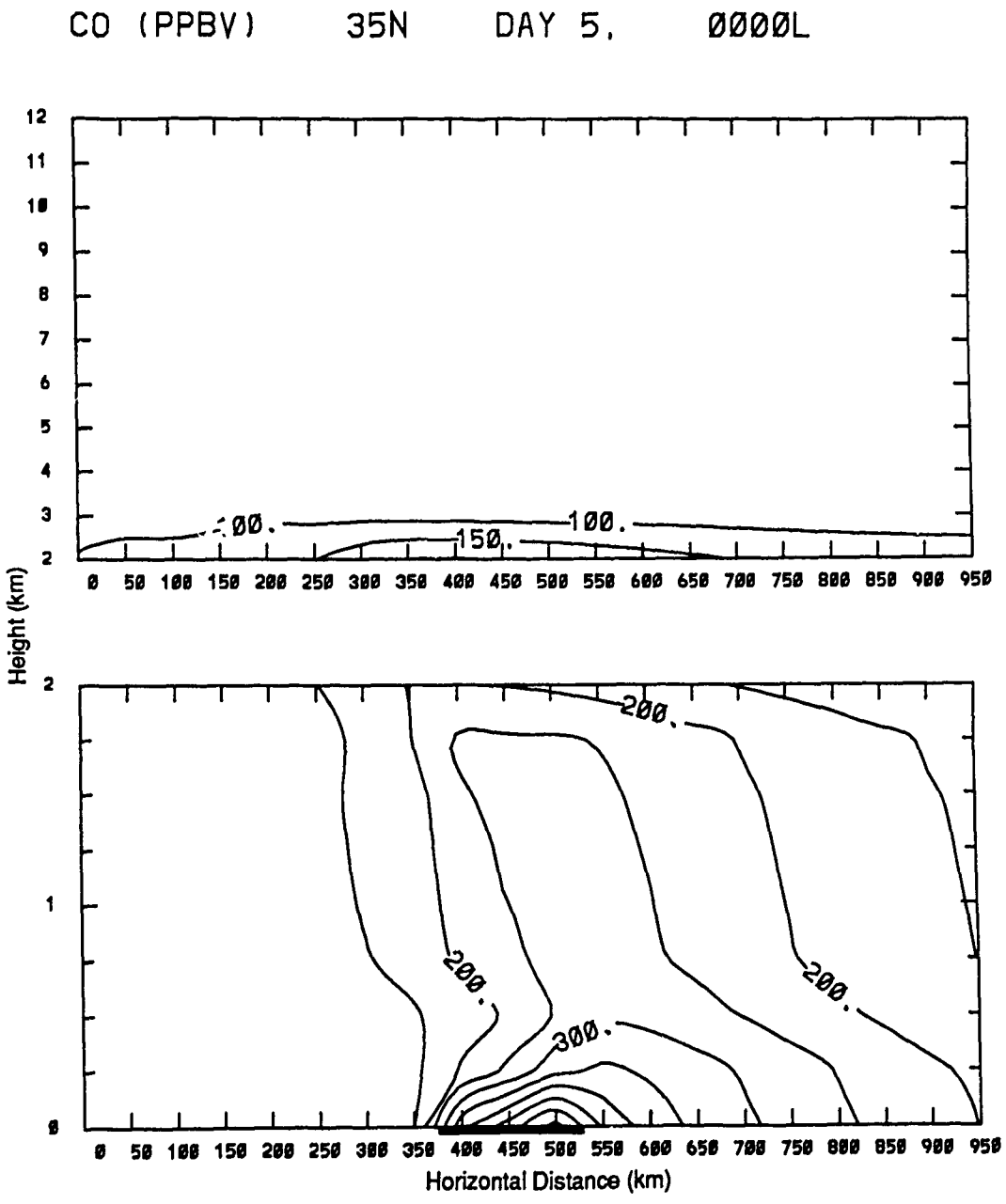

Figure 35: Forecast distribution of CO for Case I at 0000L on day 5. C ntour increment is 50 ppbv.

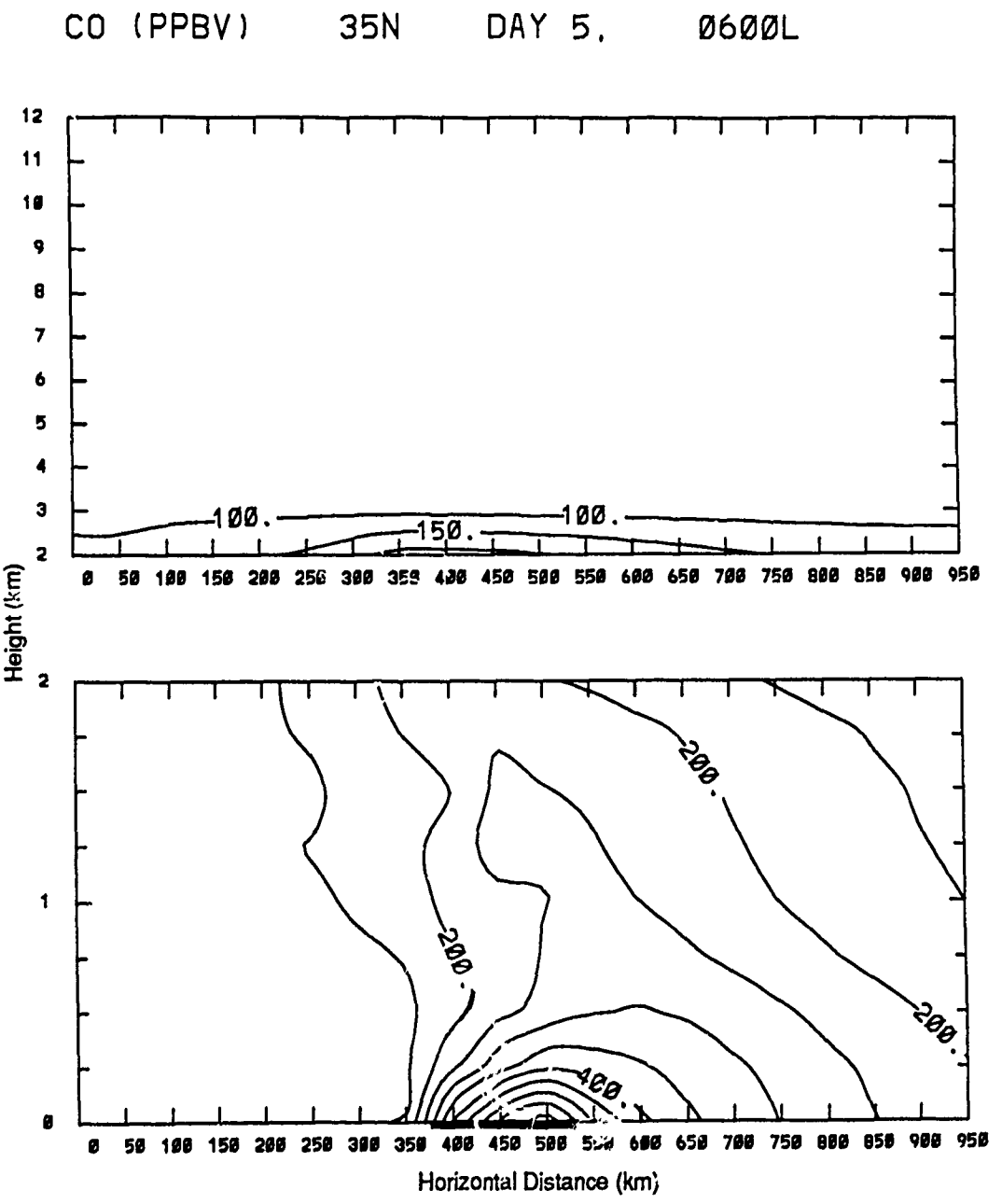

Figure 36: As in figure 35 for 0600L on day 5.

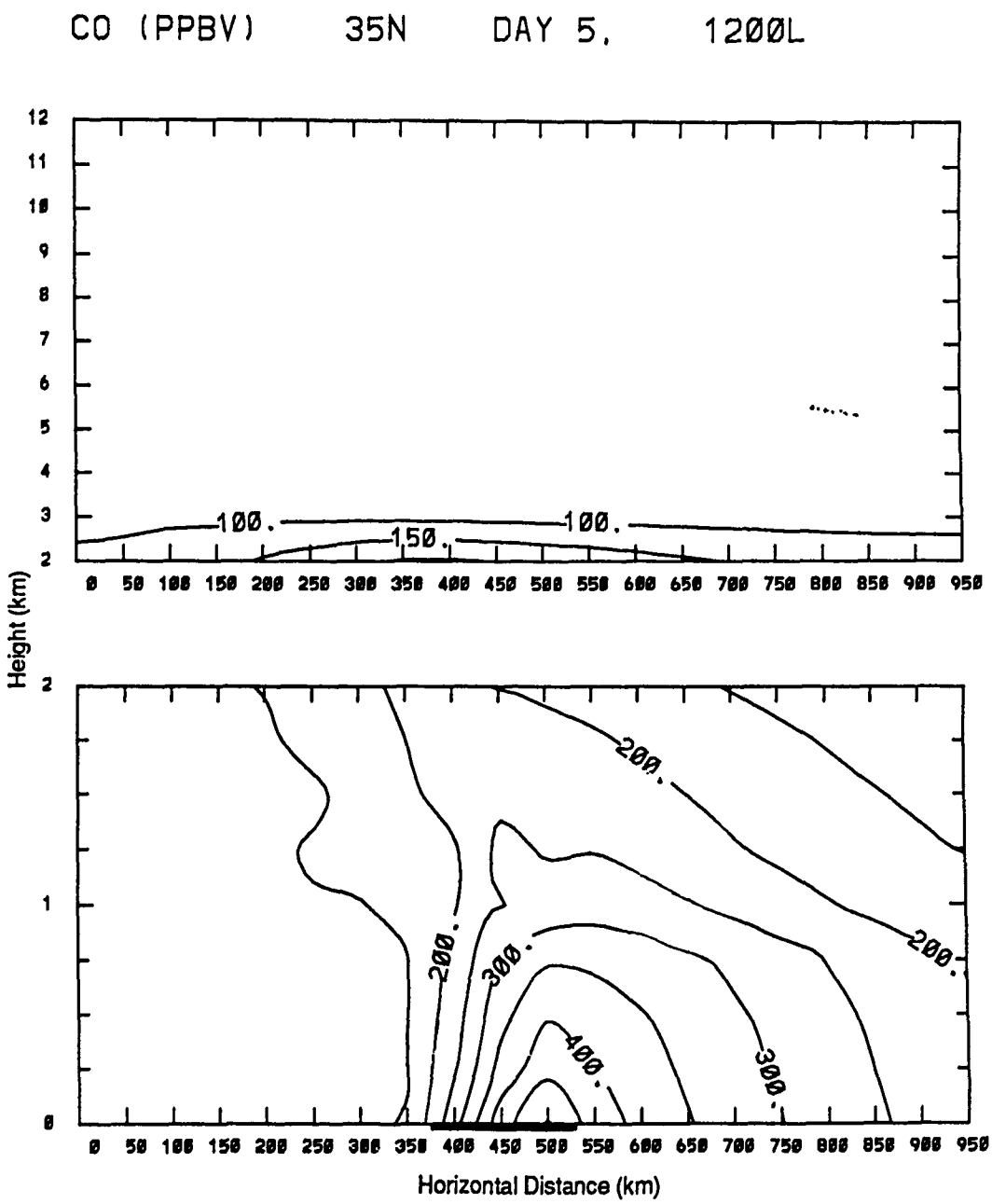

Figure 37: As in figure 35 for 1200L on day 5.

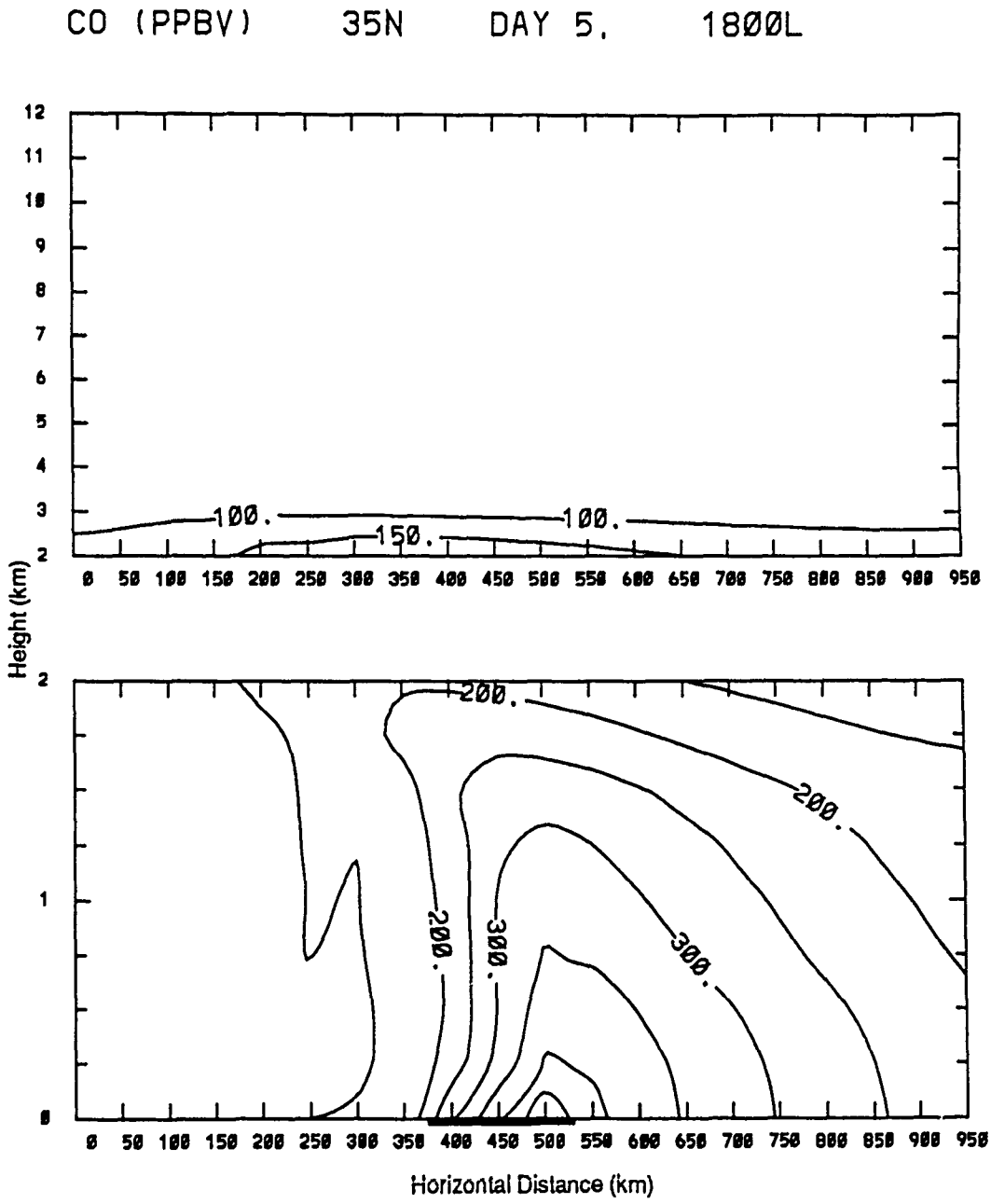

Figure 38: As in figure 35 for 1800L on day 5.

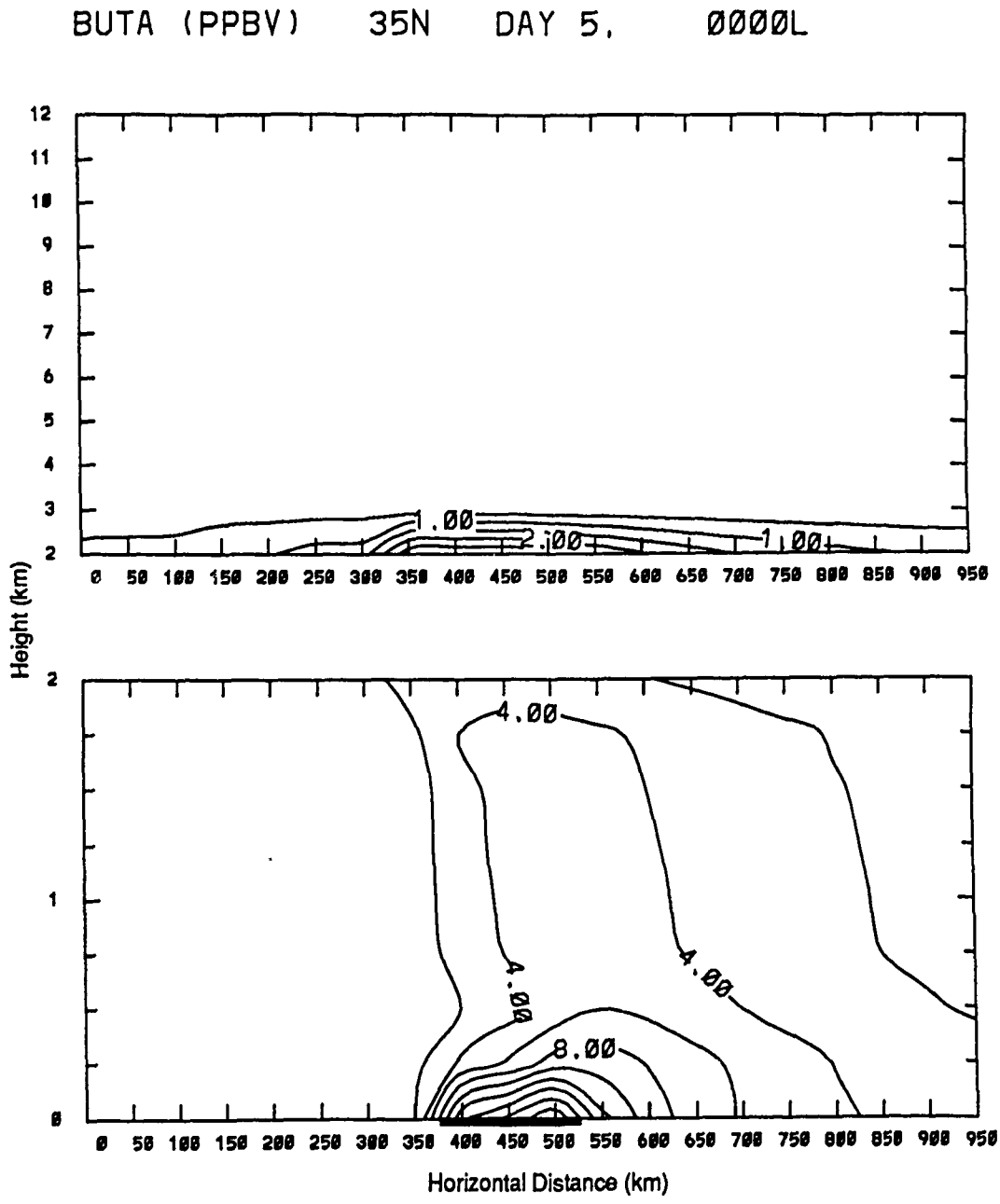

Figure 39: Forecast distribution of butane Case I at 0000L on day 5. Contour increment is 1 ppbv for the top figure, 2 ppbv for the bottom figure.

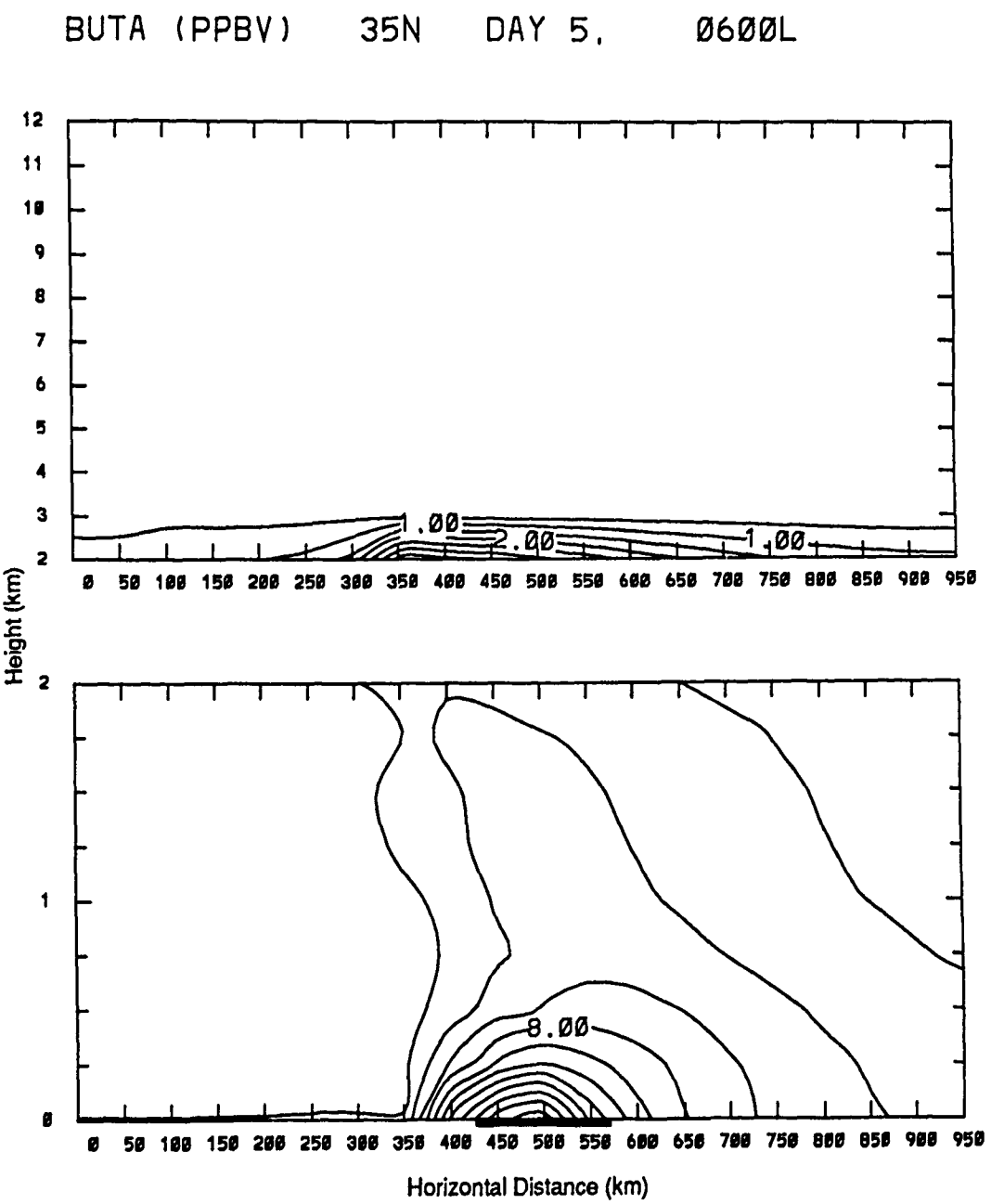

Figure 40: As in figure 39 for 0600L on day 5.

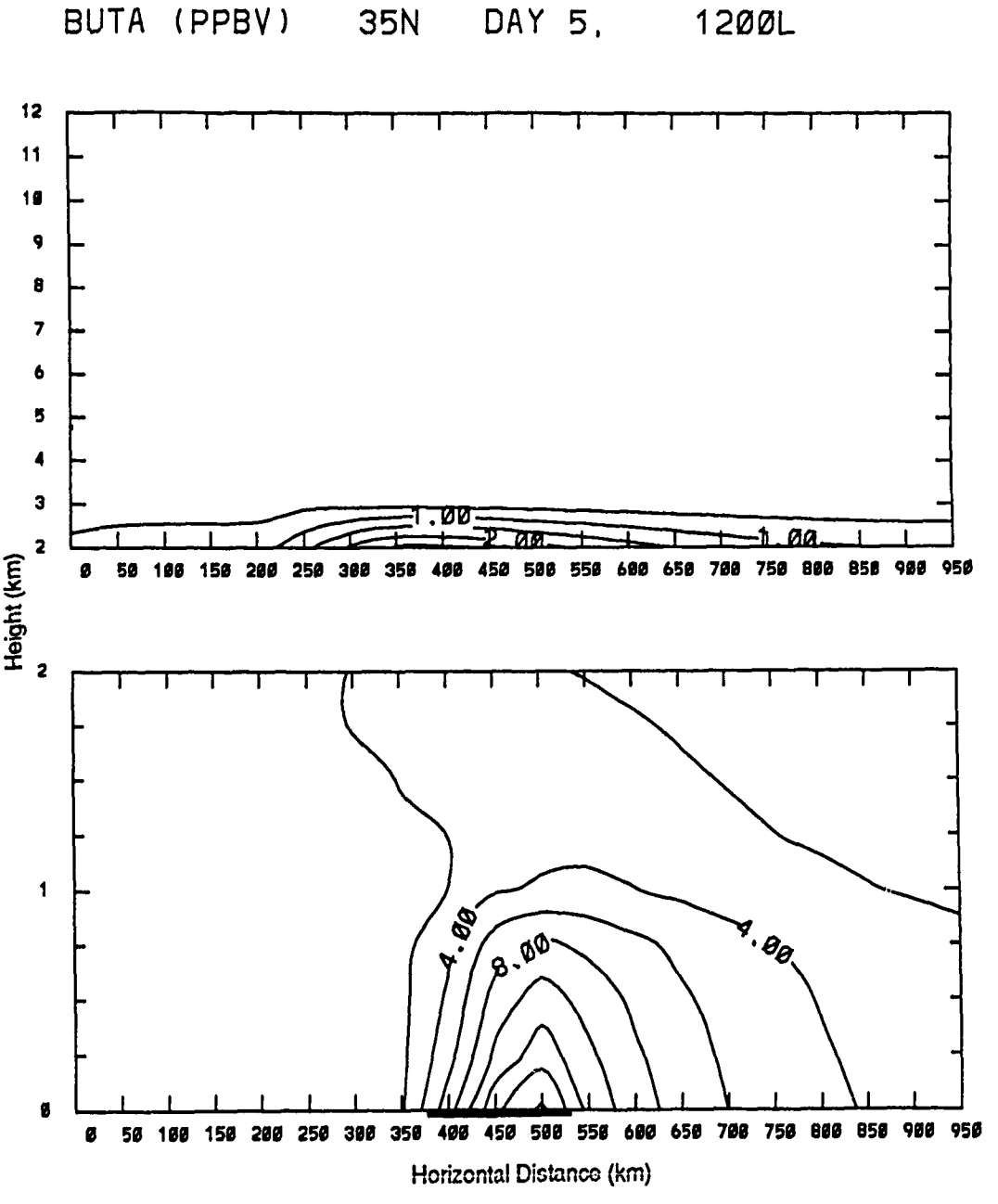

Figure 41: As in figure 39 for 1200L on day 5.

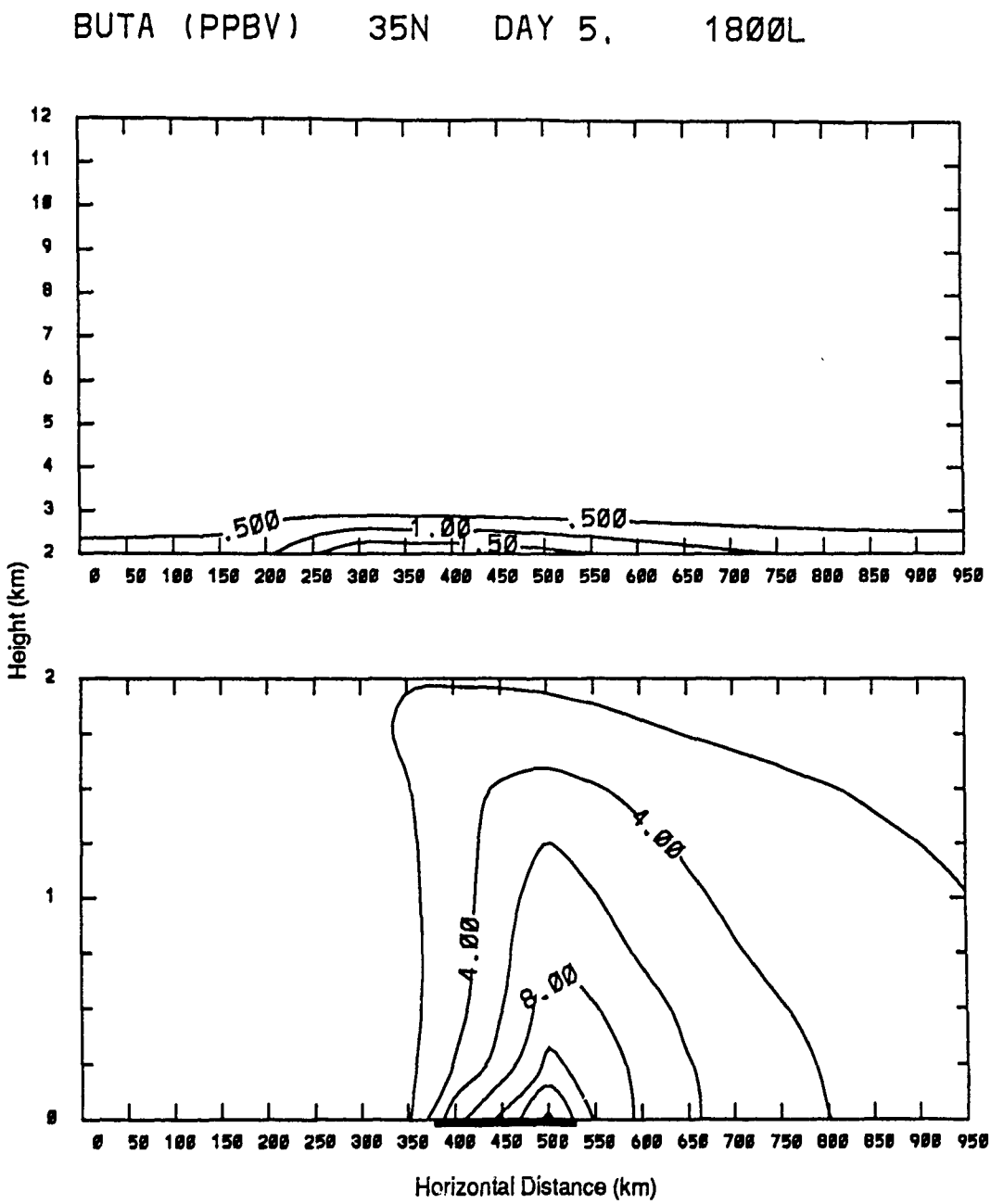

Figure 42: As in figure 39 for 1800L on day 5.

D Trace Gas Distibutions - Case II

Figures 43 through 46 depict ozone distribution for 0000L, 0600L, 1200L and 1800L on day 5 of the Case II model run. Figures 47 through 50 depict NO_x distribution for 0000L, 0600L, 1200L and 1800L on day 5 of the Case II model run. Figures 51 through 54 depict CO distribution for 0000L, 0600L, 1200L and 1800L on day 5 of the Case II model run. Figures 55 through 58 depict Butane distribution for 0000L, 0600L, 1200L and 1800L on day 5 of the Case II model run.

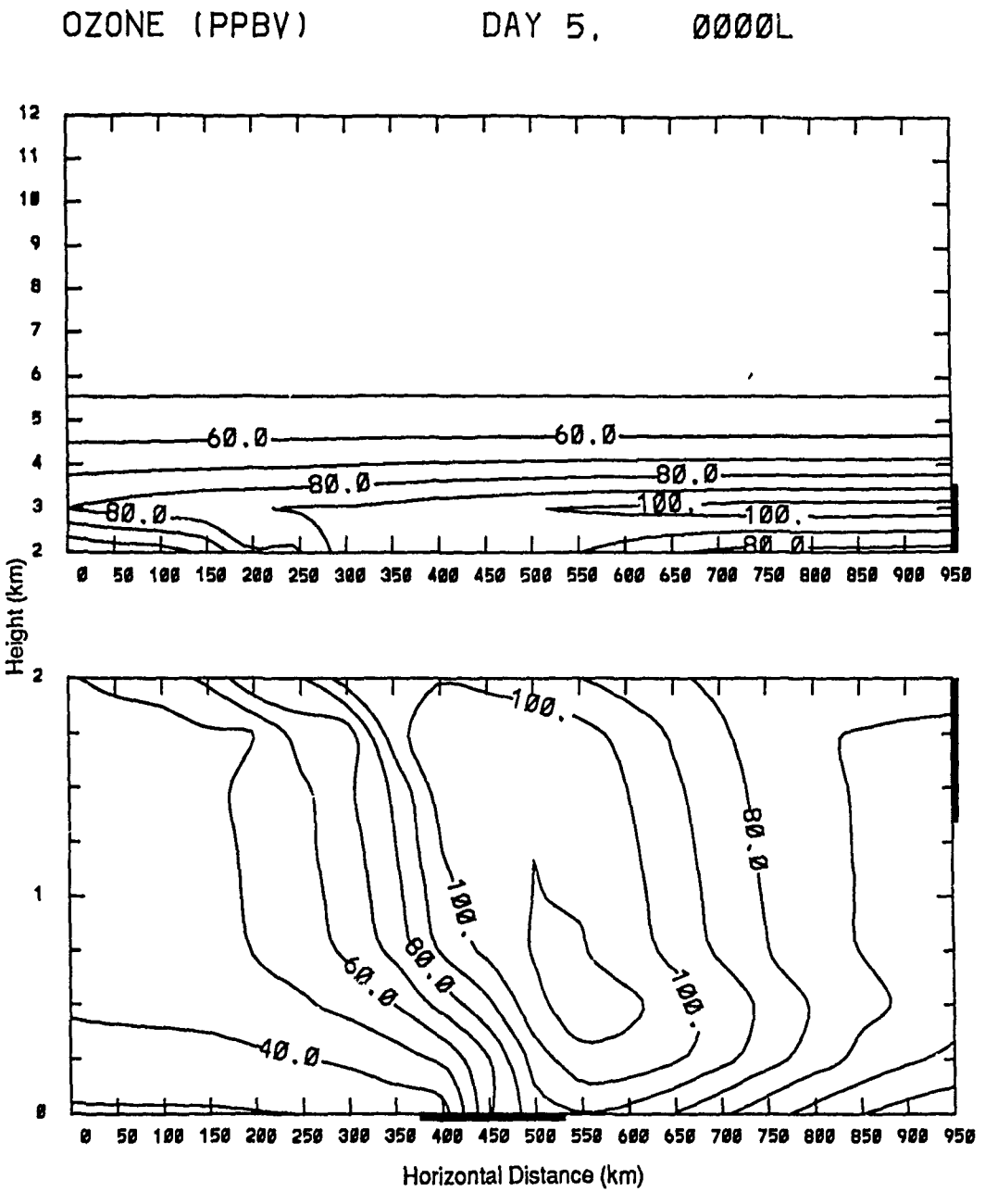

Figure 43: Forecast distribution of ozone for Case II at 0000L on day 5. Contour increment is 10 ppbv. The top of the figure shows the troposphere from 2-12 km, while the bottom figure expands the ordinate to show detail in the PBL. The abscissa indicates the horizontal extent of the computational domain.

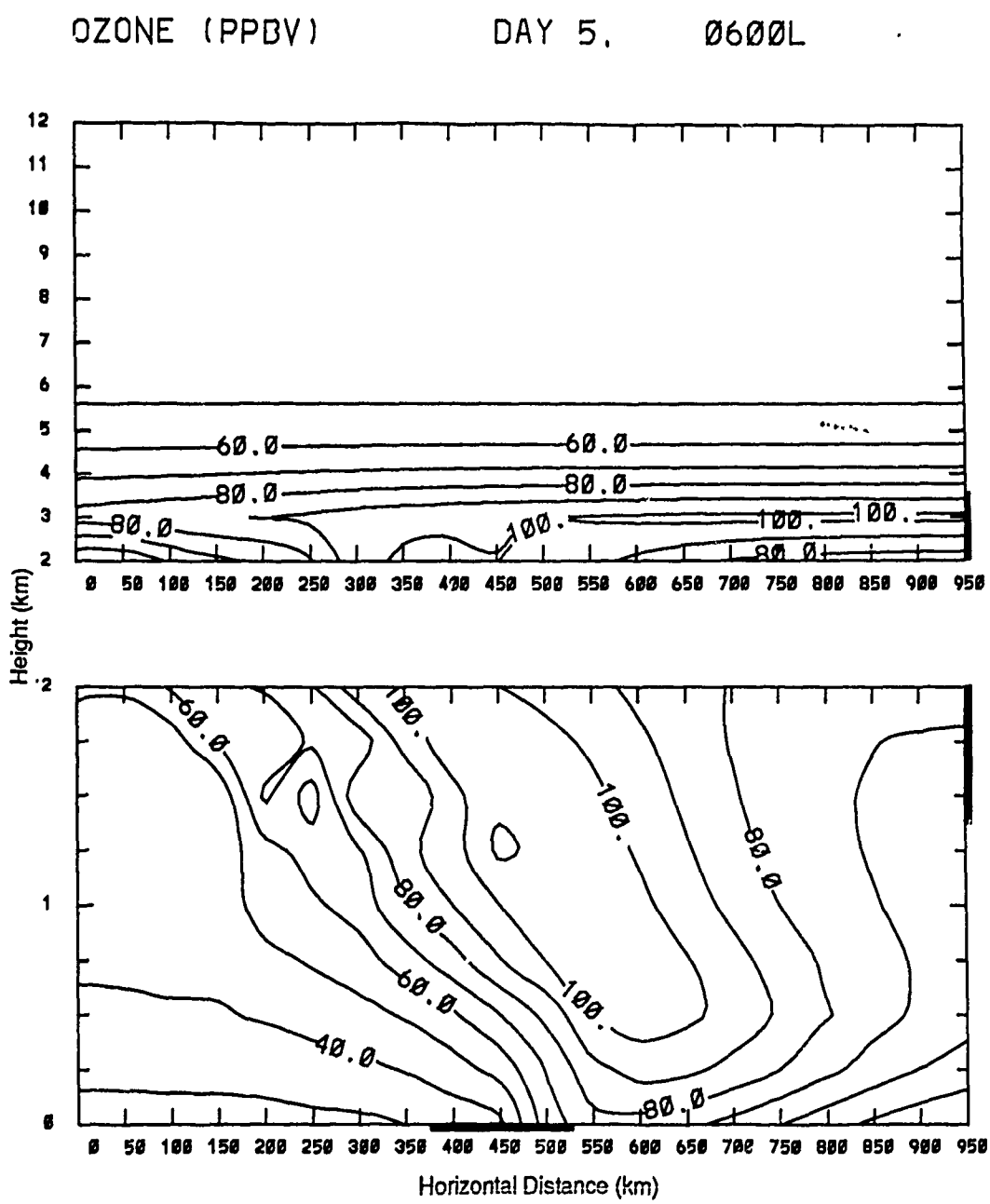

Figure 44: As in figure 43 for 0600L on day 5.

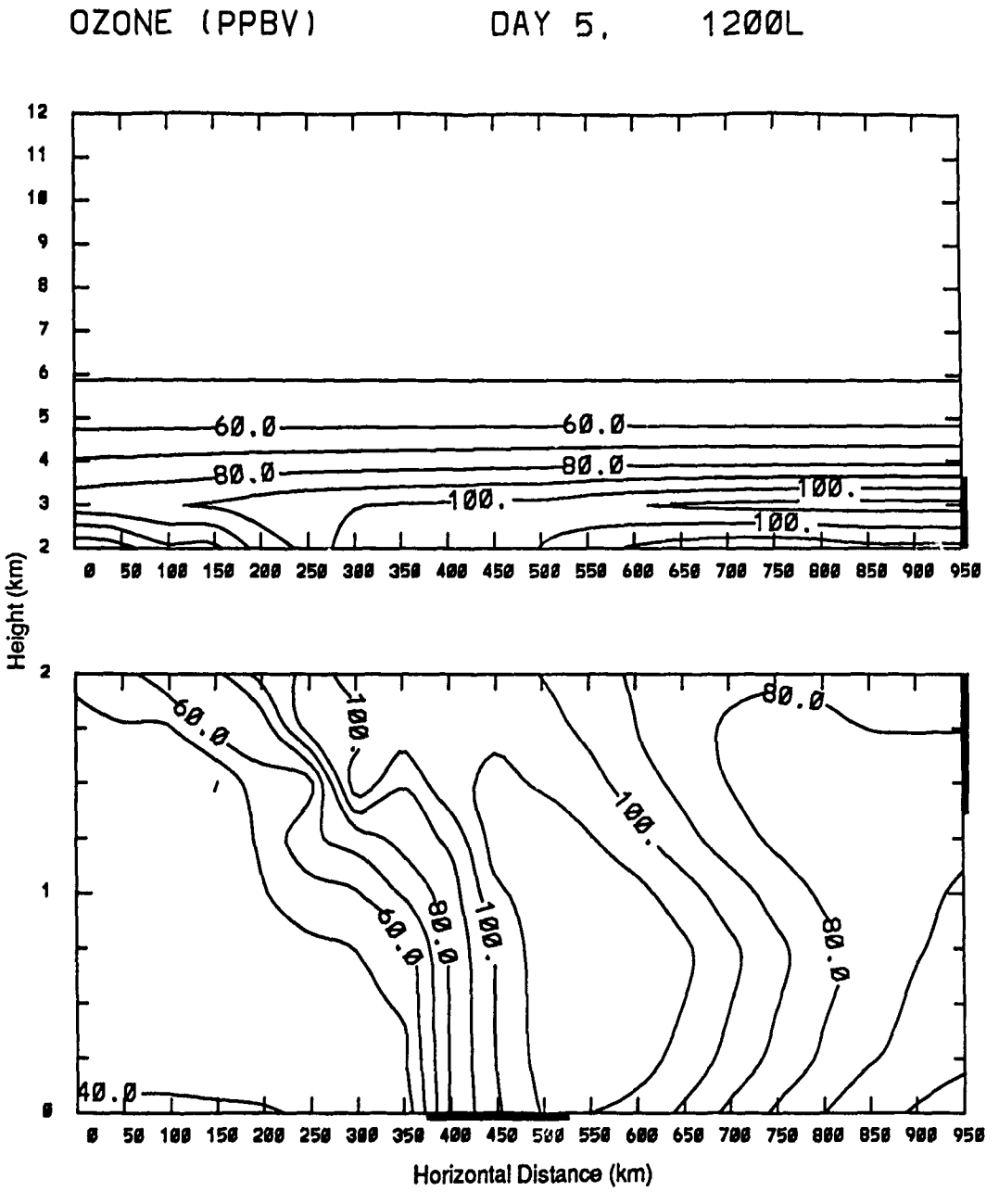

Figure 45: As in figure 43 for 1200L on day 5.

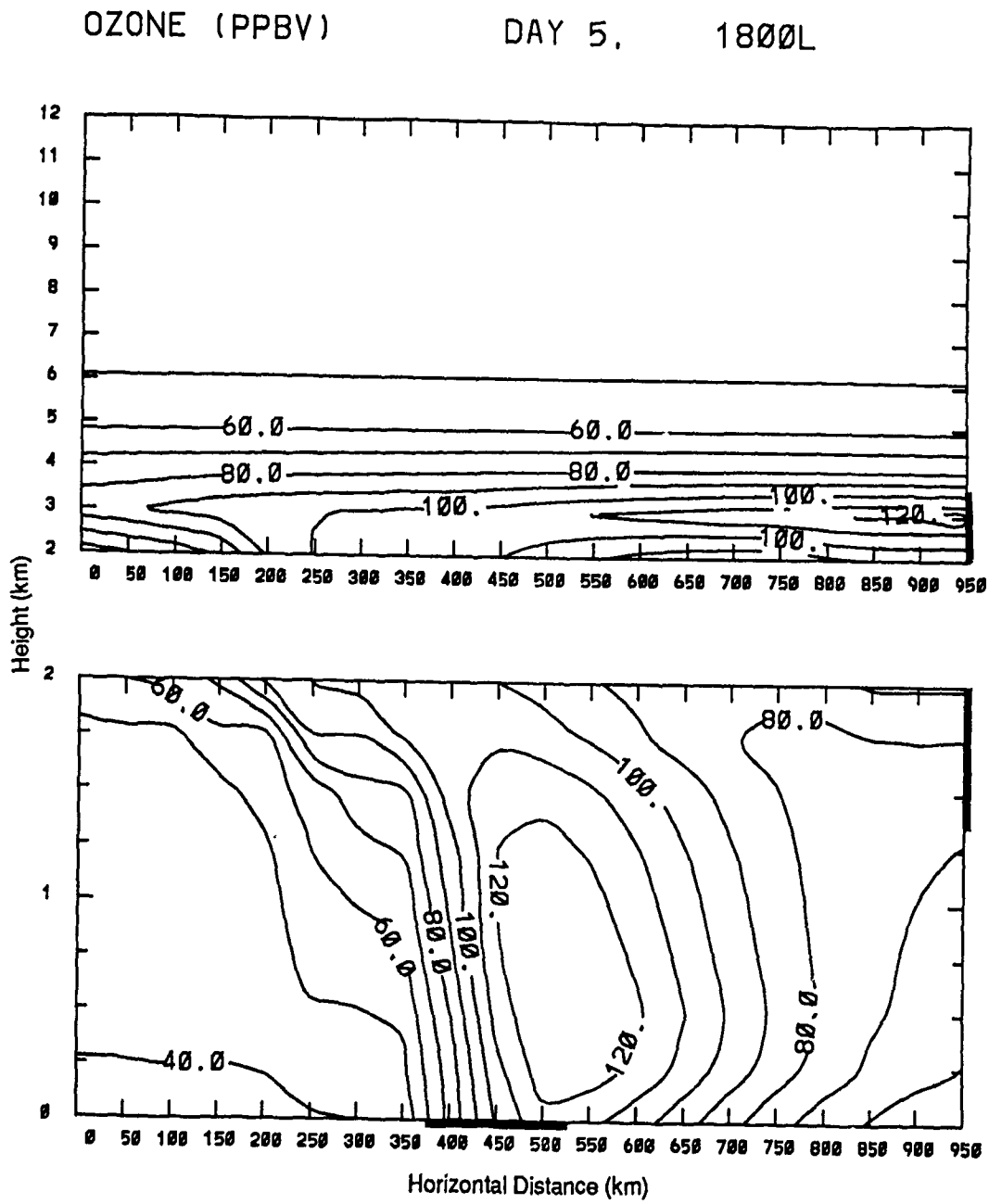

Figure 46: As in figure 43 for 1800L on day 5.

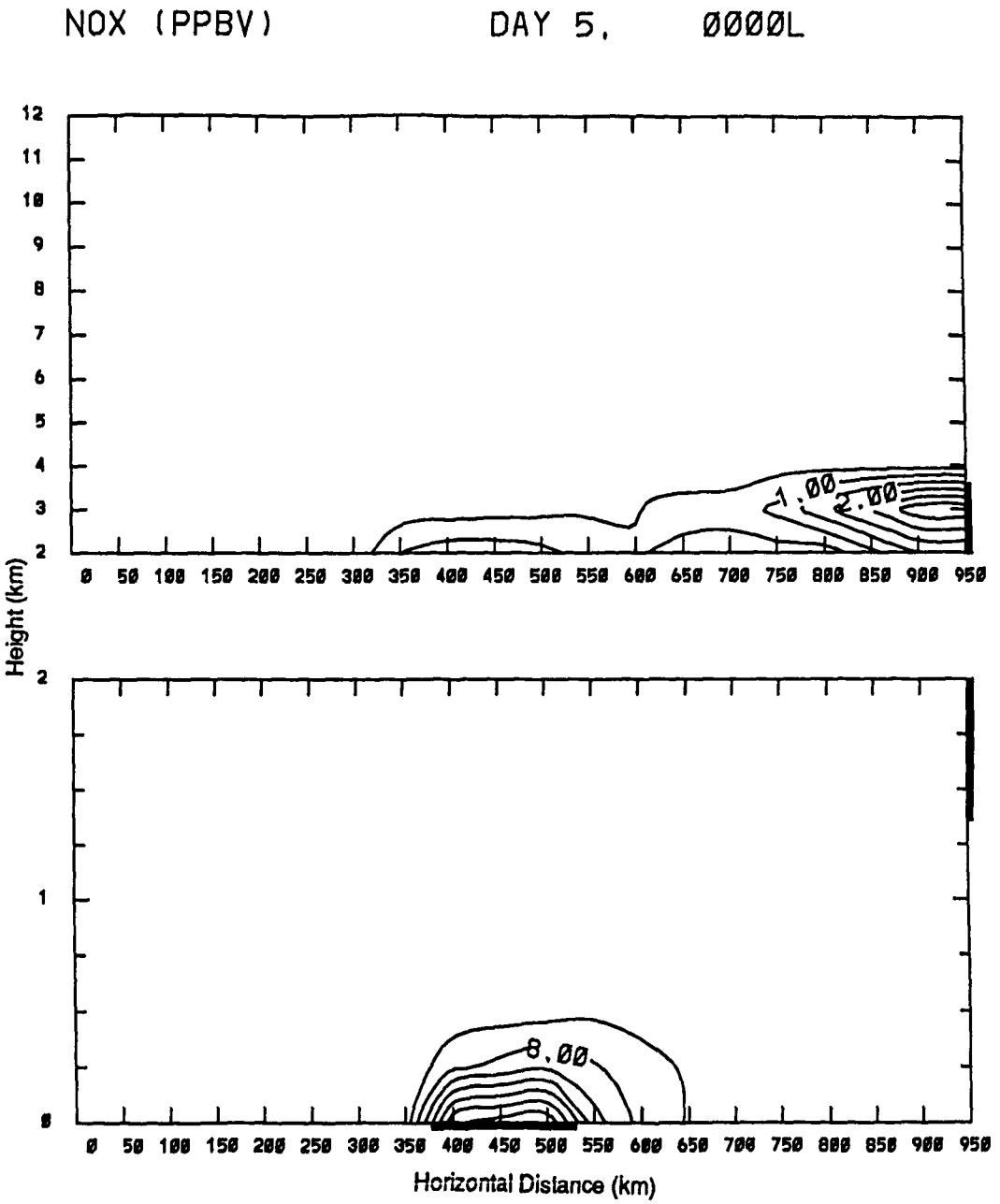

Figure 47: Forecast distribution of NO_x for Case II at 0000L on day 5. Contour increment is 0.2 ppbv for the top plot, 4 ppbv for the bottom plot.

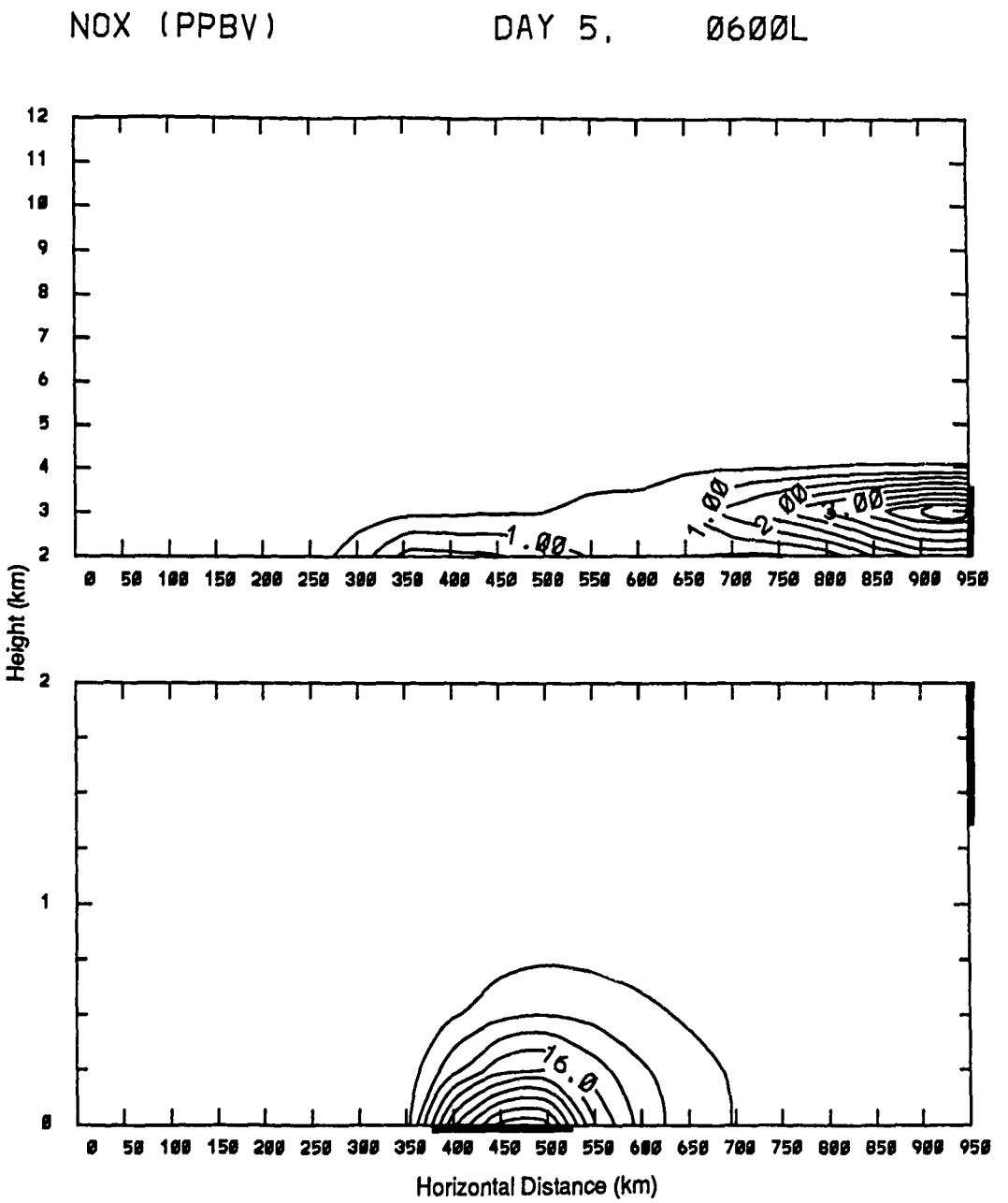

Figure 48: As in figure 47 for 0600L on day 5.

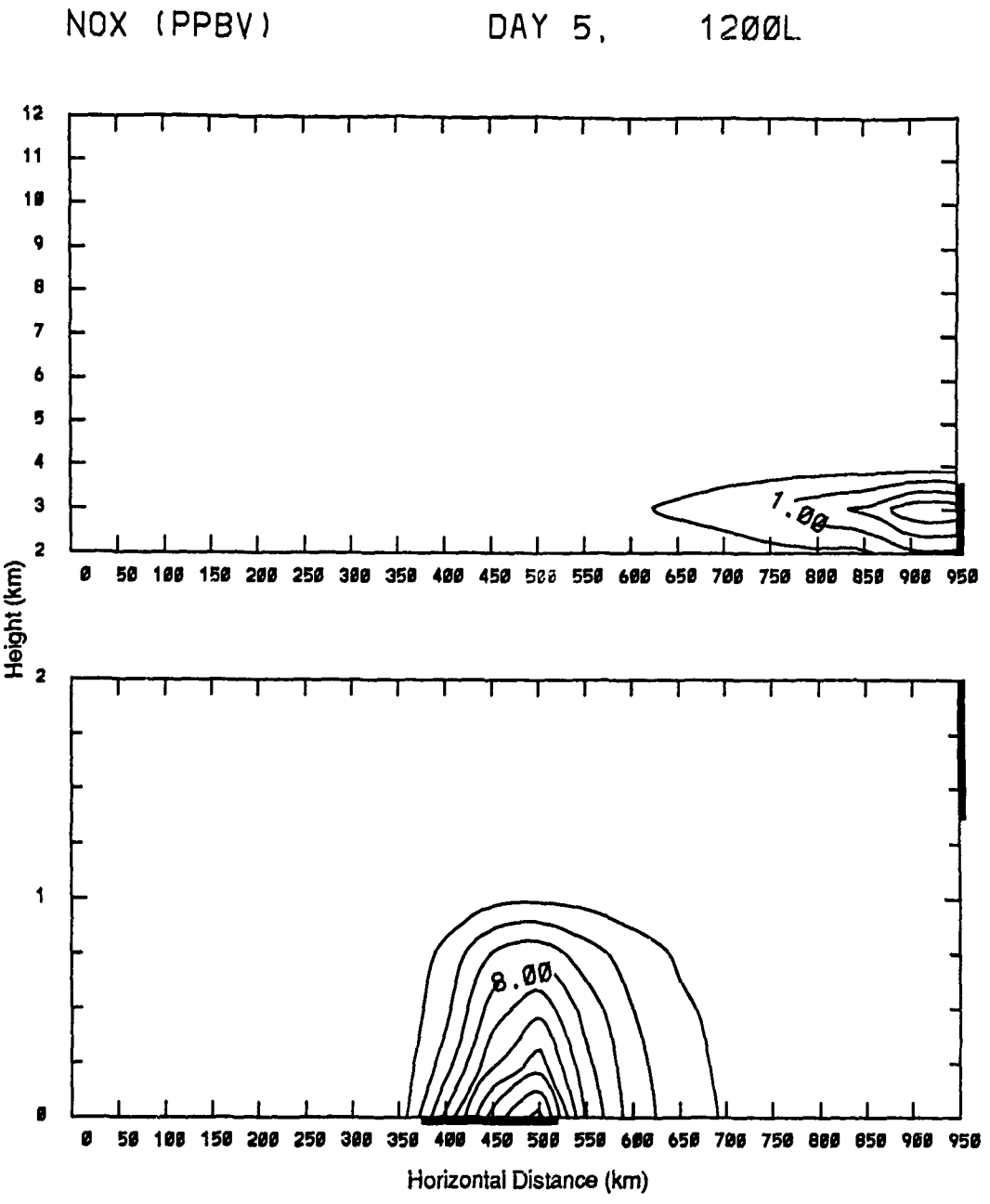

Figure 49: As in figure 47 for 1200L on day 5. Contour increment is 0.1 ppbv for the top plot, 2 ppbv for the bottom plot.

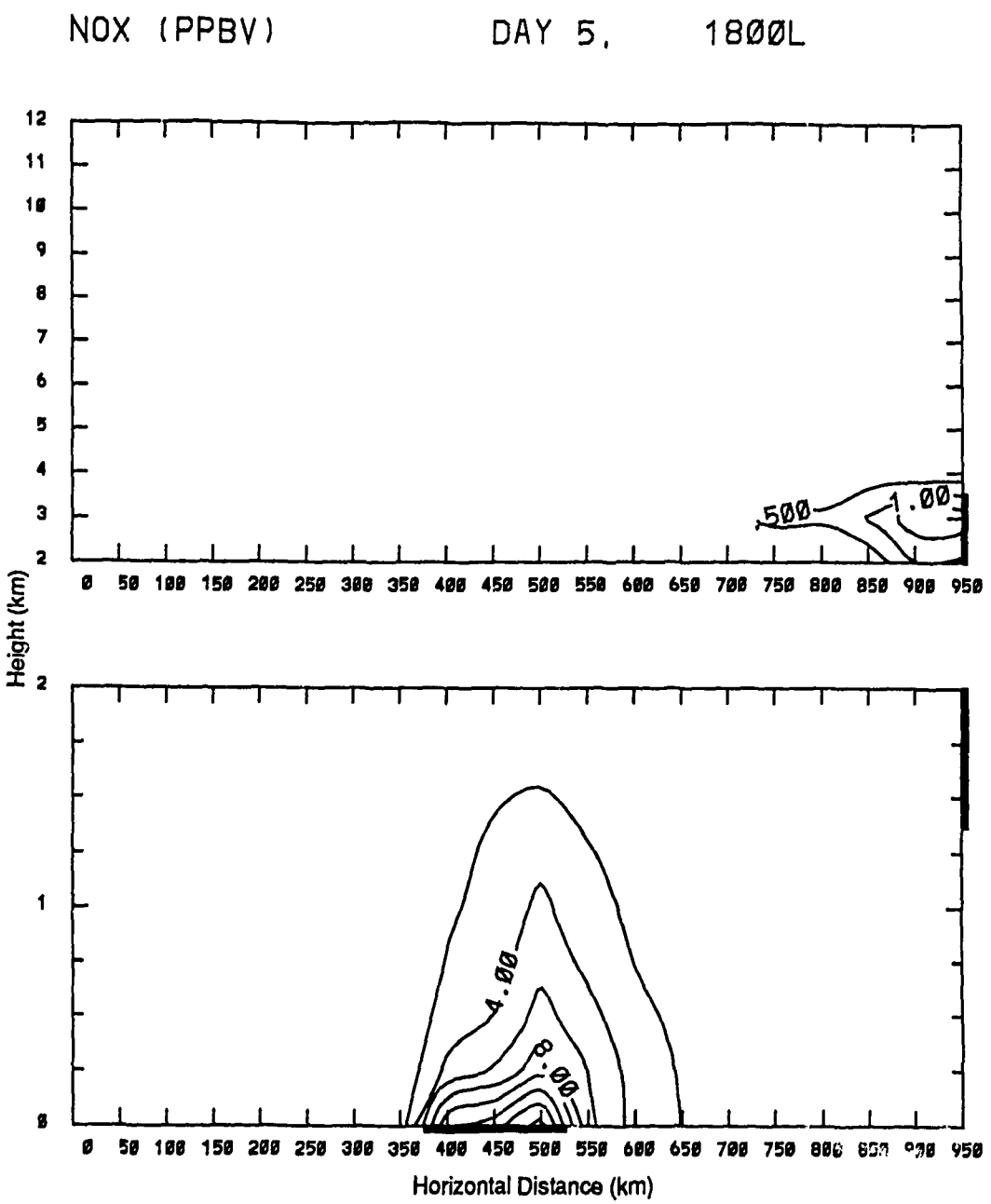

Figure 50: As in figure 47 for 1800L on day 5.

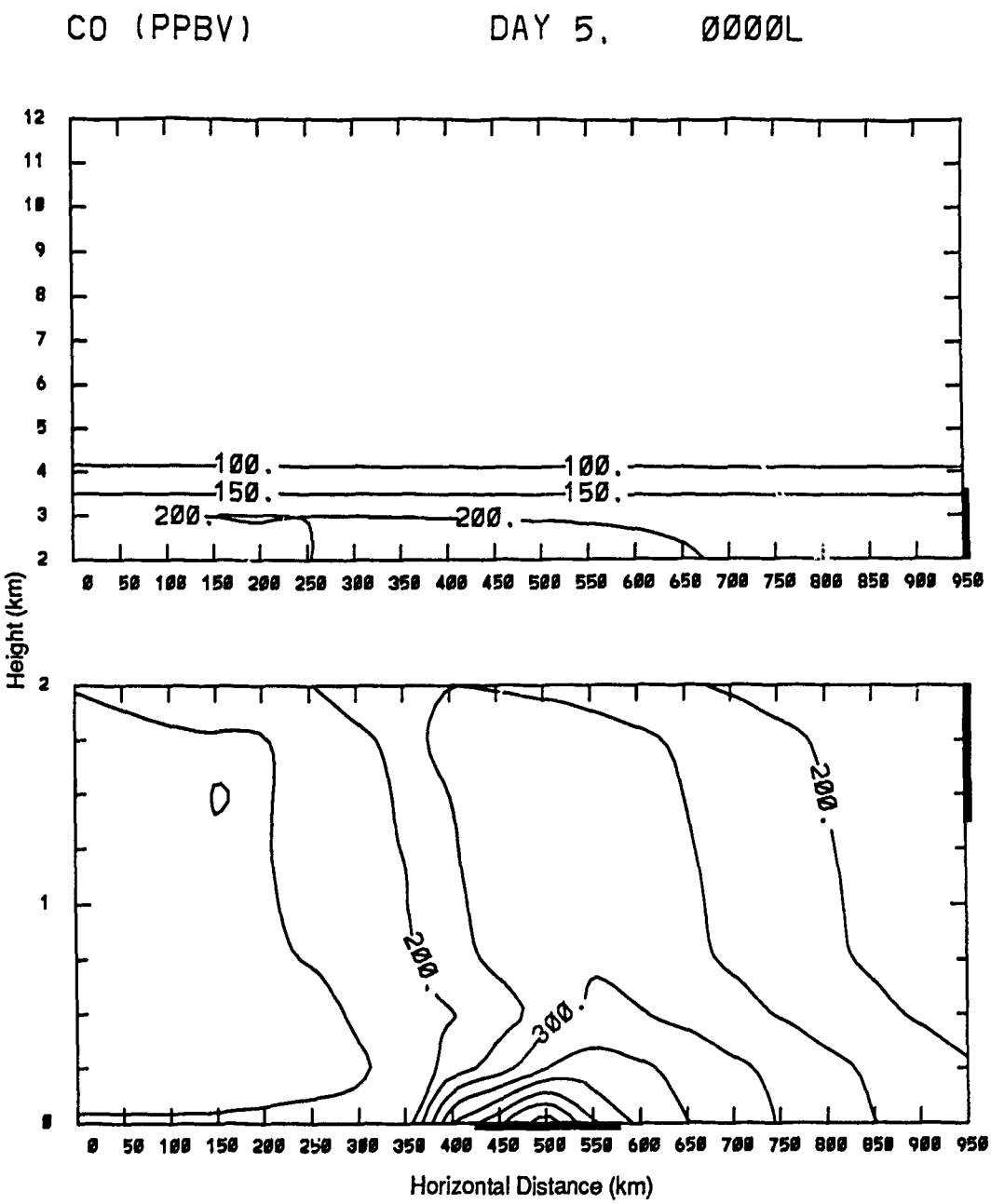

Figure 51: Forecast distribution of CO for Case II at 0000L on day 5. Contour increment is 50 ppbv.

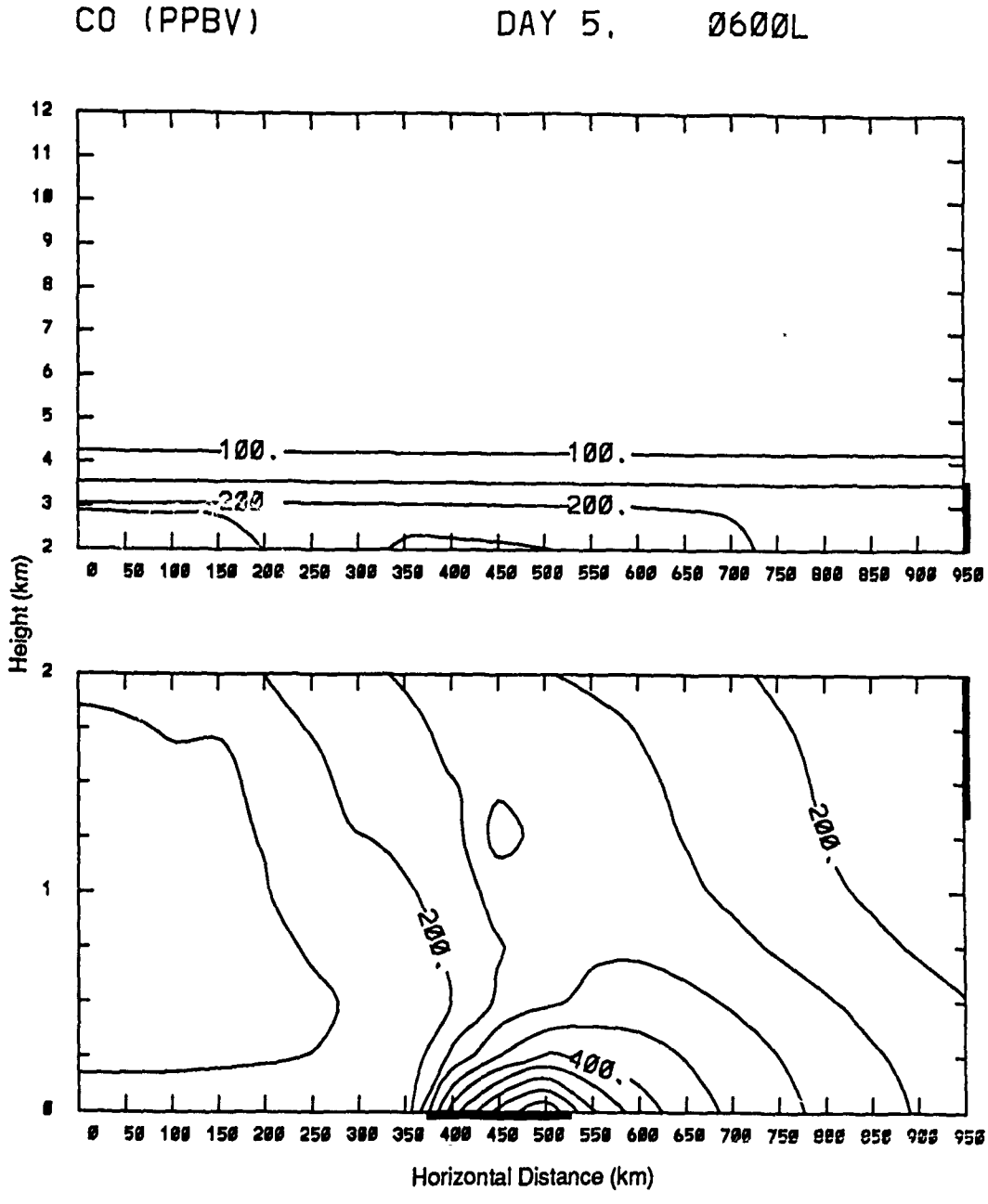

Figure 52: As in figure 51 for 0600L on day 5.

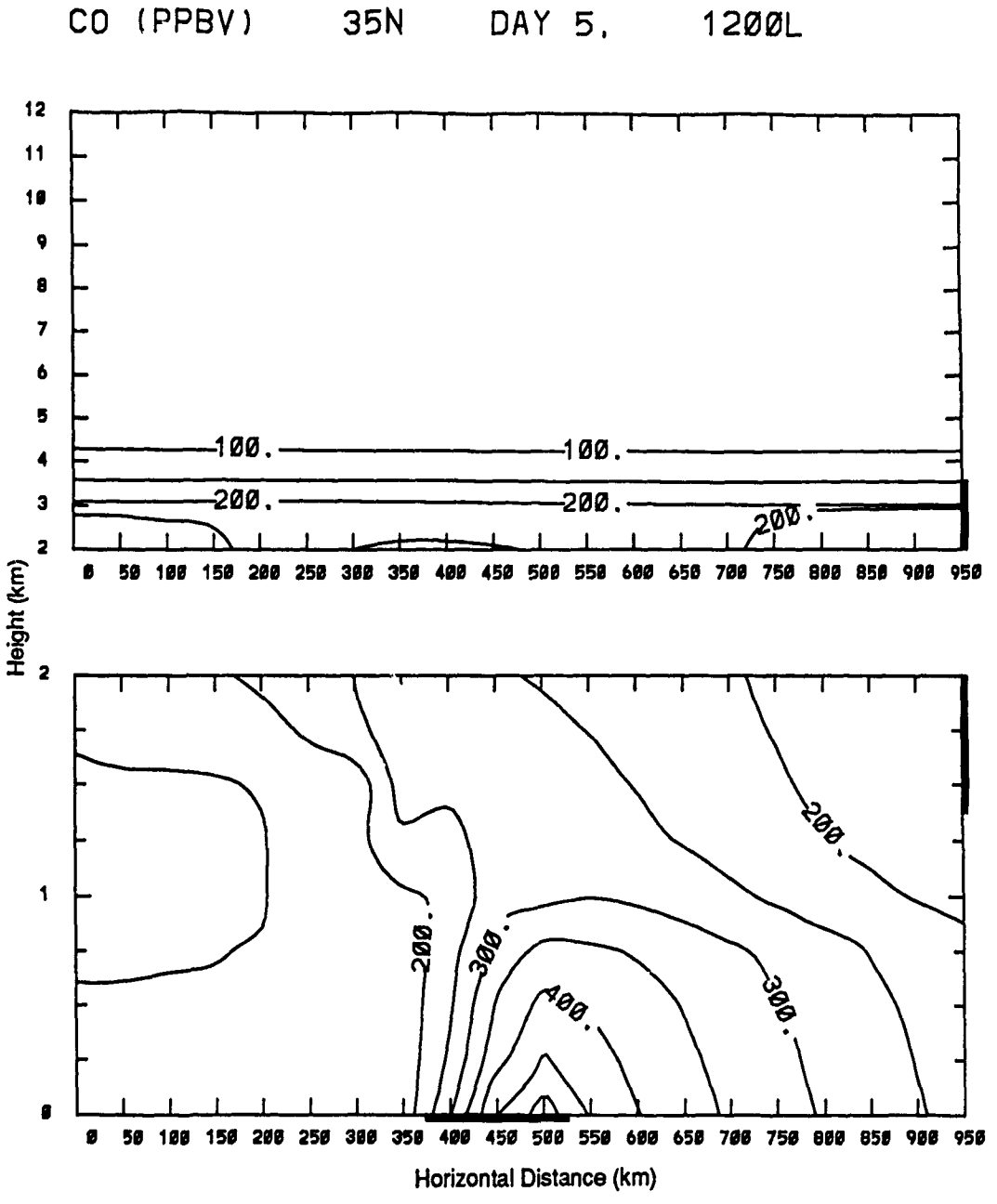

Figure 53: As in figure 51 for 1200L on day 5.

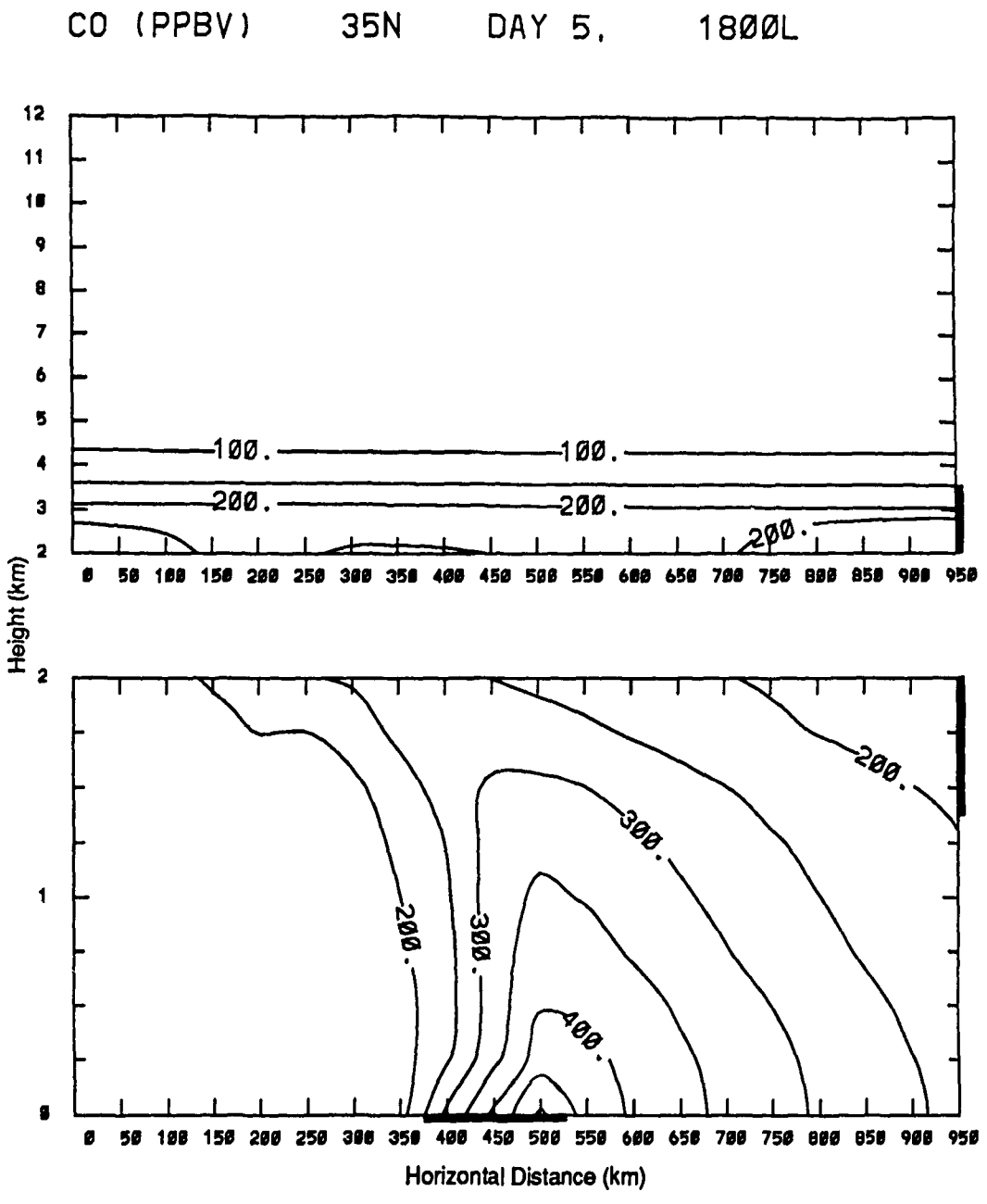

Figure 54: As in figure 51 for 1800L on day 5.

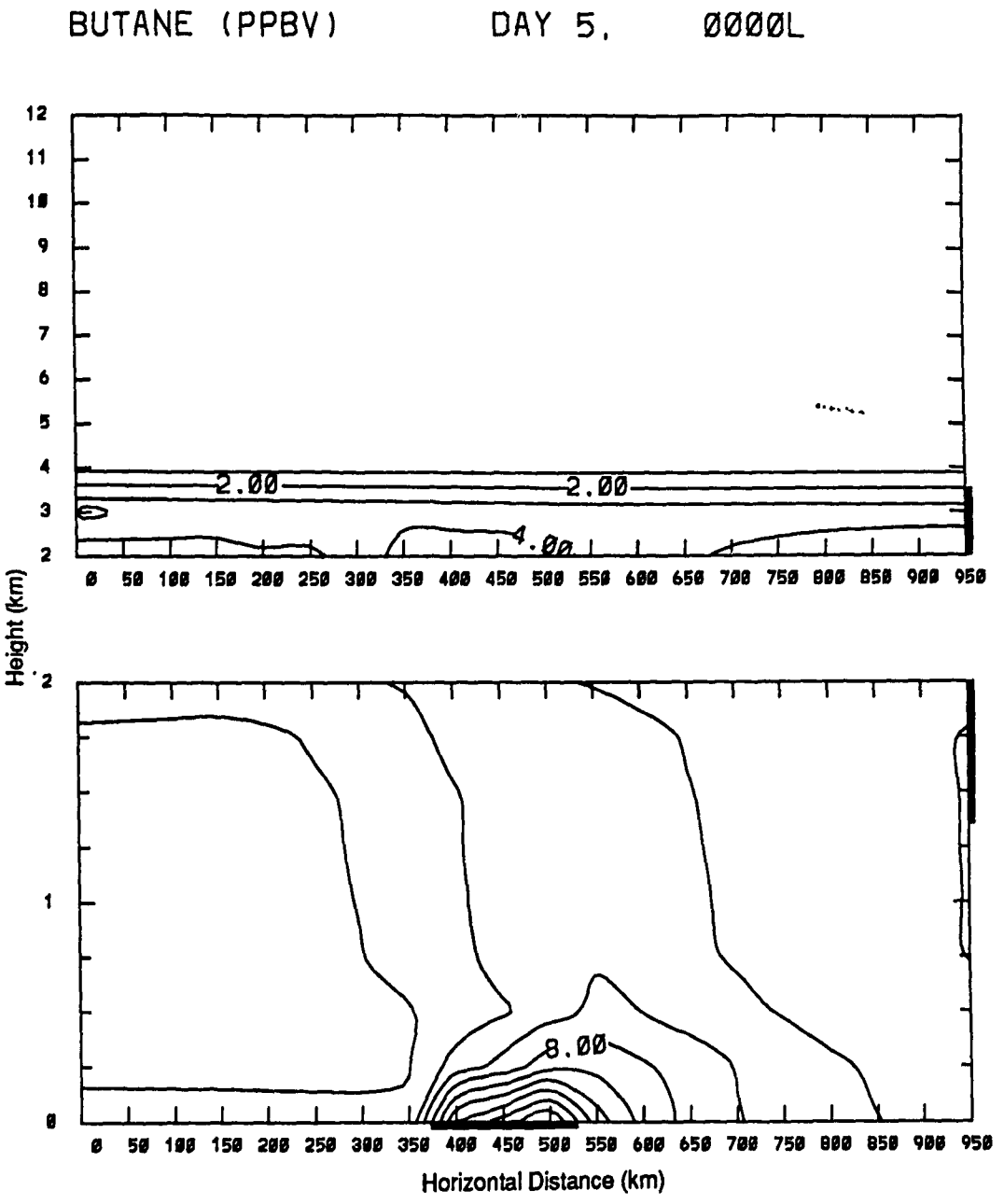

Figure 55: Forecast distribution of butane for Case II at 0000L on day 5. Contour increment is 1 ppbv for the top figure, 2 ppbv for the bottom figure.

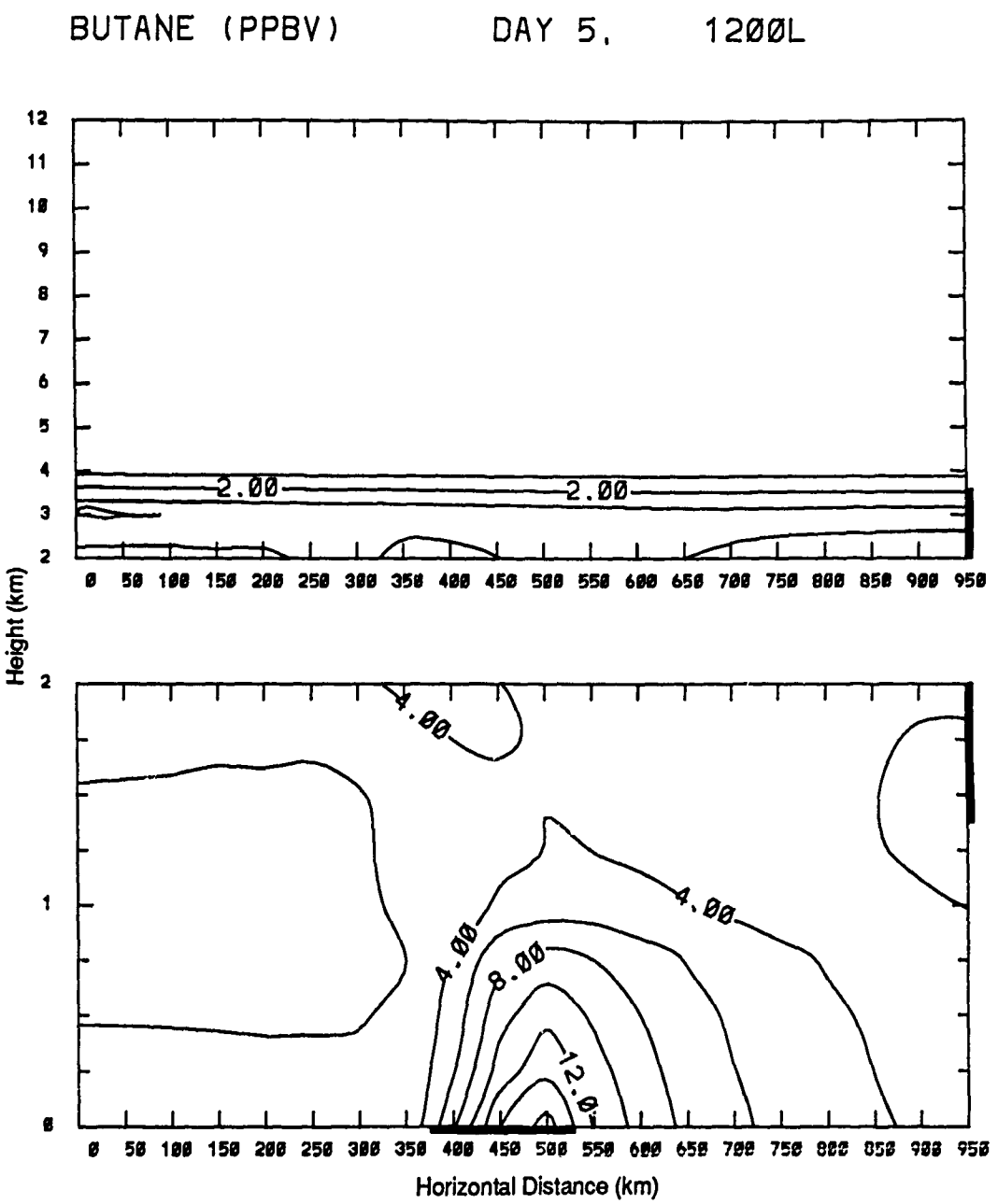

Figure 56: As in figure 55 for 0600L on day 5.

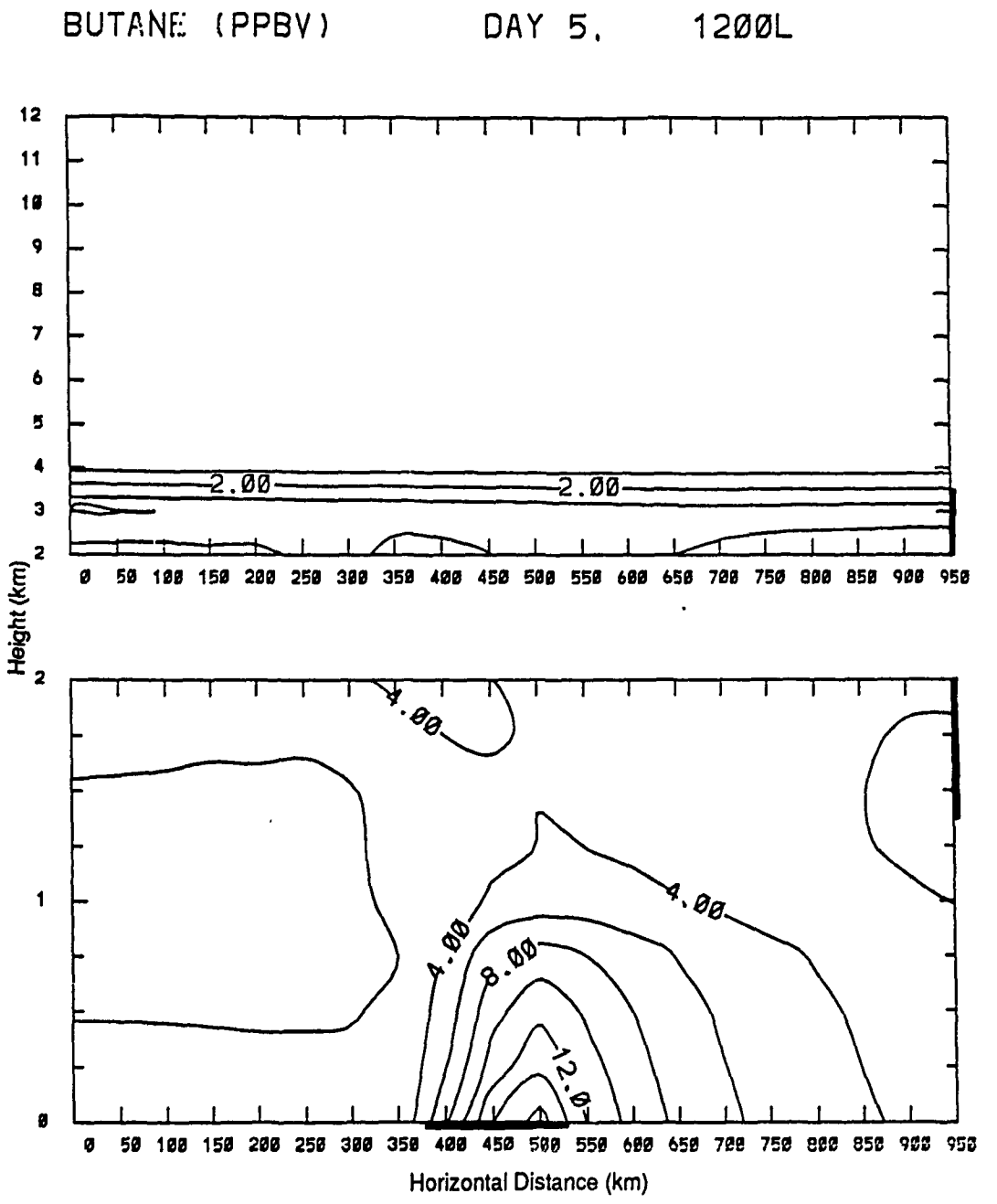

Figure 57: As in figure 55 for 1200L on day 5.

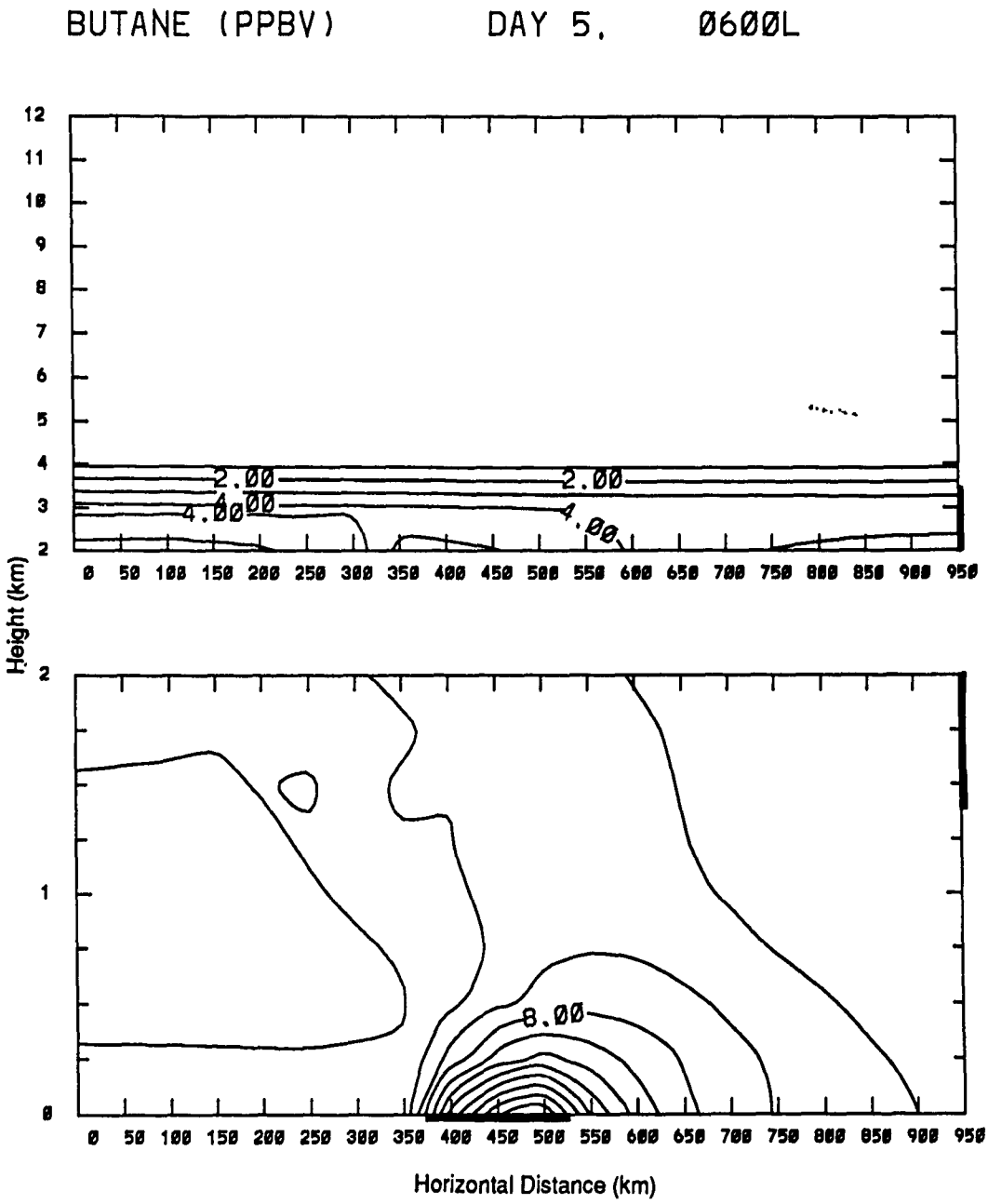

Figure 56: As in figure 55 for 0600L on day 5.

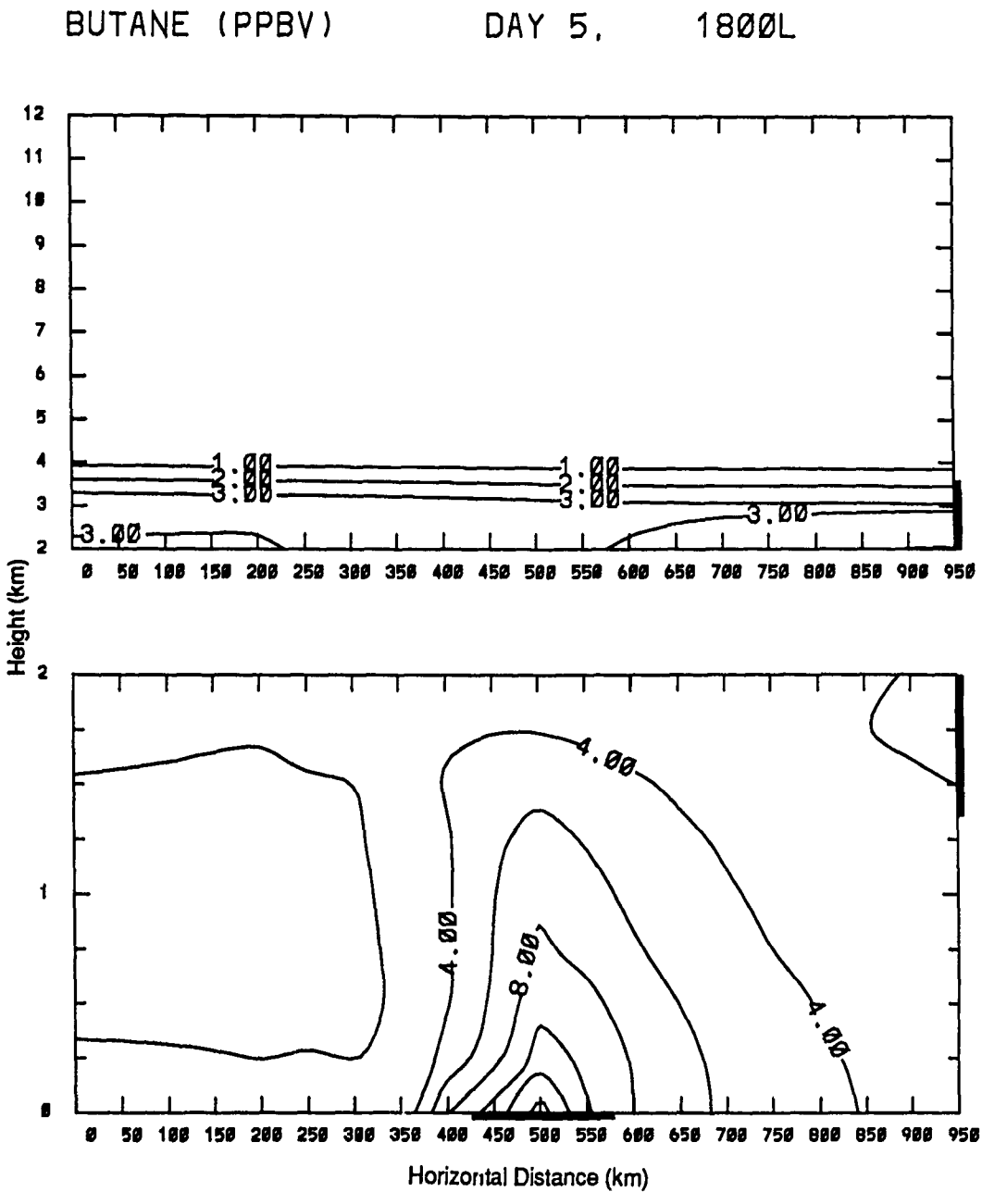

Figure 58: As in figure 55 for 1800L on day 5.

References

Benkley, C. W. and L. L. Schulman, 1979: Estimating hourly mixing depths from historical meteorological data. *J. Appl. Meteor.*, **28**, 772-780.

Buhr, M. P., D. D. Parich, R. B. Norton, F. C. Fehsenfeld, R. E. Sievers and J. M. Roberts, 1990: Contribution of organic nitrates to the total reactive nitrogen budget at a rural eastern U.S. site. *J. Geophys. Res.*, **95**, 9809-9816.

Carney, T. A., 1984: An investigation of the vertical distribution of trace constituents in the troposphere with a one-dimensional photochemical model and simple models of the planetary boundary layer, PhD Dissertation, Saint Louis University, St Louis MO. (available from University Microfilms, Ann Arbor).

Chameides, W. L. and J. C. G. Walker, 1973: A photochemical theory of tropospheric ozone. *J. Geophys. Res.*, **78**, 8751-8760.

Crutzen, P. J., 1973: A discussion of the chemistry of some minor constituents in the stratosphere and troposphere. *Pure and Appl. Geophys.*, **106-108**, 1385-1399.

Daily weather maps weekly series, July 26, 1987, United States Government Printing Office, Washington, D. C.

Danielsen, E. F., 1968: Stratospheric-tropospheric exchange based on radioactivity, ozone and potential vorticity. *J. Atmos. Sci.*, **25**, 502-518.

DeMore, W. R., R. Watson, F. Kaufman, D. Golden, R. Hampson, M. Karylo, C. Howard, M. Molina, A. Ravishankara, 1982: Chemical kinetic and photochemical data for use in stratospheric modeling. *Evaluation No. 5, JPL Publ. No. 82-57*, Jet Propulsion Laboratory, Pasadena, CA.

Fabian, R. and P. G. Pruchniewicz, 1973: Meridional distribution of ozone from ground based registrations between norway and south africa. *Pure and Appl. Geophys.*, **106-108**, 1027-1035.

Fishman, J., 1977: A numerical investigation of the meteorological and photochemical

processes which influence tropospheric ozone and other tace constituents. Ph.D. Dissertation, Saint Louis University, Saint Louis, MO.

Fishman, J., 1985: Ozone in the troposphere. In *Ozone in the Free Atmosphere*, eds R. C. Whitten and S. S. Prasad, VanNostrand Reinhold Company, New York.

Fishman, J. and T. A. Carney, 1984: A one-dimensional photochemical model of the troposphere with planetary boundary-layer parameterization. *J. Appl. Meteor.*, **1**, 351-376.

Fishman, J. and P. J. Crutzen, 1978: The origin of ozone in the troposphere. *Nature*, **274**, 855-858.

Fishman, J., V. Ramanathan, P. J. Crutzen and S. C. Liu, 1979: Tropospheric ozone and climate. *Nature*, **282**, 818-820.

Fishman, J., F. M. Vukovich and E. V. Browell, 1985: The photochemistry of synoptic-scale ozone synthesis: implications for the global tropospheric ozone budget. *J. Appl. Meteor.*, **3**, 299-320.

Fishman, J., C. E. Watson, J. C. Larsen and J. A. Logan, 1990: Distibution of tropospheric ozone determined from satellite data. *J. Geophys. Res.*, **95**, 3599-3617.

Florida Department of Environmental Regulation, 1990: Research Priorities, Tallahassee.

Folinsbee, L. J., W. F. McDonnell and D. H. Horstman, 1988: Pulmonary function and symptom responses after 6.6 hour exposure to 0.12 ppm ozone with moderate exercise. *J. Air Pol. Cont. Assoc.*, **38**, 28-35.

Heck, W. W., O. C. Taylor, R. Adams, G. Bingham, J. Miller, E. Preston and L. Weinstein, 1982: Assessment of crop loss from ozone. *J. Air Pol. Cont. Assoc.*, **32**, 353-361.

Jacob, D. and S. Wofsy, 1988: Photochemistry of biogenic emissions over the amazon forest. *J. Geophys. Res.*, **93**, 1477-1486

Kircher, C., J. Margitan and S. Sander, 1984: Pressure and temperature dependence of the reaction $NO_2 + NO_3 + M \rightarrow N_2O_5 + M$. *J. Phys. Chem.*, **88**, 4370-4375.

Levy, H., J. D. Mahlman and W. J. Moxim, 1980: A statospheric source of reactive nitrogen in the unpolluted troposphere. *Geophys. Res. Lett.*, **7**, 441-444.

Logan, J. A., 1985: Tropospheric ozone: Seasonal behavior, trends, and anthropogenic Influence. *J. Geophys. Res.*, **90**, 10,463-10,482.

Logan, J. A., 1989: Ozone in rural areas of the United States. *J. Geophys. Res.*, **94**, 8511-8532.

Lurmann, F. W., A. C. Lloyd and R. Atkinson, 1986: A Chemical mechanism for use in

long-range transport/acid deposition computer modeling. *J. Geophys. Res.*, **91**, 10,905-10,936.

Mahlman, J. D., H. Levy and W. J. Moxim, 1980: Three-dimensional tracer structure and behavior as simulated in two ozone precusor experiments. *J. Atmos. Sci.*, **37**, 655-685.

Malko, M. and J. Troe, 1982: Analysis of the unimolecular reaction $N_2O_5 + M \leftrightarrow NO_2 + NO_3 + M$. *Int. J. Chem. Kinet.*, **14**, 399-416.

Matsuno, T., 1966: Numerical intergrations of the primitive equations by a simulated backward difference method. *J. Meteor. Society of Japan*, **44**, 76-84.

McNider, R. T. and G. N. Cox, 1989: A preliminary analysis of an elevated ozone event in the southeast July 25 - 31, 1987. Submitted to SERON Steering Committee, April 1989.

Niki, H., E. Daby and B. Weinstock, 1984: Mechanisms of smog reactions. *Adv. Chem. Series*, **113**, 16-57.

O'Brien, J. J., 1970: A note on the vertical structure of th eddy exchange coefficient in the planetary boundary layer. *J. Atmos. Sci.*, **27**, 1213-1215.

Prather, M. J., 1986: Numerical advection by conservation of second-order moments. *J. Geophys. Res.*, **91**, 6671-6681.

Ramanathan, V., 1988: The greenhouse theory of climate change: A test by an inadvertent global experiment. *Science*, **240**, 293-299.

Richardson, J. L., 1988: The role of biogenic hydrocarbons in the photochemical production of tropospheric ozone in the Atlanta, Georgia region., M.S. Thesis, Georgia Institute of Technology, Altanta, GA.

Richardson, J. L, J. Fishman and G. L. Gregory, 1990: Ozone budget over the Amazon: Regional effects from biomass burning emissions., Submitted to *J. Geophys. Res.*, July 1990.

Sillman, S., J. A. Logan, and S. C. Wofsy, 1990: A regional scale model for ozone in the United States with subgrid representation of urban and power plant plumes. *J. Geophys. Res.*, **95**, 5731-5748.

Smeda, M. S., 1979: Incorporation of planetary boundary layer processes into numerical forecasting models. *Boundary-Layer Meteor.*, **16**, 115-129.

Smolarkiewicz, P. K., 1983: A simple positive definite advection scheme with small implicit diffusion. *Mon. Wea. Rev.*, **111**, 479-486.

Sun, M., 1988: Tighter ozone acandard urged by scientists. *Science*, **240**, 1724,1725.

Wang, W. C., Y. L. Yung, A. A. Lacis, T. Mo and J. E. Hansen, 1976: Greenhouse effects

due to man-made perturbations of trace gases. *Science*, **194**, 685-690.

Vukovich, F. M. and J. Fishman, 1986: The climatology of summertime O_3 and SO_2. *Atmos. Environ.*, 2423-2433.

Zeman, O. and H. Tennekes, 1977: Parameterization of the turbulent energy budget at the top the the daytime atmospheric boundary layer. *J. Atmos. Sci.*, **34**, 111-123.

A Two-dimensional Photochemical Model of the Troposphere

by Meade W. Carlson, Capt, USAF

1990
99 pages
Degree Awarded: M.S. by The Florida State University

Abstract

An experiment using a time-dependent, two-dimensional photochemical model of the troposphere to model the vertical and zonal distribution of ozone and its precursors is presented. The experiment examines two cases. Case I simulates vertical transport due to diffusion and zonal transport due to advection, with surface emissions of ozone precursors in the center of the model domain representing an urban environment with light wind conditions favorable for the formation of ozone in concentrations greater than 80 parts per billion by volume (ppbv). In Case II, an elevated source of ozone and its precursors is introduced at the upstream boundary in order to investigate the role of advection of these chemical species on ozone concentrations.

The first simulation produces surface ozone concentrations greater than 120 ppbv in the air above the urban area, and the second simulation produces an increase of 3 – 10 percent in this region. A comparison of Case I and Case II results shows that enhanced photochemical production of ozone due to the addition of ozone's precursors plays an important role in this increase.

VITA

Meade William Carlson was born on August 27, 1962, in Wells, Minnesota, and spent his childhood in Kiester, Minnesota. He studied at Concordia College in Moorhead, Minnesota and graduated with a Bachelor of Arts degree in Physics and Mathematics in 1984. Upon graduation, he was commissioned a Second Lieutenant in the United Stated Air Force and was assigned to the Air Force Institute of Technology Basic Meteorology Program at San Jose State University through Spring of 1985. From 1985 to 1988, he was assigned to Wurtsmith Air Force Base, Michigan as a Wing Weather Officer supporting the 379th Bombardment Wing. In 1988 he was promoted to Captain and entered the graduate progam in meteorology at the Florida State University under the Air Force Institute of Technology Civilian Institution's Advanced Degree Program.